Mohammad Khaled Shakfa

Localization Effects in Disordered III-V Semiconductor Nanostructures

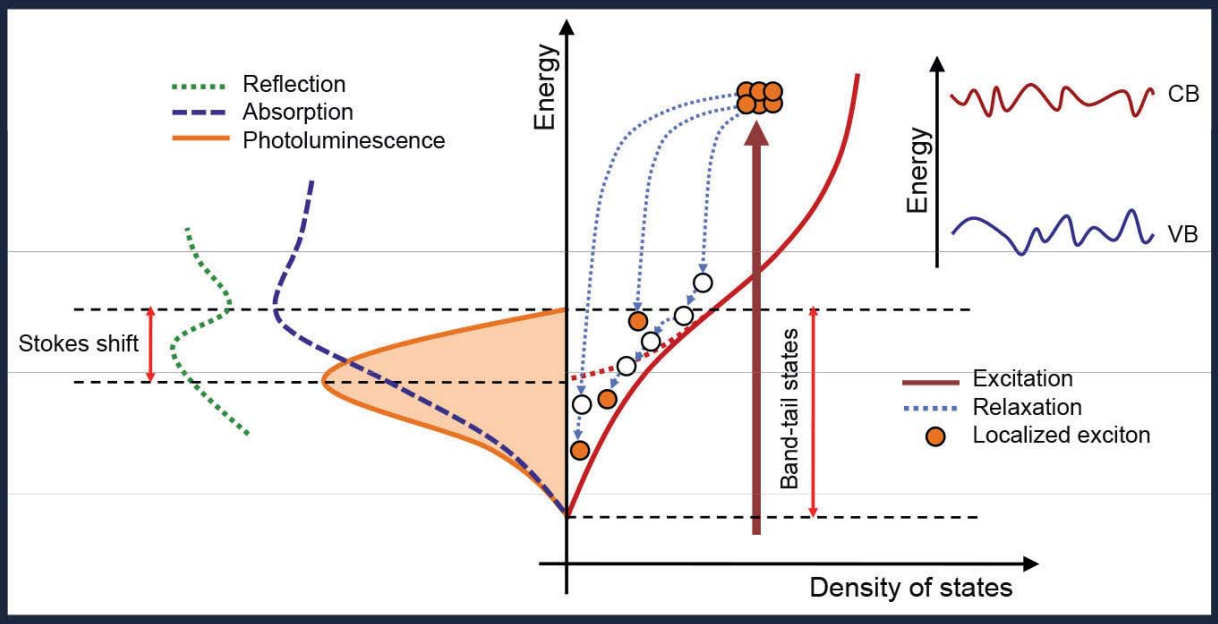

Cuvillier Verlag Göttingen
Internationaler wissenschaftlicher Fachverlag

Localization Effects in Disordered III-V Semiconductor Nanostructures

Dieses Werk ist copyrightgeschützt und darf in keiner Form vervielfältigt werden noch an Dritte weitergegeben werden.
Es gilt nur für den persönlichen Gebrauch.

Dieses Werk ist copyrightgeschützt und darf in keiner Form vervielfältigt werden noch an Dritte weitergegeben werden.
Es gilt nur für den persönlichen Gebrauch.

Localization Effects in Disordered III-V Semiconductor Nanostructures

Der Fakultät für Elektrotechnik, Informationstechnik, Physik
der Technischen Universität Carolo-Wilhelmina zu Braunschweig

zur Erlangung des Grades eines Doktors

der Ingenieurwissenschaften (Dr.-Ing.)

genehmigte Dissertation

von Dipl.-Phys. Mohammad Khaled Shakfa
aus Homs, Syrien

eingereicht am:	22.06.2015
mündliche Prüfung am:	29.07.2015
1. Referent:	Prof. Dr. rer. nat. Martin Koch
2. Referent:	Prof. Dr. rer. nat. Tobias Voss

2015

Dieses Werk ist copyrightgeschützt und darf in keiner Form vervielfältigt werden noch an Dritte weitergegeben werden.
Es gilt nur für den persönlichen Gebrauch.

Bibliografische Information der Deutschen Nationalbibliothek

Die Deutsche Nationalbibliothek verzeichnet diese Publikation in der Deutschen Nationalbibliographie; detaillierte bibliografische Daten sind im Internet über http://dnb.d-nb.de abrufbar.

1. Aufl. - Göttingen: Cuvillier, 2015
Zugl.: (TU) Braunschweig, Univ., Diss., 2015

Dissertation an der Technischen Universität Braunschweig,
Fakultät für Elektrotechnik, Informationstechnik, Physik

© CUVILLIER VERLAG, Göttingen 2015
Nonnenstieg 8, 37075 Göttingen
Telefon: 0551-54724-0
Telefax: 0551-54724-21
www.cuvillier.de

Alle Rechte vorbehalten. Ohne ausdrückliche Genehmigung
des Verlages ist es nicht gestattet, das Buch oder Teile
daraus auf fotomechanischem Weg (Fotokopie, Mikrokopie)
zu vervielfältigen.
1. Auflage, 2015
Gedruckt auf umweltfreundlichem, säurefreiem Papier aus nachhaltiger Forstwirtschaft.

ISBN 978-3-7369-9160-6
eISBN 978-3-7369-8160-7

Dieses Werk ist copyrightgeschützt und darf in keiner Form vervielfältigt werden noch an Dritte weitergegeben werden.
Es gilt nur für den persönlichen Gebrauch.

To my family

Making a mistake is not a big deal as long as you have learned from ...

Dieses Werk ist copyrightgeschützt und darf in keiner Form vervielfältigt werden noch an Dritte weitergegeben werden.
Es gilt nur für den persönlichen Gebrauch.

Dieses Werk ist copyrightgeschützt und darf in keiner Form vervielfältigt werden noch an Dritte weitergegeben werden.
Es gilt nur für den persönlichen Gebrauch.

Acknowledgements

During my years as a PhD-student at the *Braunschweig University of Technology* and then at the *Philipps University of Marburg* I have had the pleasure of meeting and working with many great people who contributed to this work in various ways. It would be impossible to properly express my full gratitude and heartfelt thanks to all of them for their help and support in just a few lines. Nevertheless, I will try to make an attempt.

First and foremost, I would like to express my sincere gratitude to my doctoral father, Prof. Dr. Martin Koch for having given me the great opportunity to learn and work in his group. My deepest appreciation goes to him for giving me the freedom to pursue the research that seemed interesting to me. He gave me the opportunity to work on several different experiments. His broad and deep knowledge combined with his insights and criticisms were valuable as well as invaluable at times. I have enormously benefited from our many discussions on various topics and from the nice environment he has created with his good humour and energy. I am grateful to him for all kinds of support he has given me. He has always been ready to offer his help whenever needed, to discuss solutions to the many roadblocks I encountered on the way, and to solve seemingly insurmountable problems. Without his consistent encouragement, trust, guidance, and mentorship, it would have been impossible for me to complete this thesis.
Prof. Koch, I have learnt a lot of things from you which I will carry with me as I move forward, not only in the academic aspect, thank you for a fantastic PhD experience!

I extend my appreciation to the members of the thesis defense committee, Prof. Dr. Tobias Voss and Prof. Dr. Andreas Waag from the the *Braunschweig University of Technology* for their genuine interest in my research topic, for the time and effort they put into reading this work, and for generously offering me valuable feedback and recommendations to improve my thesis.

Beside my supervisor, it has been a great privilege and pleasure for me to work with Prof. Dr. Sergei Baranovski, Dr. Kakhaber Jandieri, and Martin Wiemer. Their profound knowledge and insightful thoughts in disordered semiconductor physics have been a crucial resource that I have enormously benefited in my studies. Without their unflagging mentorship and the invaluable discussions I had with them, it would have been impossible for me to do this thesis. At this point, I am very grateful to Martin Wiemer for his wise advice and very constructive and useful comments regarding the text of my thesis.

I would like to equally thank Prof. Dr. Kerstin Volz; Dr. habil. Wolfgang Stolz; and Priv. Doz. Dr. Sangam Chatterjee from the *Philipps University of Marburg*, Prof. Dr. Dan A. Beaton from the *University of British Columbia*, and Prof. Dr. Thomas Tiedje from the *University of Victoria*, for providing me semiconductor structures. I would like to thank the *German Science Foundation* (DFG) through the Research Training Group (GRK 1782) and MARA - *MArburg University Research Academy* through the DAAD STIBET Program for the financial support.

Dieses Werk ist copyrightgeschützt und darf in keiner Form vervielfältigt werden noch an Dritte weitergegeben werden.
Es gilt nur für den persönlichen Gebrauch.

I am indebted to Alexej Chernikov who introduced to me the experimental setup and was always open for discussions. I would like to thank Marina Gerhard and Ronja Woscholski for sharing their experimental skill and experience, and for many useful scientific discussions. During my PhD, I had the honor to supervise two students; Dimitri Kalincev for his diploma thesis and Tashneem Ara Islam for her master thesis, thank you both for your great work. Many thanks goes to our VECSEL team; Christoph Möller, Mahmoud Gaafar, Fan Zhang, and Arash Rahimi Iman for the very fruitful collaboration. Thanks in particular to Matthias Wichmann for the great time together.

A big thanks goes out to Ibraheem Al-Naib and Mohammed Salhi for their genuine support, tips and advices in my early time in Braunschweig and for their sincere friendship, or rather brothership, over the years. I would like to offer my sincerest gratitude to Nico Vieweg for being a good friend and perfect colleague. I am deeply indebted to him for his help, support, and the great time together in the laboratory. It has been an absolute pleasure working with him. The time I spend with Nico has been quite memorable.

My thanks are due to other current and past colleagues and PhD-students in our research group including, Amin Soltani, Thorsten Probst, Sina Lippert, Claudia Goy, Norman Born, Stefan Sommer, Oday Abdulmunem, Muhaned Bilal, Christian Jansen, Christian Jördens, Benedikt Scherger, Ole Peters, and Matthias Stecher, to name a few, for the friendly working environment and ever helping attitude.

With all my respect, I am very grateful to my family and would like to especially thank my parents for everything they have done for me to overcome all of the difficulties throughout my life and for their constant guidance and encouragement to reach this advanced education that they have missed in their own lives. My siblings; Hala, Khozama, and Mohammad, you have always been an inspiration to me. My little son, Hassan, no words can express my happiness when I see your smiley innocent face. You have made my life busy but enjoyable and worthwhile. Last but certainly not least, I reserve my deepest gratitude to my beloved wife, Dalia for her sacrifice, patience, unconditional support, and always believing in me.

Marburg, in June 2015 M. Khaled Shakfa

Dieses Werk ist copyrightgeschützt und darf in keiner Form vervielfältigt werden noch an Dritte weitergegeben werden.
Es gilt nur für den persönlichen Gebrauch.

Dieses Werk ist copyrightgeschützt und darf in keiner Form vervielfältigt werden noch an Dritte weitergegeben werden.
Es gilt nur für den persönlichen Gebrauch.

Dieses Werk ist copyrightgeschützt und darf in keiner Form vervielfältigt werden noch an Dritte weitergegeben werden.
Es gilt nur für den persönlichen Gebrauch.

Contents

Dieses Werk ist copyrightgeschützt und darf in keiner Form vervielfältigt werden noch an Dritte weitergegeben werden.
Es gilt nur für den persönlichen Gebrauch.

Dieses Werk ist copyrightgeschützt und darf in keiner Form vervielfältigt werden noch an Dritte weitergegeben werden.
Es gilt nur für den persönlichen Gebrauch.

1 Introduction

Smartphones are a perfect example of how modern technologies influence our daily lives. Nowadays it is possible to share the information worldwide within a few fractions of a second through internet connection. This amazing facility makes our world as small as a village, and it is not surprising to call the last four decades as the information age associated with the digital revolution. In addition to the development of optical fibers, the key component of this revolution is indisputably the manufacturing of semiconductors.

Due to the increasing demands industrially as well as scientifically on new optoelectronic devices for specific applications, semiconductor materials with desired energy band-gap are needed. Band gap engineering afforded by the development of the growth techniques allows the construction of novel semiconductor materials which have their band gaps at custom-designed energies that meet the requirements for particular applications [1]. In addition to binary compound semiconductors, this opens up numerous possibilities of three-elements (ternary), four-elements (quaternary), or even five-elements (quinary) semiconductor compounds (or rather alloys). In principle, these higher-order compositions can be synthesized by alloying various semiconductors together [2]. Alloying provides the ability to tailor the energy band gap of a semiconductor through the manipulation of its constituent composition. Furthermore, the ability to adjust the lattice constant of a semiconductor alloy by changing the composition of an involved compound enables the development of heterostructures, which is actually the key element of the design high performance optoelectronic devices [2, 3, 4].

Among semiconductors, dilute III-V nitride and/or bismide semiconductor alloys have emerged as a subject of considerable research efforts over the last two decades driven by not only their unique physical properties but also their great potential for photonic devices [5, 6]. In this thesis, it is focused on two III-V-based compound semiconductor nanostructures: Ga(NAsP) and Ga(AsBi). In particular, quaternary Ga(NAsP) semiconductor structures are promising for the fabrication of intermediate band solar cells [7], for infrared laser emission [8, 9], and, with a tremendous potential, for the realization of monolithic optoelectronic integrated circuits on silicon substrate (silicon photonics) [5, 9]. On the other hand, ternary Ga(AsBi) semiconductor structures have been employed for a variety of applications such as photoconductive terahertz antennas [10], light-emitting diodes (LEDs) [11], and both optically pumped [12] and electrically injected [13] laser diodes.

In the studied GaAs-based compounds band-gap engineering is achieved by varying the amount of the incorporated V-element, i.e., nitrogen or bismuth. Despite the advantage of a shrinking in the band-gap energy, the introduction of a small amount of a V-element, acting as isoelectronic impurities, to a III-V host structure results in an increase in the disorder potential due to the differences, e.g., in size and electronegativity between the incorporated and

Dieses Werk ist copyrightgeschützt und darf in keiner Form vervielfältigt werden noch an Dritte weitergegeben werden.
Es gilt nur für den persönlichen Gebrauch.

substituted anions [5, 6]. The presence of disorder effects within a semiconductor can significantly influence its electronic structure, i.e., the density of localized states (DOS) is increased. Disorder-induced localized states drastically affect carrier recombination processes in semiconductors. The changes in carrier dynamics can be revealed by investigating, e.g., electrical and optical properties of disordered semiconductors [14].

This thesis aims to enrich the understanding of disorder effects on the semiconductor properties. It gives a qualitative as well as quantitative description to some unusual experimentally observed behaviors related to the carrier localization effects due to the disorder potential within the semiconductor structure. Such descriptions provide a useful method that can be unitized to characterize the experimental observation from a semiconductor structure. The adverse disorder-induced effects can be reduced by improving the growth conditions of semiconductor materials. Consequently, the performance of the optoelectronic devices would be enhanced if these conditions are specifically optimized.

After this introduction, the thesis is organized as follows. **Chapter 2**: This chapter gives an overview of the most important aspects with respect to disorder effects in semiconductors. Furthermore, a brief review of the radiative recombination mechanisms in semiconductors resulting is presented. The last part of this chapter deals with the band anti-crossing (BAC) model. This model was developed to explain the peculiar behavior of the composition dependence of the energy band-gap of dilute III-V nitride and/or bismide semiconductors. **Chapter 3**: This chapter gives a description of the experimental setups employed to investigate the semiconductor nanostructures. Besides, a brief overview of the growth conditions of these structures is given. **Chapter 4**: A qualitative explanation of the most prominent photoluminescence characteristics of disordered semiconductors are presented in this chapter. The impact of both, the excitation intensity and the lattice temperature is also discussed. The last part of this chapter contains a detailed study on carrier dynamics and localization effects in Ga(AsBi)/GaAs single quantum well's. **Chapter 5**: Within its first part, this chapter introduces, some theoretical approaches used for the interpretation of the non-monotonous disorder-induced PL features. While, in the second part of this chapter, the compositional dependence of the theoretically extracted energy scales for disorder is discussed for the investigated nanostructures. **Chapter 6**: A peculiar feature of the PL thermal quenching is experimentally observed in Ga(AsBi)/GaAs heterostructures under relatively low excitation intensities. This chapter provides a well-approved theoretical analysis used to explore this odd behavior. The presented approach is based on the suggestion that the density of localized sates consists of, at least, two different components. **Chapter 7**: A summary of the thesis is given in this chapter.

Dieses Werk ist copyrightgeschützt und darf in keiner Form vervielfältigt werden noch an Dritte weitergegeben werden.
Es gilt nur für den persönlichen Gebrauch.

2 Background

2.1 Introduction

In order to provide a reasonable interpretation of an unusual behavior of semiconductors, it is important to develop a detailed understanding of the underlying physical properties. Since this thesis tries to give an explanation of some experimental observations of disordered semiconductors, an overview of the most important aspects regarding disordered semiconductors is presented in this chapter.

The chapter is organized as follows. Section 2.2[1] deals with the origin of disorder in semiconductors translated in crystalline defects including impurity, inhomogeneities, dislocations, grain boundaries, clusters, and so on. The last part of this section shows some examples of the disorder effects in Ga(NAsP) and Ga(AsBi) semiconductor nanostructures. The second part of this chapter, Section 2.3[2], gives a brief review on the origin and types of the luminescence emission. Besides, recombination mechanisms within semiconductors are presented. Here, radiative recombination processes resulting in the photoluminescence signal are discussed in detail. The last part of the chapter, Section 2.4, introduces the band anti-crossing (BAC) theory, which was developed to interpret the unusual behavior of the composition dependence of the energy band gap dilute III-V nitrides and/or bismides. A comparison between the experimental results and the predictions of the BAC theory is also shown for the anti-crossing of the conduction band and the valence band, respectively.

2.2 Disorder in Semiconductors

From a structural point of view solids, including semiconductors can be classified into three types; ideal crystalline, real crystal, and purely amorphous. An ideal crystalline semiconductor has a periodic structure that is based on the chemical properties of its constituent atoms, i.e., all atoms in the crystal lattice are in equilibrium due to their orderly arrangement. In contrast, the atoms are more or less statistically distributed in space in a purely amorphous semiconductor. Here, no long- or even short-range order can be observed. However, a real semiconductor is not perfect–as an ideal one, but still has a degree of order.

The presence of defects, i.e., a degree of disorder, in a semiconductor influences most of its properties such as mechanical strength, electrical conductivity, and optical response, and hence, influences the performance of the semiconductor in applications. The disorder potential

[1] Section 2.2 is based on Refs. [4, 15]
[2] Section 2.3 is based on Refs. [16, 17, 18]

Dieses Werk ist copyrightgeschützt und darf in keiner Form vervielfältigt werden noch an Dritte weitergegeben werden.
Es gilt nur für den persönlichen Gebrauch.

in a real semiconductor crystal arises from the chemical disorder and displacive disorder. The **chemical disorder** is attributed to the disarrangement of the atomic species within the crystal structure, while the **displacive disorder** can be presented in a semiconductor due to, e.g., the existence of voids or vacancies in its crystal structure [19]. Furthermore, a degree of disorder is also expected for multilayer semiconductor structures, such as quantum wells, resulting from imperfect interfaces between the constituent layers.

Beside the abovementioned rough classification of defects in real semiconductors, they are broadly categorized into four groups according to their dimension (D); point defects (0D), line defects (1D), planer defects (2D), and volume defects (3D).

2.2.1 Point Defects

According to their origin, point defects can be divided in two main categories; intrinsic and extrinsic.

Intrinsic Point Defects

From a thermodynamic point of view, intrinsic point defects naturally occur in semiconductor materials without any external action at thermal equilibrium. In particular, for temperatures above zero-Kelvin, the atoms in a semiconductor do thermal vibrations. When the vibrations are intense enough a single atom is able to jump to a different location leaving a **vacancy** behind, Fig. 2.1(b). This atom can jump to an interstitial position within the crystal lattice; **Frenkel defect**, or to the surface of the crystal; **Schottky defect**. Such defects can increase the disorder positional of a semiconductor crystal if the lattice temperature is increased.

The presence of vacancies in a crystal can enhance the rate of chemical diffusion. The latter takes place when an atom of the same or a different type is able to move through the crystal of a semiconductor over time. Chemical diffusion can also happen in a semiconductor that contains at least two kinds of atoms. In this case, it is possible for two atoms to exchange positions in the lattice, forming a new type of intrinsic point defect which is known as **anti-site defect**.

Extrinsic Point Defects

These kinds of defects are present when at least one foreign atom is embedded within a semiconductor crystal. Such process is common in semiconductor physics and known in this case as **doping**. The doping is widely employed to modify the electrical as well as optical properties of a semiconductor. Depending on the location of the embedded atom within the lattice one defines two kinds of extrinsic point defects:

1. **Substitutional impurity**; when the embedded atom is placed on a lattice site, replacing the native atom, Fig. 2.1(d).
2. **Interstitial impurity**; here, the embedded atom is located at an interstitial lattice site, (e) and (g) in Fig. 2.1.

Dieses Werk ist copyrightgeschützt und darf in keiner Form vervielfältigt werden noch an Dritte weitergegeben werden.
Es gilt nur für den persönlichen Gebrauch.

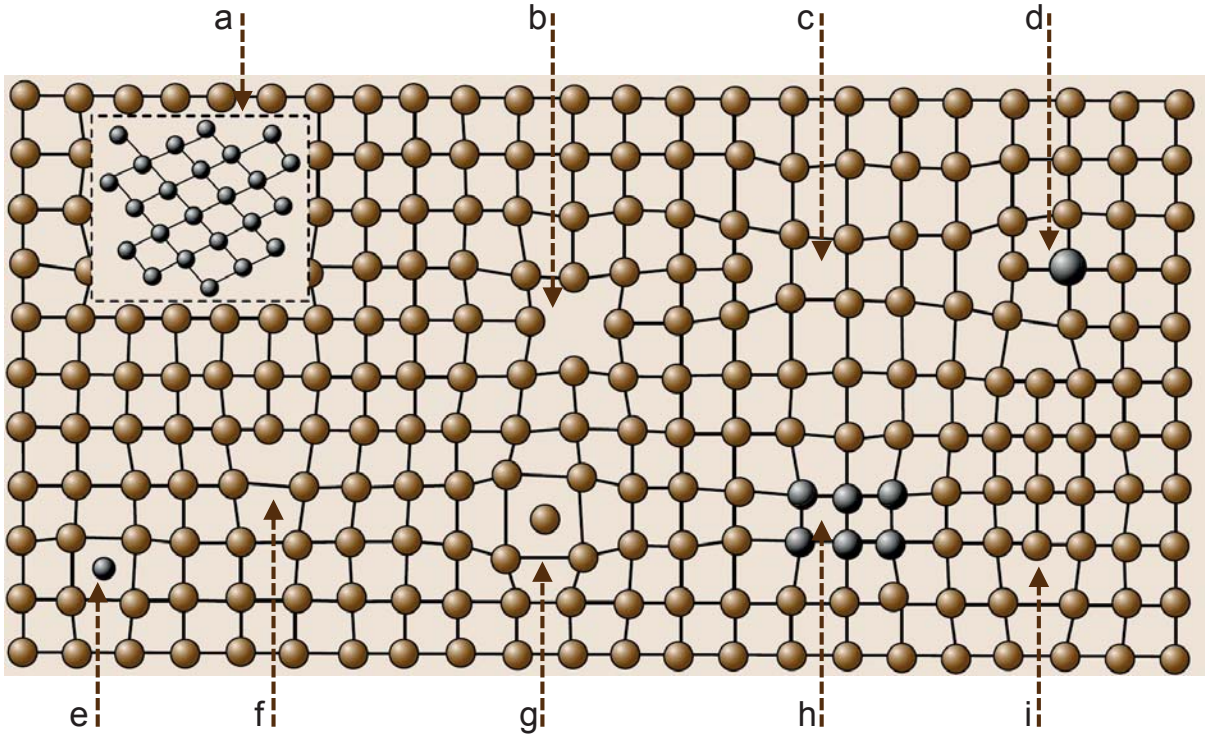

Figure 2.1: Schematic illustration of a crystal lattice with some kinds of defects: (a) incongruous inclusion (cluster), (b) vacancy, (c) vacancy-type dislocation loop, (d) substitutional impurity atom (e) interstitial impurity atom, (f) edge dislocation, (g) self-interstitial atom (h) precipitate of impurity atoms (cluster), and (i) interstitial-type dislocation loop (taken from [15]).

2.2.2 Line Defects

Line defects are purely geometrical faults and called exclusively dislocations. Dislocation lines may be straight or follow irregular curves or closed loops. However, dislocations are classified into two main types. One type is named **edge dislocation** and it happens when an extra plane of atoms is inserted into the lattice, resulting in a localized strain to be introduced into the lattice, Fig. 2.1(f). In contrast, when one side of a crystal is undergone shear stress and displaced by at least one lattice plane, while the opposite side is held fixed. This type of line defects is known as **screw dislocation**. However, several complicated **mixed dislocations** can be formed when edge and screw dislocations are both present in a semiconductor structure.

2.2.3 Planar Defects

Planar defects denote to geometrical irregularities in a crystalline lattice which occur across a planar surface of the crystal. These irregularities are caused either by an internal error in the crystal structure or by imperfect interfaces between two different semiconductor structures. The **internal planar defects** can be divided into

Dieses Werk ist copyrightgeschützt und darf in keiner Form vervielfältigt werden noch an Dritte weitergegeben werden.
Es gilt nur für den persönlichen Gebrauch.

- **Stacking faults** take place when a single plane of atoms within the crystalline lattice is misoriented or out of order.
- **Twin boundaries** are formed when a stacking fault reorients the rest of the crystal, resulting in a mirror plane within the crystal.
- **Grain boundaries** can be found in a crystalline lattice when two or more single crystals of different orientation are get together.
- **Interphase boundaries** arise when one crystalline material shares an interface with another crystalline material.

For the last case of interphase boundaries, and depending on the properties of each material, the interface between the constituent lattices can be

- **Coherent interphase boundaries** are formed when the two lattices have similar geometries. In this case, no defects will be found but a small amount of strain may be introduced due to the material change.
- **Semi-coherent interphase boundaries** occur when the two lattices have similar geometries but a larger lattice mismatch. Here, edge dislocations tend to form due to increased strain within the structure.
- **Incoherent interphase boundaries** are found in materials with a high degree of disorder, i.e., they occur at interfaces of a structure consisted of materials with significantly different geometries.

In contrast to the internal planar defects, **external planar defects** refer to surface defects that are caused by an interaction of the crystal with a gas or liquid environment. Consequently, the crystal periodicity can be interrupted and bonds can also be broken. Such defects occur at the crystal's surface and affect the outermost atomic layers, or surface region.

2.2.4 Volume Defects

This kind of defects is also known as bulk defects and happens when a significant number of point defects are spatially gathered in a so-called **cluster**. Clusters of defects appear generally when a semiconductor crystal is super-saturated with respect to some kind of point defect due to the excessive increase in the concentrations of this defect. In this case, the crystal can achieve an equilibrium condition by condensing the excess defects into clusters with different phase regions.

Clusters of vacancies forming small regions within the semiconductor material, where there are no atoms, are called **voids** or bubbles. In contrast, clusters of foreign atoms forming small regions of different phase are called **precipitates**, Fig. 2.1(h). The presence of precipitates in a semiconductor crystal is attributed to the retrograde solubility of native point defects. Another mechanism of the foreign particle formation is called **inclusion** incorporation, Fig. 2.1(a). Inclusions result from the capture melt-solution droplets from the diffusion boundary layer adjacent to the growing interface. This is enriched by the rejected excess component.

Dieses Werk ist copyrightgeschützt und darf in keiner Form vervielfältigt werden noch an Dritte weitergegeben werden.
Es gilt nur für den persönlichen Gebrauch.

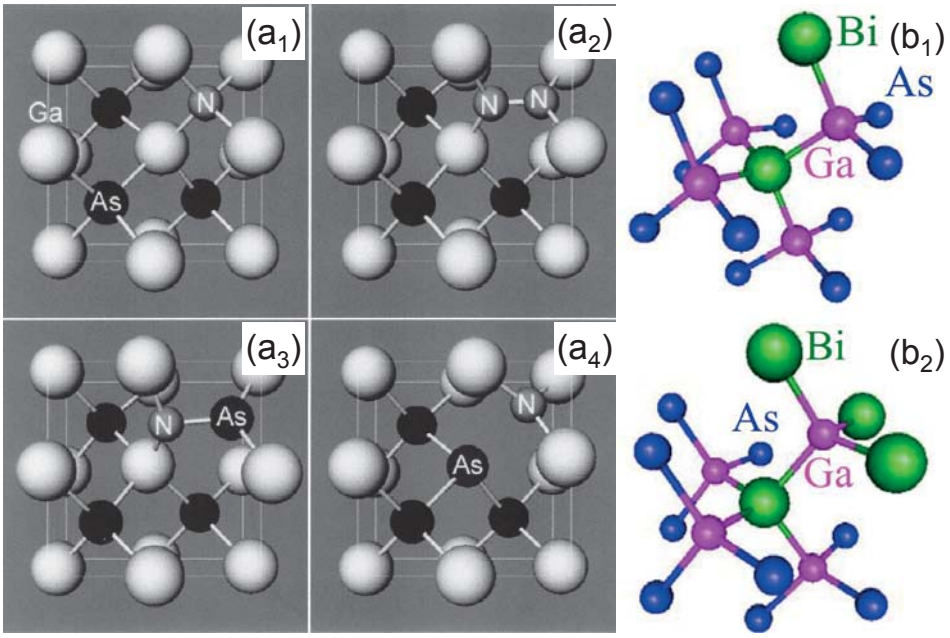

Figure 2.2: Atomic positions in Ga(NAs) for (a_1) substitutional N, (a_2) N–N, (a_3) N–As split interstitials, and (a_4) $(As_{Ga}–N_{As})_{nn}$ complex. Dark and light circles indicate As and Ga atoms, respectively, where N atoms are labeled (aftre Zhang and Wei [20]). Atoms distribution within the Ga(AsBi) lattice for (b_1) next-nearest-neighbor Bi pairs and (b_2) Bi clusters (after Ciatto *et al.* [23]).

2.2.5 Disordered III-V Semiconductors

In this sub-section, it is focused on the defects in dilute III-V nitride and/or bismide semiconductor alloys. Several types of N-induced defects in dilute III-V nitride semiconductors have been reported in the literature. Zhang and Wei have presented some types of N-related point defects in epitaxial Ga(NAs) alloys [20], which are shown in Fig. 2.2 as follows:

- **The substitutional N** is formed when an N atom is placed on a lattice site of an As atom, Fig. 2.2(a_1)
- **The N-N split interstitial** appears when N_2 molecule replaces an As atom, Fig. 2.2(a_2).
- **The N-As split interstitial** is assumed as a variation to N-N, Fig. 2.2(a_3). Here, the N-As bond length is longer than the N-N bond length.
- **The $(As_{Ga}–N_{As})_{nn}$ pair** is obtained when the N_{As} attracts the As_{Ga}, where nn stands for nearest neighbor, Fig. 2.2(a_4). The N_{As} is associated with compressive strain due to the small size of N atom, while As_{Ga} is associated with tensile strain due to two extra electrons in the non-bonding orbital.
- **The $(V_{Ga}–N_{As})_{nn}$ pair** with very low binding energy occurs when some Ga atoms are missed in the lattice structure (V_{Ga}: Ga vacancy).

The inhomogeneous N incorporation in Ga(NAsP) results in a degree of disorder, long-range compositional disorder, and can be revealed, e.g., in the cross-sectional transmission electron micrograph (TEM) [21]. Fig. 2.3(a) shows a dark field image of a cross-sectional TEM of

Dieses Werk ist copyrightgeschützt und darf in keiner Form vervielfältigt werden noch an Dritte weitergegeben werden.
Es gilt nur für den persönlichen Gebrauch.

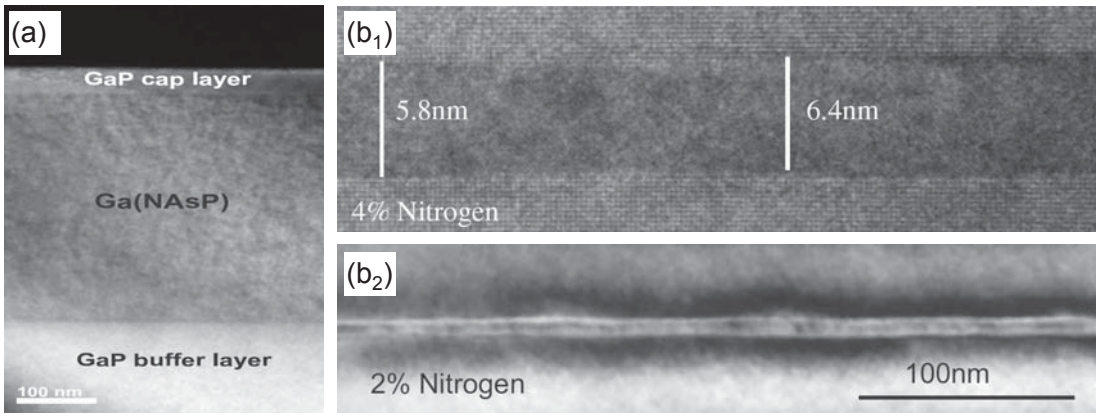

Figure 2.3: (a) dark field image of a cross-sectional TEM of Ga(NAsP) layer grown on GaP, using the strain sensitive (202) reflection (aftre Jandieri *et al.* [21]). (b_1) high resolution TEM [010] micrographs of a Ga(NAsP)/GaP QW with 4%-N content. (b_2) strain-contrast (202) TEM micrograph of a Ga(NAsP)/GaP QW with 2%-N content. Both b_1 and b_2 are adopted from Ref. [22].

Ga(NAsP) layer grown on GaP, using the strain sensitive (202) reflection. The fluctuations in the intensity indicate the local strain due to lattice constant changes caused by N-related defects. Furthermore, fluctuations in the layer thickness are also responsible for long-range disorder in the case of semiconductor heterostructure such as quantum wells. A high resolution TEM [010] micrograph of a Ga(NAsP)/GaP QW with an N content of 4% is shown in Fig. 2.3(b_1) and it demonstrates a fluctuation in the thickness of the QW as high as about 1 nm [22]. On the other hand, a strain-contrast fluctuation within the QW material can be an additional source of disorder. Such a fluctuation at a scale of 10–50 nm is presented in Fig. 2.3(b_2) for a Ga(NAsP)/GaP QW with an N content of 2% [22].

The aforementioned disorder effects in dilute III-V nitrides are also expected in Bi containing III-V semiconductor structures, since the relatively large size of Bi atom results in a degree of disruption in the lattice of the new materials, i.e., dilute III-V bismides. Using x-ray absorption spectroscopy and an appropriate theoretical simulation method, Ciatto *et al.* investigated the local structure around Bi atoms in Ga(AsBi) layers grown on GaAs as a function of Bi content aiming to detect short-range order [23]. It was found that static disorder in the Bi next-nearest-neighbor interatomic distances dramatically increase when the Bi content is increased. In particular, the Bi atoms are randomly distributed for a Bi content of 1.2%, tend to form next-nearest-neighbor pairs when the Bi content is increased up to 1.9%, and form small Bi clusters for higher Bi content (2.4%). Figs. 2.2(b_1) and 2.2(b_2) show two different local configurations of atom distribution within the lattice structure of Ga(AsBi) in the case of a next-nearest-neighbor Bi pair and for a Bi tetramer (cluster), respectively. In the second case, a central Bi atom is surrounded by three Bi next-nearest-neighbors, where all Bi atoms are next nearest neighbors of each other. However, the existence of Bi clusters within Ga(AsBi) structures is confirmed by Wu *et al.*, even for Bi content as low as 1.5% [24]. This can be seen in high resolution TEM micrographs of the corresponding sample as presented in Fig. 2.4(a_1). Here, clusters remain coherent to the matrix and tend to be formed in spherical shape. A cluster

Dieses Werk ist copyrightgeschützt und darf in keiner Form vervielfältigt werden noch an Dritte weitergegeben werden.
Es gilt nur für den persönlichen Gebrauch.

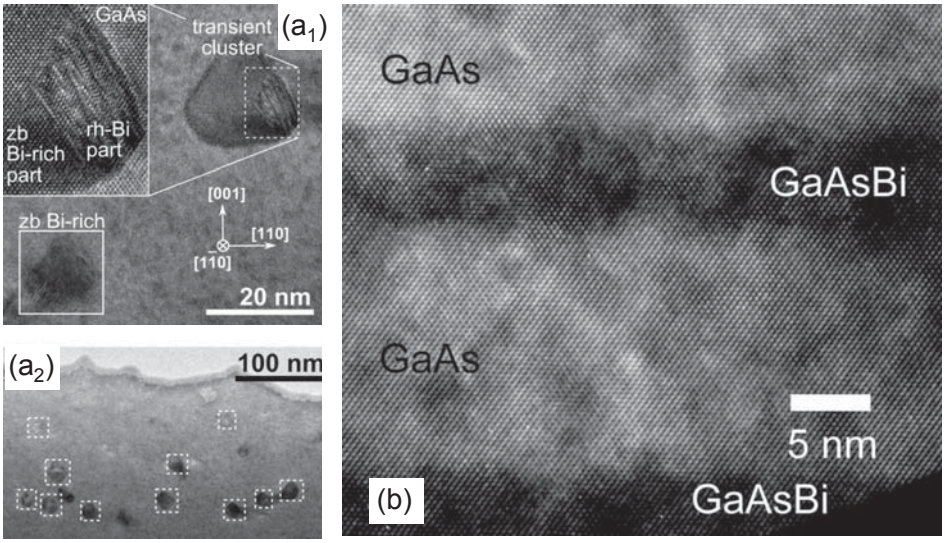

Figure 2.4: (a_1) high resolution and (a_2) bright field TEM image for a Ga(AsBi) layer with Bi content of 1.5% and 4.7%, respectively. (b) cross-sectional TEM image of a Ga(AsBi)/GaAs MQWs-sample with Bi content of 4.8% (zb: zincblende and rh: rhombohedra). (a_1) and (a_2) are adopted from Ref. [24] while (b) from Ref. [25].

diameter ranging between 12 and 22 nm is obtained for a Ga(AsBi) layer with Bi content of 4.7%, shown in Fig. 2.4(a_2) Furthermore, imperfect interfaces are also observed in the case of Ga(AsBi) heterostructures. An example is shown in Fig. 2.4(b) for a Ga(AsBi)/GaAs MQWs-sample with Bi content of 4.8% [25]. Here, fluctuations in layer thickness are demonstrated through TEM measurements.

2.3 Photoluminescence

Luminescence is a light signal produced by spontaneous emission in a material in which electrons in excited states drop down to lower levels. However, depending on the excitation method luminescence can be mainly categorized as follows [26],

- **Photoluminescence (PL)**; the luminescence takes place when a light source, e.g., laser, is used to excite the carriers in the material.
- **Cathodoluminescence (CL)**; in this method an electron beam is used as excitation source. This technique is utilized to obtain extremely high spatial resolution of the luminescence beyond the optical diffraction limit. Here, the luminescence signal is usually detected using a system based on a scanning electron microscope (SEM).
- **Electroluminescence (EL)**; the luminescence is caused by an electric current flowing through the material. This phenomenon is employed in many optoelectronic devices such as the light emitting diode (LED).
- **Chemiluminescence**; the luminescence is caused by a chemical reaction. When chemiluminescence happens in an organism, it is called bioluminescence

Dieses Werk ist copyrightgeschützt und darf in keiner Form vervielfältigt werden noch an Dritte weitergegeben werden.
Es gilt nur für den persönlichen Gebrauch.

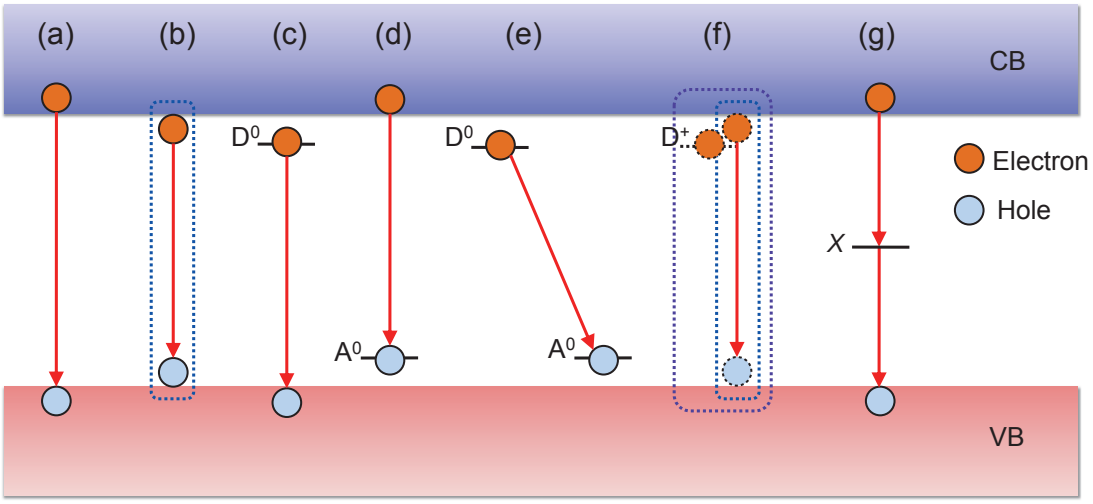

Figure 2.5: Schematic illustration of optical transitions in semiconductors.

Next, it is focused on the photoluminescence (PL), since it is the method which is employed to characterize the semiconductor structures presented in this thesis. Analyzing the PL signal provides much important information about the photo-excited material system, for example, but not limited to, impurity levels. Furthermore, the PL intensity could be the best way to check the optical efficiency as well as the material quality of a semiconductor, since it reflects the interplay between the usually desirable radiative and defect-induced non-radiative recombination.

Optical Transitions in Semiconductors

When a photon is absorbed into a semiconductor material an electron in the valence band (VB) is able to rise to an excited state –higher in energy– leaving a so-called *hole* behind. However, this photo-excited electron can undergo different processes, including thermal relaxation and energetic (optical) transitions. Optical transitions in semiconductors results in either radiative or non-radiative recombination, and can be furthermore categorized into two groups; intrinsic and extrinsic. When an electron and a hole recombine through radiative recombination, a photon is emitted and its energy is dependent on the energetic distance between these electron and hole.

If the photon energy of the excitation source is high enough, excited-electrons can reach the conduction band (CB). An excited-electron can directly drop to VB and radiatively recombine with a hole; this process is named **band-to-band** radiative transition and takes place at relatively high temperatures, Fig. 2.5(a). The band-to-band transition in indirect gap semiconductors such as GaP is called an indirect transition and it needs phonon assistance in order to keep the momentum conservation. In contrast, Direct-gap semiconductors such as GaAs do not necessarily need phonon assistance for radiative transitions.

At low temperatures, an excited electron can be united with a hole through the Coulomb attractive force arose between them. This form of an *electron-hole (e-h) pair* is usually called a **free exciton** (FE). Here, the intrinsic PL emission occurs via excitonic recombination instead of band-to-band transition–in the pure semiconductors, Fig. 2.5(b).

Dieses Werk ist copyrightgeschützt und darf in keiner Form vervielfältigt werden noch an Dritte weitergegeben werden.
Es gilt nur für den persönlichen Gebrauch.

However, if some impurities are intentionally incorporated into a semiconductor, new energy level states will be created in the energy band gap, i.e., *donor* (D) and *accepter* (A). Depending on the position of their energy levels donors and accepters are commonly classified into two types; *shallow* and *deep*. In particular, for the case of donors, the donor levels just below the CB are defined as shallow donors, while deep donors indicate the donors that have energy levels far away from the CB within the energy band gap. The extrinsic PL occurs between an electron trapped by a donor, that is, a neutral donor state D^0 and a hole at the top of VB and/or between an electron at the bottom of CB and a hole of the neutral acceptor state A^0, both possibilities are sketched in Fig. 2.5(c) and (d), respectively. Such processes are known as **free-to-bound** transitions. When both types of impurities (D^0 and A^0) are present as compensated semiconductors, **donor-acceptor pair** (DAP) recombination occurs through radiative tunneling, Fig. 2.5(e). On the other hand, in the case of extrinsic semiconductors, an FE can be captured by a neutral impurity state (D^0 or A^0), *ionized* impurity state (ionized donor D^+ or ionized acceptor A^-), or by a defect state forming a **bound exciton** (BE); Fig. 2.5(f) presents the case of a BE that is captured by a D^+. Such excitonic recombination processes become more prominent in semiconductor quantum structures, e.g., quantum wells due to the increased exciton-binding energy by quantum confinement.

In addition to impurity levels, defects in the semiconductor structure result in non-radiative centers, called also *defect centers*, deeply located in the energy band gap, shown as *X* level in Fig. 2.5(g). Indeed, such defect centers exist even in very pure materials, and they capture electrons and/or holes initially by non-radiative transitions associated by multi-phonon emission. Then the captured electrons and/or holes are charged and recombine non-radiatively with other carriers.

2.4 Band Anti-crossing Model

When an atom in a compound semiconductor is replaced with an atom of an element belonging to the same column of the periodic table, it is referred to as an *isovalent* or *isoelectronic* center. Although both atoms have the same valence, they may differ in many other aspects like a different atom size and different electronegativity. If these differences are significant, they may result in local defect potential associated with the isovalent impurities. If the electron affinity of the introduced atom is larger than that of the constituent atom, this atom becomes an electron trap, playing the role of donor, and the corresponding energy level is placed below or in resonance with the conduction band edge, i.g., N-induced localized states in dilute III-V nitride semiconductor alloys. Similarly, the introduced atom plays the role of accepter if its electron affinity is smaller than that for the constituent atom. Here, on the other hand, the isovalent energy level is placed above or in resonant with the valence band edge, such as in dilute III-V nitride bismide semiconductor alloys.

Dilute III-V nitride and/or bismide alloys are categorized under the name of highly mismatched semiconductor alloys (HMAs). The mismatching in an HMA originates from the great differences of electronegativity, size, and/or ionization energy of the constituents [5]. However, the energy band-gap of HMAs as a function of the composition shows a great bowing in

Dieses Werk ist copyrightgeschützt und darf in keiner Form vervielfältigt werden noch an Dritte weitergegeben werden.
Es gilt nur für den persönlichen Gebrauch.

comparison to the same dependence for conventional semiconductor alloys. In the following, an advanced theory used to interpret the anomalous compositional behavior of the energy band-gap of HMAs is presented.

2.4.1 Bandgap Bowing in Semiconductor Alloys

Since the band-gap energy and the lattice constant are the most important parameters of a semiconductor, the prediction of them has been a task of crucial importance for researchers. In particular, an optoelectronic device can be engineered according to the band-gap energy of based semiconductor structure(s), e.g., the functioning of an emitter or detector. In contrast, the mismatching between the lattice constants of two semiconductors constructed a structure can degrade the optical efficiency of the device due to the increasing defects, i.e., non-radiative centers.

Conventionally, both the band-gap energy and the lattice constant of a semiconductor alloy are determined from the properties of the endpoint constituent compounds. The lattice constant of an AB_xC_{1-x} semiconductor alloy consists of two compounds of similar character, AB and AC, can be extracted as follows

$$\alpha^{ABC} = x\alpha^{AB} + (1-x)\alpha^{AC} \ , \tag{2.1}$$

where x is the concentration of the component B, and α^{ABC}, α^{AB}, and α^{AC} are the lattice constants of AB_xC_{1-x}, AB, and AC, respectively. This relation, Eq. (2.1) is commonly known as Vegard's Law [27] and is the key concept of the Virtual Crystal Approximation (VCA). In the framework of VCA approach disorder effects, e.g., compositional fluctuations, are neglected. In other words, semiconductor alloy acts as a pure crystalline materials and the potential of the periodic crystal is taken as an average over the atomic potentials of the endpoint constituent compounds [28].

In contrast to the lattice constant, the band gap energy of real semiconductor alloys cannot be well estimated using a linear relation between the band gap energies of the binary compounds, AB and AC. Indeed, the band gap energy of AB_xC_{1-x} semiconductor alloy varies –with composition– between the band gap energies of the constituent compounds with some degree of bowing away from the linear trend . This dependence is commonly interpolated by the following quadratic expression [29]

$$E_g^{ABC} = xE_g^{AB} + (1-x)E_g^{AC} - bx(1-x) \ , \tag{2.2}$$

where b is the bowing parameter that represents the deviation of the energy band gap from the linear interpolation, and E_g^{ABC}, E_g^{AB}, and E_g^{AC} are the bandgap energies of AB_xC_{1-x}, AB, and AC, respectively. A successful exploitation of Eq. (2.2) is reported for $(Al_xGa_{1-x})N$ semiconductor alloys [30] as shown in Fig. 2.6(a): one can clearly see a considerable deviation of the experimental data from the theoretical zero-bowing calculation represented by the dashed line.

The bowing parameter, b is typically considered to be independent of the composition, x. However, early studies show that phenomenological Eq. (2.2) can be reproduced taking into

Dieses Werk ist copyrightgeschützt und darf in keiner Form vervielfältigt werden noch an Dritte weitergegeben werden.
Es gilt nur für den persönlichen Gebrauch.

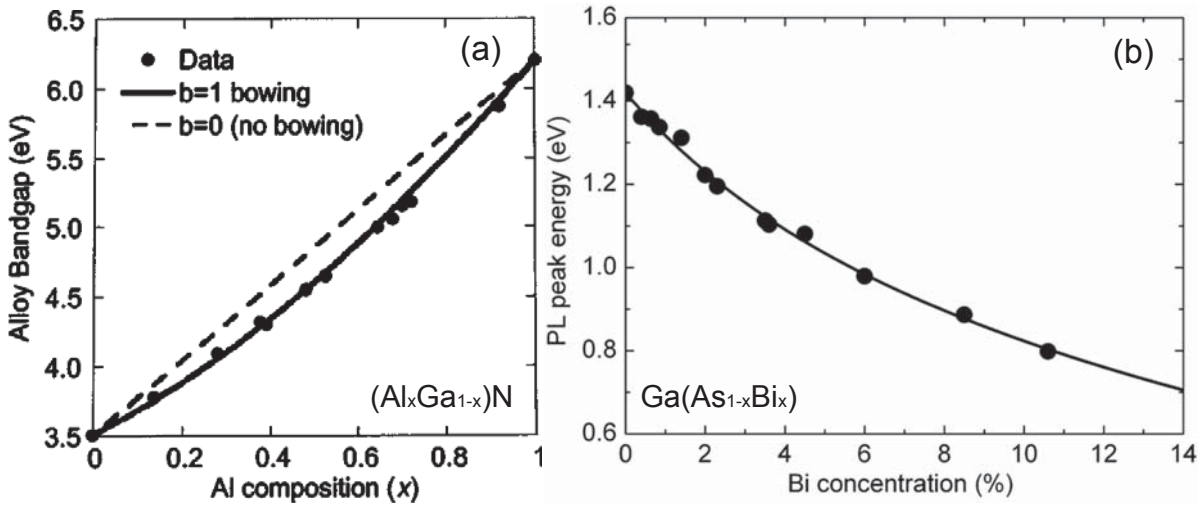

Figure 2.6: (a) composition dependence of the energy gaps for $(Al_xGa_{1-x})N$ alloys. The solid line is obtained from Eq. (2.2). The dashed line represents the case of zero bowing (after Yun *et al.* [30]). (b) experimental data for the PL peak energy as a function of Bi concentration in $Ga(As_{1-x}Bi_x)$. The solid line is a fit to the experimental data using Eq. (2.4) (after Lu *et al.* [34]).

account the disorder effects within a given semiconductor alloy [28, 31], and the bowing parameter can also be dependent on the composition [32]. In this context, it has been reported that the bowing parameter is well described by the following empirical expression [33].

$$b(x) = \frac{b_1}{1 + b_2 x} \,, \tag{2.3}$$

here b_1 and b_2 are fitting parameters. By substituting Eq. (2.3) into Eq. (2.2) the band gap energy of, e.g., Ga(AsBi) can be estimated by

$$E_g^{GaAsBi} = xE_g^{GaBi} + (1-x)E_g^{GaAs} - \frac{b_1 x(1-x)}{1 + b_2 x} \,. \tag{2.4}$$

This expression is utilized by Lu *et al.* [34] to describe the behavior of the PL peak energy of $Ga(As_{1-x}Bi_x)$ as a function of Bi content (x). Here, b_1 and b_2 are found to be 9.5 and 10.4, respectively, and $E_g^{GaBi} = -0.36$ eV was considered as a fitting parameter due to the fact that GaBi compound has never been synthesized up to now and, hence, its band gap energy is unknown. Fig. 2.6(b) shows the corresponding data.

So far the discussion has been limited to the characterization of the band-gap energy in ternary semiconductor alloys. However, the picture becomes more complicated for quaternary – or even quinary– semiconductor alloys [35, 36], since all binary and ternary constituents should be taken into account in order to provide a reasonable description of electronic and structural properties of a given quaternary alloy. E.g., in the case of $Ga(As_{1-x-y}N_xBi_y)$ semiconductor alloys presented in Ref. [37], the lattice constant of these alloys is obtained from

$$\alpha^{GaAsNBi}(x,y) = (1-x-y)\alpha^{GaAs} + x\alpha^{GaN} + y\alpha^{GaBi} \,, \tag{2.5}$$

Dieses Werk ist copyrightgeschützt und darf in keiner Form vervielfältigt werden noch an Dritte weitergegeben werden.
Es gilt nur für den persönlichen Gebrauch.

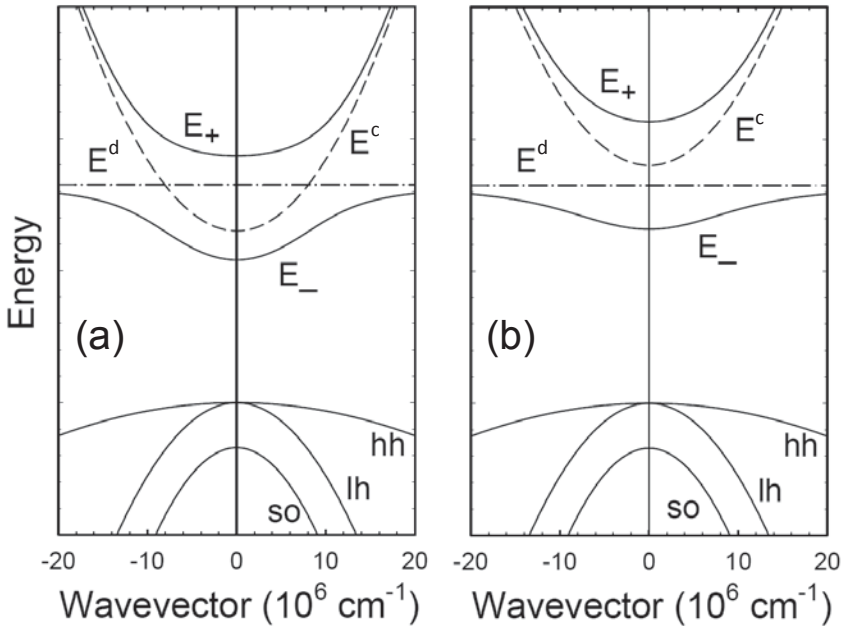

Figure 2.7: BAC model in the vicinity of the Γ point minimum: the localized impurity-related states are located (a) within or (b) below the conduction band of the host semiconductor. The solid curves are the restructured E_+ and E_- sub-bands resulting from the band anti-crossing interaction between the localized states (dash-dotted line) and the extended states of the conduction band (broken line), (after Shan *et al.* [48]).

while the band gap energy is given by

$$E_g^{GaAsNBi} = (1-x-y)E_g^{GaAs} + xE_g^{GaN} + yE_g^{GaBi} - \left[b^{GaAsN}x(1-x) + b^{GaAsBi}y(1-y) + b^{GaAsNBi}xy\right] \quad , \quad (2.6)$$

where α^{GaAs}, α^{GaN}, and α^{GaBi}, and E_g^{GaAs}, E_g^{GaN}, and E_g^{GaBi} are the lattice constants and band gap energies for GaAs, GaN, and GaBi binary compounds, respectively, while b^{GaAsN}, b^{GaAsBi}, and $b^{GaAsNBi}$ are the bowing parameters for Ga(AsN), Ga(AsBi), and Ga(AsNBi) semiconductor alloys, respectively. Theoretical calculations based on Eqs. 2.5 and 2.6 predict a promising construction, in which $y = 1.7x$, that is lattice matched GaAs, and which has a band-gap energy of 1 eV [37].

The VCA approach has been widely used to fit the energy band gap bowing of much semiconductor alloys. However, it fails to well model the composition dependence of the energy band-gap in dilute III-V nitrides and/or bismides where a relatively huge bowing parameter was extracted: $b = 16.2$ eV in the case of Ga(N_xAs_{1-x}) [38].

2.4.2 Conduction Band Anti-crossing Model

Many theoretical models have been suggested to explain the large bowing in the energy band-gap in HMAs, e.g., dilute III-V nitride and/or bismide semiconductor alloys. Wei and Zunger suggested an approach based on a composition dependent bowing parameter and resulting from

Dieses Werk ist copyrightgeschützt und darf in keiner Form vervielfältigt werden noch an Dritte weitergegeben werden.
Es gilt nur für den persönlichen Gebrauch.

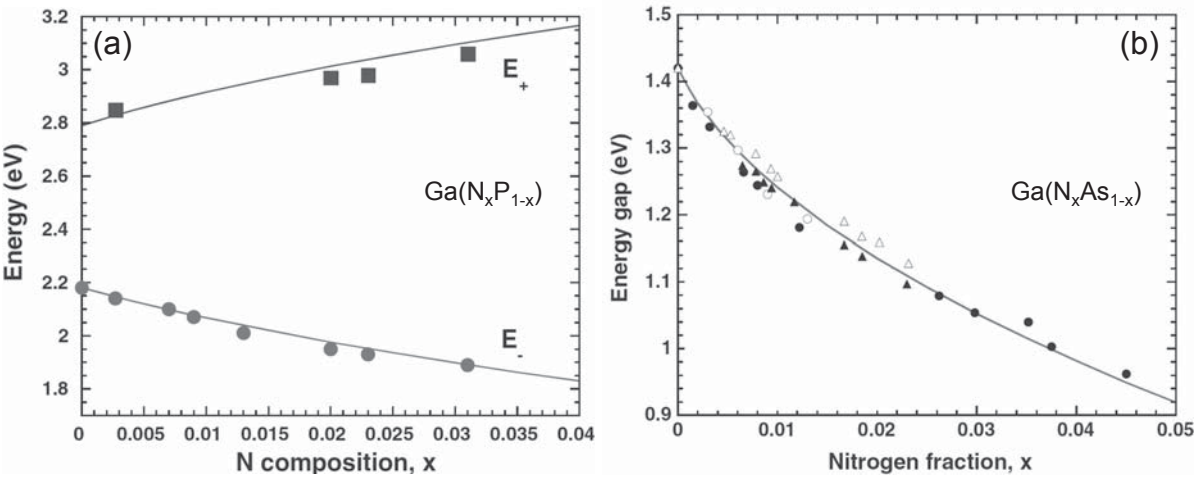

Figure 2.8: (a) energy sub-bands, E_+ and E_- as a function of N fraction for $GaP_{1-x}N_x$: the symbols are obtained from photoreflectance measurements and lines are calculated using two-band BAC model. (b) energy band-gap of Ga(NAs) vs. the N fraction. The solid line indicates the theoretical calculations based on BAC model. The symbols represent the experimentally-determined values adopted from [50] (closed circles), [51] (open circles), [52] (open triangles), and [53] (closed triangles). Both (a) and (b) are taken from Ref. [41]

local density approximation (LDA) calculations in Ga(NAs) [39]. However, the LDA model was replaced by empirical pseudopotential calculations due to some errors concerning the energy band-gap were risen by applying the LDA model [40]. In addition to the aforementioned approaches, an elegant model has been suggested to describe electronic structure of dilute III-V nitride semiconductor alloys [41, 42, 43], and later extended for the dilute III-V bismide semiconductor alloys [44, 45, 46]. This approach considers the anti-crossing interaction between the localized impurity-induced states and the delocalized states of the host semiconductor. Not surprisingly, this model is named the band anti-crossing (BAC)[3].

The BAC calculations are carried out within the many-impurity Anderson model [47] considering the simplest possible manner of a two-band anti-crossing situation [5]. In particular, a narrow resonant energy band formed by the N states strongly interacts with the energy level associated with the extended states of the conduction band of the host semiconductor's matrix. This anti-crossing interaction causes a restructuring of the conduction band of the host semiconductor, i.e., the conduction band is split into two non-parabolic sub-bands. The newly formed sub-bands have energy dispersion relations given by [42]

$$E_{\pm}(k) = \frac{1}{2}\left[\left(E^c(k) + E^d\right) \pm \sqrt{\left(E^c(k) - E^d\right)^2 + 4C^2x}\right], \tag{2.7}$$

where k is the electron wavevector, x is the N fraction, $E^c(k)$ is the energy dispersion of the lowest conduction band of the host semiconductor, E^d is the energy of the localized states derived from the substitutional N atoms, and C describes the coupling between the localized N-

[3]It is widely common to drop "conduction" from the name of this model for the case of dilute III-V nitrides, in which the conduction band anti-crossing interacts with the resonant N-impurity states.

Dieses Werk ist copyrightgeschützt und darf in keiner Form vervielfältigt werden noch an Dritte weitergegeben werden.
Es gilt nur für den persönlichen Gebrauch.

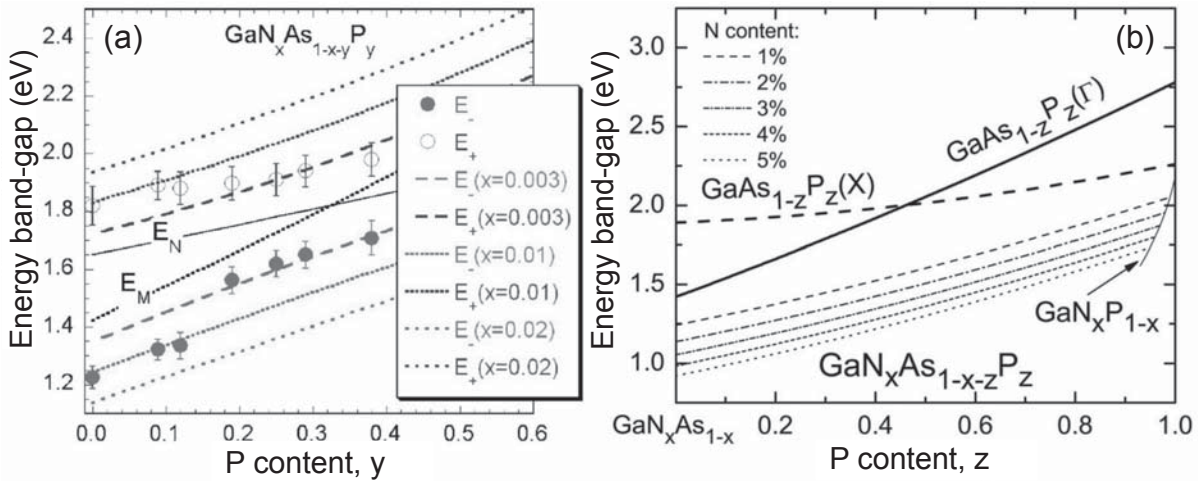

Figure 2.9: (a) measured and calculated values of lower E_- and upper E_+ conduction sub-bands in Ga(N$_x$As$_{1-x-y}$P$_y$). E_M is the energy band-gap of Ga(As1 $-$ yP$_y$) and E_N is the N energy level in Ga(N$_x$As$_{1-x-y}$P$_y$), (After Yu *et al.* [54]). (b) energy band-gaps of Ga(As$_{1-z}$P$_z$), Ga(N$_x$As$_{1-x}$), Ga(N$_x$P$_{1-x}$) and Ga(N$_x$As$_{1-x-z}$P$_z$) alloys (after Kudrawiec [55]). All values in (a) and (b) are plotted as a function of P content.

related states and the band states of the host semiconductor [41]. Furthermore, at the Brillouin zone centre, the effective mass of a dilute III-V nitride semiconductor alloy is approximated by the density-of-state electron effective mass and can be estimated by [41]

$$m_{\mathrm{e}}(x) = \frac{2m_0^e}{1 - \dfrac{E^c(0) - E^d}{\sqrt{\left(E^c(0) - E^d\right)^2 + 4C^2x}}}, \tag{2.8}$$

where m_0^e is the electron effective mass in the host semiconductor.

It is worth mentioning that the BAC model remains valid, not only if the the localized states are located within the conduction band such as in Ga(NAs) [48], but even if the localized states lie below the conduction-band edge, e.g., ZnMnOTe [49]. Theoretical predictions of the BAC model have been verified by experimental observations for different dilute III-V nitride semiconductor alloys. Two examples which demonstrate excellent agreement between the experimental results and BAC model calculations are shown in Fig. 2.8(a) and (b) for Ga(N$_x$P$_{1-x}$) and Ga(N$_x$As$_{1-x}$), respectively [41].

Ga(NAsP)

The incorporation of N atoms into Ga(AsP) alloy affects the electronic structure in similar way to their incorporation into GaAs. Consequently, the conduction band of Ga(NAsP) consists of two sub-bands (E_- and E_+) due to the anti-crossing interaction between localized N states and the conduction band of Ga(AsP). This is demonstrated by means of the photoreflectance spectra of Ga(NAsP), from which two well-resolved optical transitions are distinctly different from the energy band-gap transition of Ga(AsP) [54]. The corresponding experimental values of the

Dieses Werk ist copyrightgeschützt und darf in keiner Form vervielfältigt werden noch an Dritte weitergegeben werden.
Es gilt nur für den persönlichen Gebrauch.

energy transitions, lower E_- and upper E_+ conduction sub-bands, are shown in Fig. 2.9(a) as closed and open circles, respectively. E_M represents the energy band-gap of Ga(As$1-y$P$_y$) as a function of P content. Yu *et al.* used BAC model to characterize the electronic structure of Ga(NAsP) [54] and, on the other hand, to determine the N fraction in the studied layers. The calculated dependences of the energy transitions of Ga(N$_x$As$_{1-x-y}$P$_y$) on the P contect are plotted in Fig. 2.9(a). Here, the N content is set to x= 0.3%, 1%, and 2%, respectively. E_N indicates the N energy level in Ga(N$_x$As$_{1-x-y}$P$_y$) as a function of P content.

The BAC model is indirectly applied by Kudrawiec [55] to parameterize the energy band gap of Ga(N$_x$As$_{1-x-z}$P$_z$). In particular, the energy band gaps of both constituent ternary alloys, i.e., Ga(N$_x$As$_{1-x}$) and Ga(N$_x$P$_{1-x}$) alloys, are calculated using the BAC model,

$$E_g^{GaNAs}(x) = \frac{1}{2}\left[E_N^{GaAs} + E_g^{GaAs} - \sqrt{\left(E_N^{GaAs} - E_g^{GaAs}\right)^2 + 4\left(C^{GaNAs}\right)^2 x}\right] \tag{2.9}$$

and

$$E_g^{GaNP}(x) = \frac{1}{2}\left[E_N^{GaP} + E_g^{GaP} - \sqrt{\left(E_N^{GaP} - E_g^{GaP}\right)^2 + 4\left(C^{GaNP}\right)^2 x}\right], \tag{2.10}$$

while the energy band gap of Ga(N$_x$As$_{1-x-z}$P$_z$) is extracted using Eq. (2.2) as follows

$$E_g^{GaNAsP}(x,z) = (1-z')E_g^{GaNAs}(x) + z'E_g^{GaNP}(x) - z'(1-z')C\,, \tag{2.11}$$

where

$$z' = z + \frac{xz}{(1-x)}\,. \tag{2.12}$$

Here, E_N^{GaAs}, E_N^{GaP}, C^{GaNAs}, and C^{GaNP} are empirical parameters, and C is the bowing parameter. Both E_g^{GaAs} and E_g^{GaP} are correspond to the energy band gap of GaAs and GaP at the Γ point, respectively. Fig. 2.9(b) shows the energy band-gap of Ga(N$_x$As$_{1-x-z}$P$_z$), calculated by applying Eqs. (2.9)–(2.12), as a function of P content for different N contents, i.e., it varies between the energy band-gaps of Ga(N$_x$As$_{1-x}$) and Ga(N$_x$P$_{1-x}$). Here, the bowing parameter C is assumed to be 0.19 eV. Besides, the energy band-gap of Ga(As$_{1-z}$P$_z$) at Γ point as well as X point are presented against P content for the bowing parameters of 0.19 and 0.24 eV for Γ and X valley, respectively. The nature of the fundamental band-gap of Ga(As$_{1-z}$P$_z$) alloy changes from indirect to direct when the X valley minimum crosses below the Γ valley minimum for P content higher than 45% [55].

2.4.3 Valence Band Anti-crossing Model

Proceeding from the similarity in the trend of mismatch between N and As in Ga(NAs) as well as Bi and As in Ga(AsBi), Alberi *et al.* extended the BAC to explain the large shrinking in the energy band gap of Ga(AsBi) [45, 46]. Due to the fact that the electronegativity of Bi is lower than that for As, Bi-related impurity states are located close to the valance band of host GaAs matrix [56, 57]. Hence, in this case, instead of the conduction band, the band anti-crossing takes place between resonant Bi states and the GaAs valance band and this adapted model is consequently named as the valence band anti-crossing (VBAC) model. As a result of the

Dieses Werk ist copyrightgeschützt und darf in keiner Form vervielfältigt werden noch an Dritte weitergegeben werden.
Es gilt nur für den persönlichen Gebrauch.

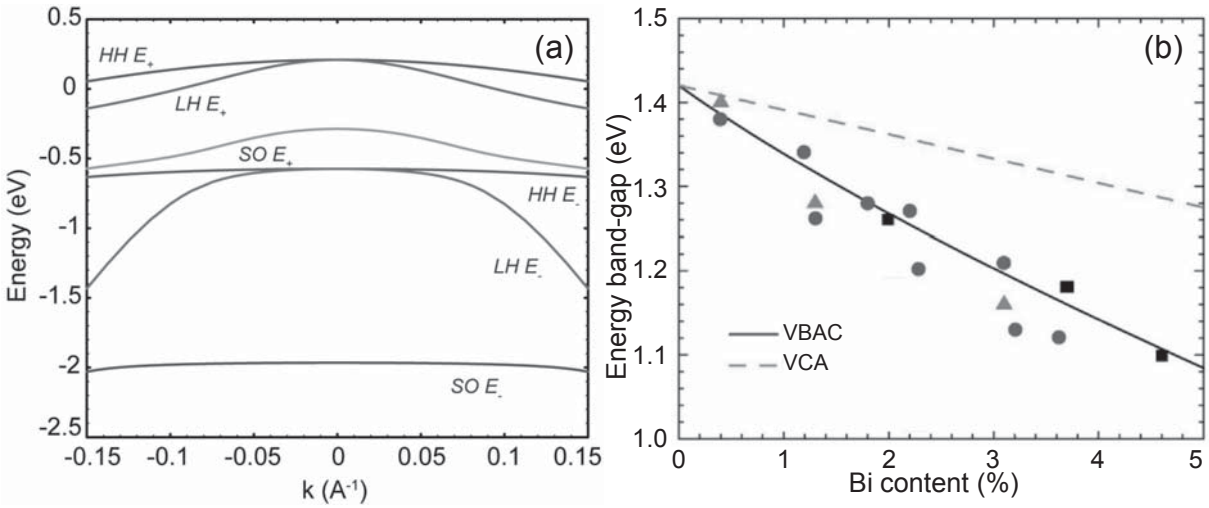

Figure 2.10: (a) dispersion relation of the $Ga(As_{0.96}Bi_{0.04})$ valence bands, consisting of the heavy hole (HH), light hole (LH), and spin-orbit split-off (SO) E_+ and E_- sub-bands, (after Alberi *et al.* [46]). (b) energy band-gap of Ga(AsBi) vs. the GaBi fraction: triangles, squares, and circles represent the experimentally-determined values which are adopted from [58], [59], and [60], respectively. The dashed and solid lines indicate the theoretical calculations based on VBAC model and VCA approach, respectively.

aforementioned coupling, the primary valence bands of GaAs split into three pairs of sub-bands as shown in Fig. 2.10(a): (E^+_{HH}, E^-_{HH}), (E^+_{LH}, E^-_{LH}) and (E^+_{SO}, E^-_{SO}) for heavy hole (HH), light hole (LH), and spin-orbit split-off (SO) bands, respectively [46].

According to the VBAC model the valence band edge is given by [44]

$$E_v^{GaAsBi}(x) = \frac{1}{2}\left[E_v^{GaA} + E_{Bi} + \sqrt{\left(E_v^{GaAs} - E_{Bi}\right)^2 + 4C_{Bi}^2 x}\right], \tag{2.13}$$

and the expression of the electron effective mass given in Ref. [41], Eq. (2.8), can be consequently modified for the hole effective mass in Ga(AsBi) as follows

$$m_h(x) = \frac{2m_0^h}{1 + \dfrac{E_v^{GaAs} - E_{Bi}}{\sqrt{\left(E_v^{GaAs} - E_{Bi}\right)^2 + 4C_{Bi}^2 x}}}, \tag{2.14}$$

where x is the Bi fraction, E_{Bi} is the energy level of embedded Bi atom measured from the valence band edge E_v^{GaAs} of GaAs, C_{Bi} is the coupling constant, and m_0^h is the effective mass of heavy holes in GaAs.

Fig. 2.10(b) shows some experimentally-reported values of the energy band gap of Ga(AsBi) adopted from Refs. [58, 59, 60] as a function of Bi content. Theoretical calculations of the energy band-gap of Ga(AsBi) based on VBAC model and VCA approach (Eq. (2.2)) are also presented as solid and dashed line, respectively in Fig. 2.10(b). While the experimental data show a large deviation from VCA results, they can be reasonably fitted to the theoretical curve obtained based on VBAC model for $E_{Bi} = -0.4$ eV and $C_{Bi} = 1.55$ eV.

Dieses Werk ist copyrightgeschützt und darf in keiner Form vervielfältigt werden noch an Dritte weitergegeben werden.
Es gilt nur für den persönlichen Gebrauch.

3 Experimental Procedure

In this chapter, the different elements composing the experimental setup for time-resolved photoluminescence spectroscopy used in this work are described in detail in Section. 3.1. Besides, the fundamental concepts of the operating principle of the streak camera are also included. The experimental setup employed to perform continuous-wave photoluminescence measurements, presented in Sction 5.5.2, is introduced in Section. 3.2. A brief overview of semiconductor structures studied in this work is given in the last part of this chapter, Section 3.3.

3.1 Time-Resolved Photoluminescence Spectroscopy

Fig. 3.1 shows a schematic drawing of the experimental setup used for time-resolved photoluminescence (TRPL) measurements presented within this thesis. A pulsed laser is used to excite the samples. The spectrally as well as temporally resolved detection of the PL signal is obtained by by the combination of a spectrometer and an ultrafast streak camera. The PL signal is ultimately recorded by a charge-coupled device (known as a CCD camera) and processed by computer software. In the following a detailed description of these steps is given.

3.1.1 Excitation Source

The excitation source for the TRPL setup is a laser system consisting of a compact titanium-doped sapphire (Ti:sapphire) mode-locked oscillator[1], pumped by an intracavity frequency-doubled neodymium-doped yttrium aluminum garnet (Nd:YAG) laser[2] operating in a continuous wave (CW) mode with a center wavelength of 532 nm and a maximum output power of 11 W.

The key component of the laser is the Ti:sapphire crystal. This crystal is produced by introducing Ti_2O_3 into a melt of Al_2O_3. Consequently, a boule of material is grown from this melt where a small fraction of Al^{3+} ions are replaced with Ti^{3+} ions. The latter ions are responsible for the lasing action of the gain medium, i.e., Ti:sapphire crystal. The Ti:sapphire laser can operate in either CW or pulsed mode and, on the other hand, its emission wavelength can be continuously tuned from 670 nm to greater than 1000 nm. This broad range of wavelengths results from the fluorescence transitions from the lower vibrational levels of the excited state to the upper vibrational levels of the ground state of the Ti^{3+} ion. Fig. 3.2(a) shows the absorption and emission spectra of Ti^{3+} in the Ti:sapphire crystal. The pulsed operation of the Ti:sapphire

[1] Spectra-Physics, Tsunami
[2] Spectra-Physics, Milennia Pro

Dieses Werk ist copyrightgeschützt und darf in keiner Form vervielfältigt werden noch an Dritte weitergegeben werden.
Es gilt nur für den persönlichen Gebrauch.

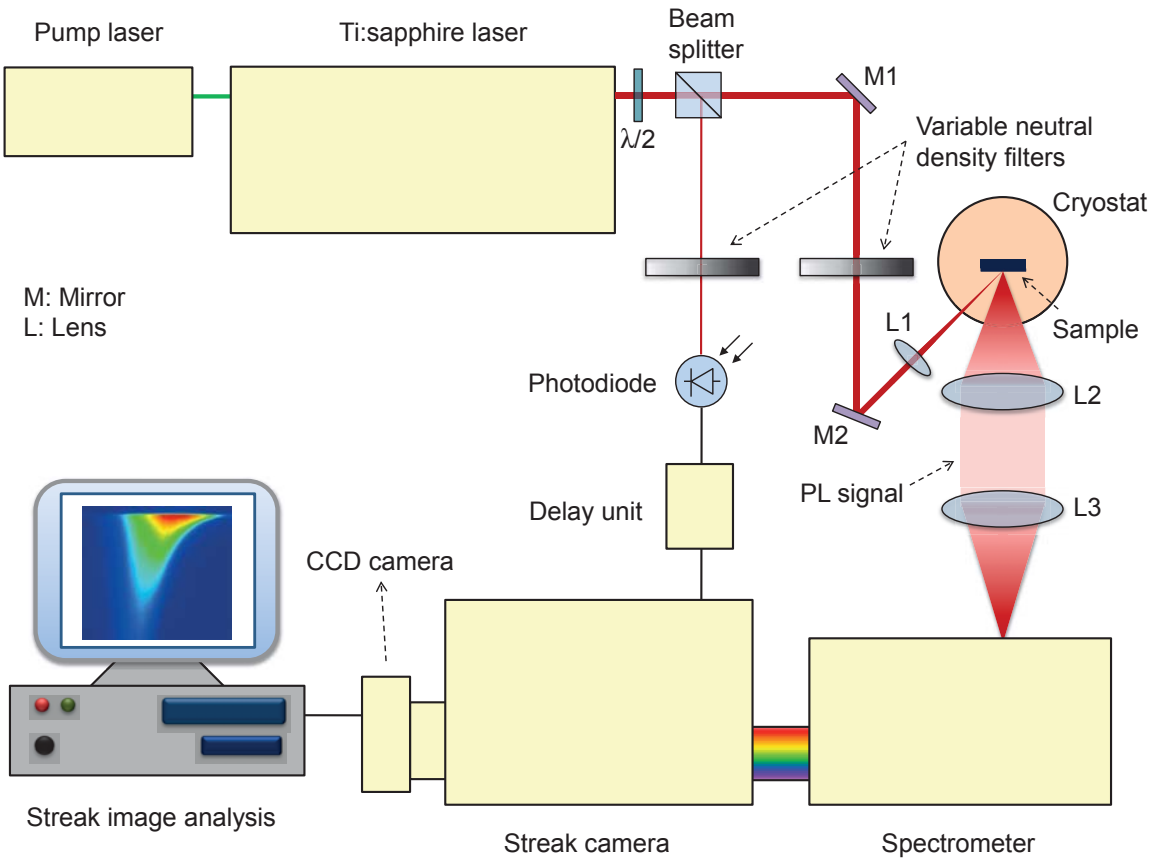

Figure 3.1: Schematic overview of the experimental setup used for time-resolved photoluminescence measurements.

laser is based on the Kerr effect inside the Ti:sapphire crystal, i.e., the intensity-dependent, nonlinear refractive index of the Ti:sapphire crystal. The wavelength tuning and the width of the laser pulse are controlled by adjustment of optical components of the laser cavity, including, in particular, a birefringent optical filter and prism pairs.

For all TRPL measurements in the present work, the laser operates in a pulsed mode with a pulse width of 100 fs and a repetition rate of 80 MHz, corresponding to a separation of 12.5 ns between each two consecutive pulses. The laser's emission wavelength is tuned between 760 nm and 800 nm with an average output power as high as 2.1 W.

3.1.2 Photoluminescence Signal

The laser beam of the Ti:Sapphire laser is split into two arms using a beam splitter: one is led to a photodiode as it will be explored in the next Section 3.1.3 and the other arm is used to excite the samples. A $\lambda/2$-wavelength-plate is applied before the beam splitter to adjust the distribution of the laser power between the two laser arms. In addition, variable neutral density filters are used to attenuate the power of the excitation beam for specific requirements of an experiment.

For all TRPL measurements presented in this work, the laser beam is focused on the sample down to a spot size of $\sim$30 μm in diameter. The samples are mounted at the end of a cold finger

Dieses Werk ist copyrightgeschützt und darf in keiner Form vervielfältigt werden noch an Dritte weitergegeben werden.
Es gilt nur für den persönlichen Gebrauch.

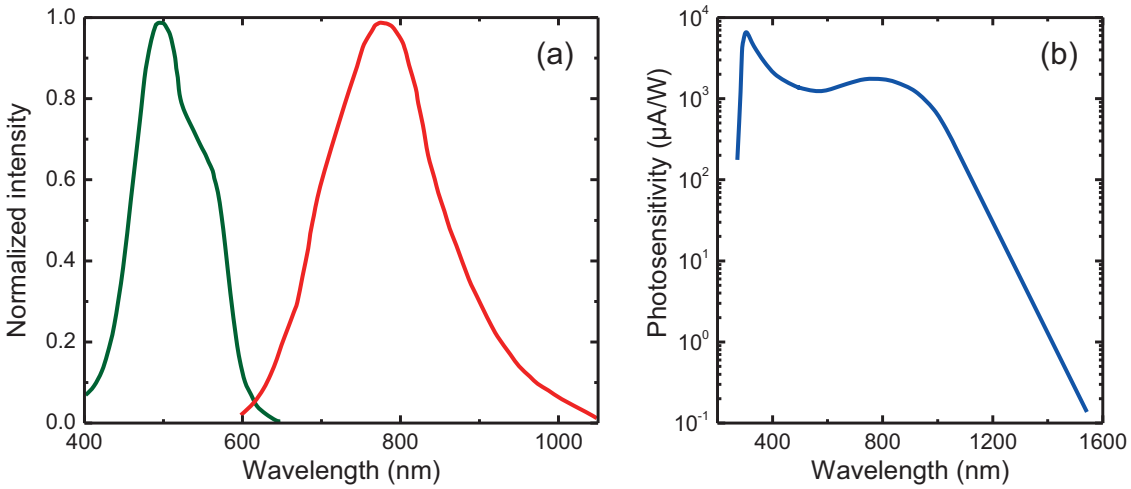

Figure 3.2: (a) absorption (green) and emission (red) spectra of Ti^{3+} ions in Ti:sapphire crystal. (b) photosensitivity of the used streak camera.

fixed inside a liquid-helium-flow microscopy-cryostat[3]. A temperature-sensor is also integrated inside the cryostat and directly connected to the temperature controller[4]. The latter is also united with a suction pump[5] used to suck up the helium that flows through the cryostat. Subsequently, the samples' temperature is adjusted between 10 K and 300 K by controlling both the sample heating and the helium flow. Furthermore, the samples are kept under a dynamic vacuum as low as 10^{-5}–10^{-6} mbar using a vacuum pump[6] in order to avoid condensation forming on the surface of the samples.

If the photon energy of the Ti:Sapphire laser is similar to or larger than the band gap of the investigated sample, each pulse of the excitation beam is absorbed in the sample and, thus, an excited state is created. Immediately thereafter, the system relaxes emitting an optical radiation, i.e., the PL signal. The PL signal emitted by a sample is collected normal to the sample surface in reflection geometry, collimated by a set of two lenses (collecting lenses), and then focused onto the entrance slit of a grating spectrometer.

Each of the lenses, i.e, laser focusing lens (L1 in Fig. 3.1) and the collecting lenses (L2 and L3 in Fig. 3.1), as well as the cryostat is mounted on a manually actuated XYZ stage to ensure precise positioning and focusing, and in order to minimize and restrict the effect of the sample-drift on the detected PL signal. This drift can take place when the temperature is changed (increased or decreased) during temperature-dependent measurements.

[3]Cryo Vac
[4]Cryo Vac, model TIC 304–MA
[5]Vacuubrand, diaphragm vacuum pump, model ME 4
[6]Pfeiffer Vacuum Technology AG, turbo pump, model TC600

Dieses Werk ist copyrightgeschützt und darf in keiner Form vervielfältigt werden noch an Dritte weitergegeben werden.
Es gilt nur für den persönlichen Gebrauch.

3.1.3 Detection System

The detection system is a combination of a spectrometer[7] and a streak camera[8]. This combination enables one to obtain simultaneously spectral and temporal information of the detected PL signal. Furthermore, a high-stability delay unit[9] is used to adjust the delay times of trigger signal derived from the pulsed laser via an ultrafast photodiode. The streak camera as well as the delay unit together with the spectrometer are operated using the HPD-TA (Temporal Analyzer) software developed by Hamamatsu.

Depending on the chosen grating and the slit widths of the spectrometer, the maximal spectral resolution of the measured PL signal in the TRPL setup is about 0.1 nm for a grating of 600 grooves/nm. However, a grating of 30 grooves/nm is used for all TRPL measurements presented in this work, corresponding with a spectral resolution of $\sim$1 nm. The employed streak camera can be operated in 4 different time ranges of 157, 820, 1540 and 2280 ps. The temporal resolution varies between 2 ps and 10 ps, according to the used time range of the detection-windows, i.e, the dimensions of the streak camera image.

The detection system is limited by two factors. One is the spectral sensitivity of the photocathode: the higher the detected wavelength, the lower is the response of the photocathode, as shown in Fig. 3.2(b) for the employed streak camera in this work. The second limitation of the detection system is due to trigger jitter, which affects significantly the temporal resolution.

3.1.3.1 Streak Camera Operation Principle

A streak camera is an ultra fast detector used to record extremely-short-time light-emission phenomena, e.g., photo-excited carriers in semiconductors, with a very high temporal resolution. The key component of the streak camera is an electron tube that is called “streak tube”. Fig. 3.3 shows the operating principle of the streak camera, considering a detected pulsed PL signal consists of four components, which have different optical intensities and slightly vary in terms of both time and space (wavelength or energy).

After the incident PL signal is spectrally dispersed by a grating spectrometer, its participating pulses pass through the entrance slit of the streak camera and are then conducted by optics into a slit image on the photocathode in the front of the streak camera tube. Here, incoming photons on the photocathode are converted into electrons due to the photoelectric effect. The number of generated electrons is proportional to the intensity of the incident light signal. Consequently, these four pulses are sequentially converted into electrons. Inside the tube the electrons are accelerated and conducted towards a micro-channel plate (MCP). During the travel of these accelerated electrons between the sweep electrodes a high voltage is applied, resulting in a high-speed sweep of the electrons from top to bottom. On the other hand, since the electrons are created at different times, corresponding to the different arrival time of the photons of the spectrally dispersed PL signal, they are therefore deflected vertically in slightly different angles. It should be noted that the synchronization between this sweep and the trigger signal is

[7] Bruker, model 25015
[8] Hamamatsu, model C 5680
[9] Hamamatsu, model C 6878

Dieses Werk ist copyrightgeschützt und darf in keiner Form vervielfältigt werden noch an Dritte weitergegeben werden.
Es gilt nur für den persönlichen Gebrauch.

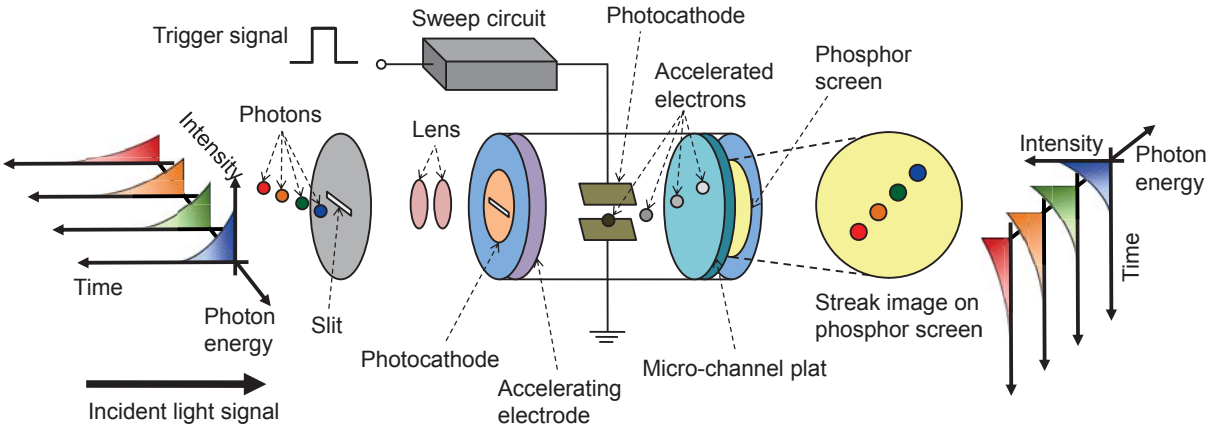

Figure 3.3: Operation principle of a streak camera, figuratively assuming that the detected PL signal consists of four pulses that have different optical intensities and slightly vary in terms of both time and energy.

secured using a delay unit connected to a photodiode which is hit by the excitation pulsed laser. At the end of their travel inside the streak tube, the accelerated electrons are multiplied several thousands of times through the MCP. The amplified electrons are converted back into photons, i.e., an optical signal, on a phosphor-screen, which is recorded at the end of the device by a high-sensitive CCD camera[10]. The brightness of the fluorescence image is in direct proportion to the intensities of incident photons of the measured PL signal. The fluorescence image corresponding to the photons which were earliest to arrive are placed in the uppermost position of the phosphor screen, followed by the other images being arranged in sequentially descending order from top to bottom. Hence, the perpendicular direction on the phosphor screen serves as the time axis. Ultimately, the detected PL signal is stored and can be plotted and processed on a computer as a 3D image using an appropriate software.

3.1.3.2 Streak Image Analysis

As above mentioned, the HPD-TA program is used to control the detection system and to automate the entire measurement procedure. This program is also developed to read out images from the Hamamatsu streak camera's phosphor screen. A streak camera image delivers intensity vs. time vs. position (wavelength or energy) information of the detected signal, cf. Fig. 3.4(d). Fig. 3.4(a) shows the PL signal from a Ga(AsBi)/GaAs single quantum well just to give an example for a typical streak camera image. While the horizontal axis represents the photon energy, the vertical one is for the time. On the other hand, the intensity is false-color coded where blue and red colors correspond to low and high intensities, respectively.

In order to improve the quality of the streak image the detected PL signal is usually integrated for relatively long time with respect, of course, to the sensitivity of the phosphor screen. Furthermore, HPD-TA program allows to automatically record a PL signal many times and digitally accumulate them. Consequently, a streak image, as shown in Fig. 3.4(a), is an average

[10]Hamamatsu, model C 4742-95

Dieses Werk ist copyrightgeschützt und darf in keiner Form vervielfältigt werden noch an Dritte weitergegeben werden.
Es gilt nur für den persönlichen Gebrauch.

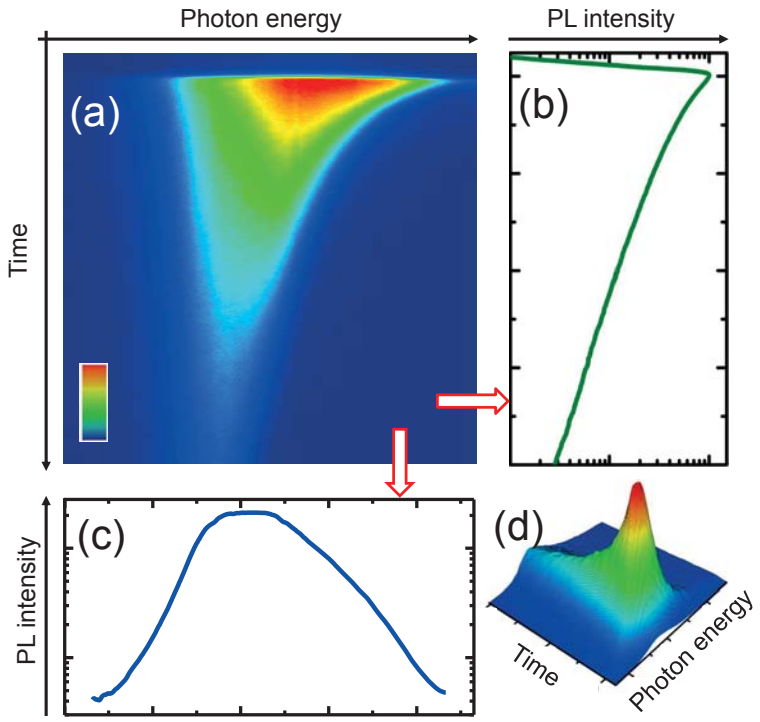

Figure 3.4: (a) an example of a PL image obtained with the streak camera. (b) PL spectra and (c) corresponding PL transients are extracted from the streak image by the integration of whole temporal intervals and spectral traces, respectively. (d) three-dimensional representation of a streak camera image.

of the recorded shots of the PL signal. This process helps to reduce excitation-independent optical signals inevitably included in the streak image. However, these excitation-independent background radiations need to be subtracted for yielding reliable data. This is achieved using a "LabView 8.0" code.

Ultimately, the acquired data are processed employing "Origin 9.0" software. PL transients for a desired wavelength range can be obtained by integrating across corresponding columns in a streak image, i.e. spectral traces. In contrast, integrating temporal intervals across rows in a streak image results in time-resolved PL spectra. The PL spectra and corresponding PL transients for the streak image presented in Fig. 3.4(a) are extracted by the integration of temporal intervals and spectral traces and shown in Figs. 3.4(b) and 3.4(c), respectively.

3.2 Continuous-Wave Photoluminescence Spectroscopy

Besides the TRPL setup, a standard continuous-wave PL (CWPL) setup is employed to characterize PL spectra of Ga(AsBi) single quantum well's, which are presented in Chapter 5. Fig. 3.5 shows a schematic drawing of the experimental setup used for CWPL measurements. Instead of the Ti:Sapphire laser used for the TRPL setup as an excitation source, a CW helium-neon

Dieses Werk ist copyrightgeschützt und darf in keiner Form vervielfältigt werden noch an Dritte weitergegeben werden.
Es gilt nur für den persönlichen Gebrauch.

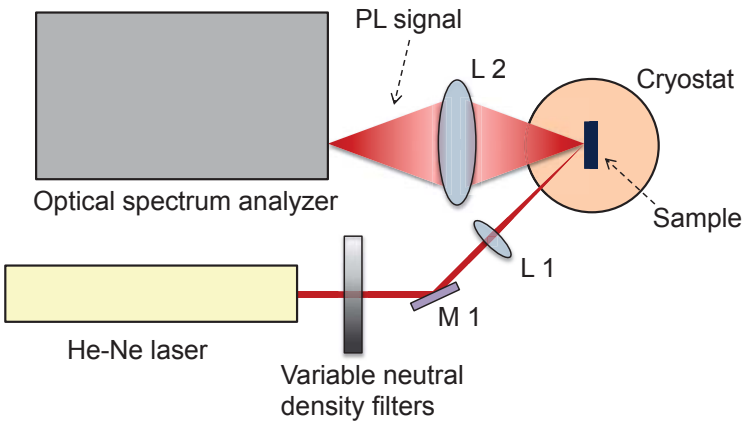

Figure 3.5: Schematic overview of the experimental setup used for time-resolved photoluminescence measurements.

(He:Ne) laser is employed to excite studied sample for CWPL experiments. The laser operates at 632.8 nm.

Alike to the TRPL measurements the samples are mounted on a holder inside a liquid-helium-flow microscopy-cryostat and kept under a very low dynamic vacuum. The PL signal is detected using a spectrometer with an integrated detector and a data processing unit, which is called optical spectrum analyzer[11] (OSA). Using the OSA, a PL signal can be plotted as a function of the wavelength with a maximal spectral resolution of 0.05 nm. The sensitivity of the OSA ranges from 330 to 1700 nm.

3.3 Samples Description

This section presents the important growth parameters used for growing the nanostructures evaluated in this work. The emphasis of this thesis is on two different semiconductor materials, i.e., dilute nitride Ga(NAsP) and dilute bismide Ga(AsBi). The Ga(NAsP)/GaP multiple quantum wells (MQWs) and the Ga(AsBi)/GaAs heterostructures were grown by the workgroup of Dr. Wolfgang Stolz and Prof. Dr. Kerstin Volz in the department of physics and material sciences center at Philipps-University of Marburg. The Ga(AsBi)/GaAs single quantum well's (SQW's) were grown by the workgroup of Prof. Dr. Thomas Tiedje in the department of physics and astronomy at University of British Columbia.

3.3.1 Ga(NAsP)/GaP Multi Quantum Wells

Three Ga(NAsP)/GaP triple QW structures with varying N and As content and almost similar well widths were grown on (001)-oriented GaP substrate by metal organic vapor phase epitaxy (MOVPE). The epitaxial growth was realised in a commercially available horizontal reactor system with gas flow rotation (AIX 200-GFR-reactor) using hydrogen carrier gas at low reactor

[11] YOKOGAWA, model AQ-6315A

Dieses Werk ist copyrightgeschützt und darf in keiner Form vervielfältigt werden noch an Dritte weitergegeben werden.
Es gilt nur für den persönlichen Gebrauch.

Table 3.1: Composition and layer thickness of the Ga(NAsP)/GaP MQWs.

Sample	N content (%)	P content (%)	As content (%)	QW width (nm)
23381	3	5	92	5.6
23384	4	6	90	6.7
23385	2	14	84	5.6
23386	4	7	89	5.4

pressure of 50 mbars. A detailed description of the growth technique and the growth conditions can be found in Ref. [61]. The Ga(NAsP) QWs were grown pseudomorphically between 100 nm GaP barriers.

High-resolution X-ray diffraction measurements were performed to determine both P and N contents within the QWs. By reducing the P content with increasing N content the macroscopic mismatch is kept around 2.5%–2.6% compressive mismatch in both layer compositions, which was verified by XRD measurements [62]. The well widths were estimated by taking the mean width observed in transmission electron microscopy (TEM), with a fluctuation of ± 1 nm. An example of TEM images on these samples is presented in Fig. 2.3. An overview of the composition and thickness of the Ga(NAsP) layers is given in Table 3.1.

3.3.2 Ga(AsBi)/GaAs Single Quantum Well

A set of Ga(AsBi) SQW's with different Bi contents were grown on a semi-insulating GaAs(100) substrate in a VG V80H solid source molecular beam epitaxy (MBE) system at a growth rate of $\sim$1 nm/min. The Bi concentration was controlled by monitoring the As flux, Bi flux, and growth temperature. The growth technique and the growth conditions are described in Ref. [34].

The structural quality was confirmed using high-resolution X-ray diffraction; these experiments include full dynamical simulations, and are independently corroborated the expected QW thicknesses and Bi contents. All samples consist of a 300 nm GaAs buffer layer, followed by a QW layer and a 20 nm GaAs cap layer. The growth parameters are summarized in Table 3.2.

Table 3.2: Growth parameters of Ga(AsBi)/GaAs SQW's.

Sample	Substrate temperature (°C)	As flux (10^{-8} mbar)	Bi flux (10^{-8} mbar)	Bi content (%)	QW width (nm)
r2016	365	14	1.70	1.1	12
r2048	280	25	1.70	6.0	14
r2049	320	25	1.70	5.5	12
r2074	300	11	0.42	2.1	13

Dieses Werk ist copyrightgeschützt und darf in keiner Form vervielfältigt werden noch an Dritte weitergegeben werden.
Es gilt nur für den persönlichen Gebrauch.

Table 3.3: Bi content and layer thickness of the Ga(AsBi)/GaAs heterostructures.

Sample	Bi content (%)	Ga(AsBi) layer thickness (nm)
17215	3.2	59
17221	2.9	60
17222	4.2	34
17225	4.5	25

3.3.3 Ga(AsBi)/GaAs Heterostructures

A series of Ga(AsBi)/GaAs heterostructures with Bi different contents were grown by MOVPE on undoped exact (001) GaAs substrates. The growth was taken place in a commercially available horizontal reactor system with gas flow rotation (AIX 200-GFR-reactor) at a reduced reactor pressure of 50 mbar using Pd purified H_2 as carrier gas and triethylgallium (TEGa), tertiarybutylarsine (TBAs) and trimethylbismuth (TMBi) as precursors. The TEGa partial pressure for the Ga(AsBi) growth was 0.042 mbar at a V/III ratio of 1.1 and a TMBi/V ratio of 0.034. The growth temperature was set to 400 °C. Further information on the growth technique and the growth conditions can be found in Ref. [63] The Bi fraction and layer thickness, which were determined using high resolution x-ray diffraction $\omega - 2\theta$ scans around the (004) reflection peak of GaAs, are summarized in Table 3.3 . All samples are deposited on a 250-nm-thick-GaAs buffer layer and capped by a 20-nm-thick-GaAs layer, both were grown at 625 °C.

Dieses Werk ist copyrightgeschützt und darf in keiner Form vervielfältigt werden noch an Dritte weitergegeben werden.
Es gilt nur für den persönlichen Gebrauch.

4 Photoluminescence of Disordered Semiconductors

4.1 Introduction

The shed light on dilute nitride III-V semiconductors was started with a dream to cover the electromagnetic spectrum range from the ultraviolet to the infrared using only one material; this magical structure was GaAsN. The supposed scenario was that the band-gap energy of GaAsN alloys can be adjusted by controlling the incorporated amount of nitrogen. Consequently, one can achieve a variation of the band-gap energy between 1.42 eV (GaAs) and 3.4 eV (GaN) [64]. However, unlike what was foreseeable, an unexpected reduction in the band-gap energy is observed for GaAsN, e.g., the incorporation of 1% of N into GaAs reduces the band-gap energy by about 180 meV [65]. This strong shrinking in the band-gap energy is typically explained by a conduction-band anti-crossing model [42], based on the interaction between the conduction band of GaAs and resonant localized N states [43]. In a similar way, the incorporation of Bi atoms into the GaAs lattice leads to a significant decrease in the band-gap energy as high as ∼62–84 meV/%Bi [58, 66, 67]. In this case, a velance-band anti-crossing model, based on the interaction between the valance band of GaAs and resonant localized Bi states is used for the interpretation of the behavior of the electronic structure [45]. Besides ternary, dilute nitride and/or bismide III-V quaternary semiconductors such as Ga(NAsBi) [68], (GaIn)(AsBi) [69], (AlGa)(NAs) [70] and Ga(NAsP) [71], have also attracted increasing attention during the last two decades in the scientific community due to their unusual physical properties and their potential for long-wavelength optoelectronic applications.

Despite the advantage of a shrinking in the band-gap energy, the introduction of a small amount of a V-element to a III-V host structure results in an increase in the disorder potential due to the differences, e.g., in size and electronegativity between the incorporated and substituted anions [5, 6]. Several reasons that contribute to (or increase) the disorder potential in semiconductors are discussed in Section 2.2. The presence of disorder effects within a semiconductor can significantly influence its electronic structure, i.e., the density of localized states (DOS) is increased [72]. Disorder-induced localized states drastically affect carrier recombination processes in semiconductors. The changes in carrier dynamics can be revealed by investigating, e.g., electrical and optical properties of disordered semiconductors [14]. In this context, photoluminescence (PL) spectroscopy is widely used for the characterization of disorder in semiconductors.

This chapter deals with most prominent PL characteristics of disordered semiconductors. A qualitative description of the disorder-related PL features is also introduced. It will be especially

Dieses Werk ist copyrightgeschützt und darf in keiner Form vervielfältigt werden noch an Dritte weitergegeben werden.
Es gilt nur für den persönlichen Gebrauch.

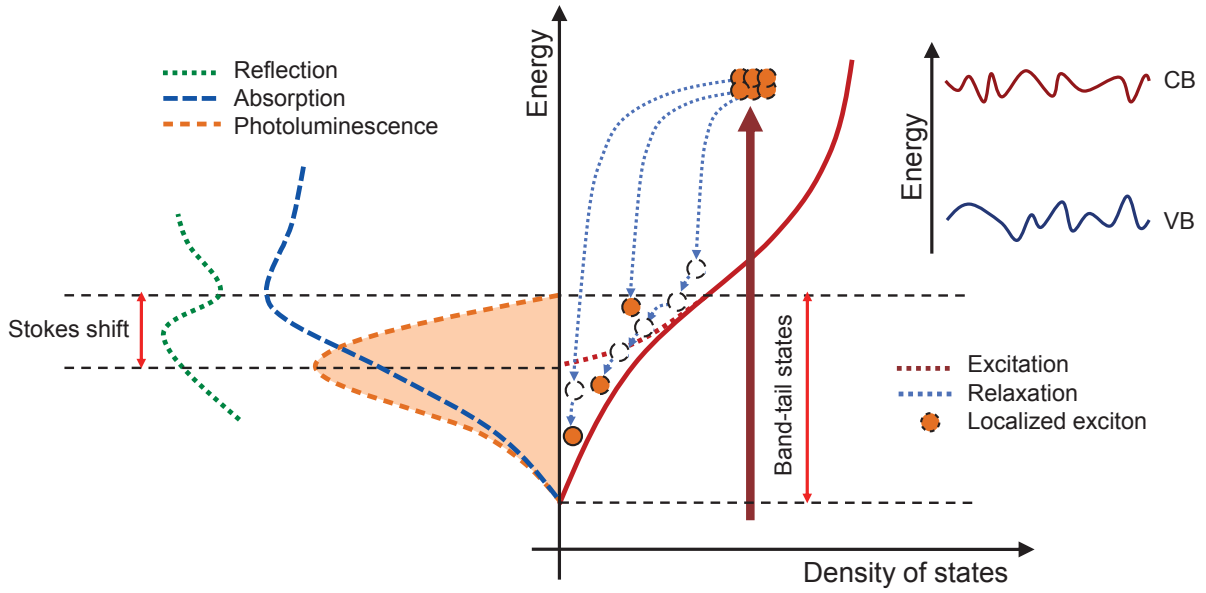

Figure 4.1: Schematic illustration of excitation-dependent exciton dynamics in a typical disordered semiconductor. The top-right inset shows the fluctuation in the edges of the conduction band (CB) and the valence band (VB) due to disorder effects.

focused, through this chapter, on the PL emission from disordered Ga(NAsP) and Ga(AsBi) nanostructures. The chapter begins with a brief description of the origin of the Stokes shift, given in Section 4.2. In Section 4.3, the impact of the excitation intensity on both the spectral shape and the temporal dynamics of the PL emission at very low temperatures as well as room temperature is presented. Different aspects of the temperature dependence of the PL emission are discussed in Section 4.4. Besides, the effect of the filling of localized states on the temperature-dependent disorder-induced PL characteristics is discussed. The distribution of PL decay times depending on the PL emission energy is described in Section 4.5. Then, a detailed study on carrier dynamics and localization effects in Ga(AsBi)/GaAs SQW's with different Bi content is presented in Section 4.6. Here, the influence of the Bi content on some PL features is described. Furthermore, the thermal evolution of carrier recombination mechanisms is discussed. Finally, Section 4.7 summarizes the results of this chapter.

4.2 Stokes Shift

Under relatively low excitation conditions, an energy red-shift between the absorption peak and the corresponding PL emission peak is widely observed in disordered semiconductors, such as dilute III-V bismides [73] as well as nitrides [74]. This phenomenon is named Stokes[1]-shift and can be described –in the case of disordered semiconductors– in terms of carrier dynamics, as illustrated in Fig. 4.1, with respect to the band-gap theory in semiconductors. In particular, photo-excited excitons relax towards energetically lowest states, so-called band-tail states [76, 77, 78, 79]. The latter reflects the fluctuations in energy band edges due to disorder effects (cf.

[1]This phenomenon had been reported for the first time by G. G. Stokes in 1852 [75].

Dieses Werk ist copyrightgeschützt und darf in keiner Form vervielfältigt werden noch an Dritte weitergegeben werden.
Es gilt nur für den persönlichen Gebrauch.

the inset of Fig. 4.1). While a fraction of these excitons can directly reach deep band-tail states, the rest emigrate downward in energy across shallow band-tail states performing some phonon-assisted tunnelling transitions [80]. The band-tail states are commonly known also as disorder-induced localized states. It has been assumed that localized excitons can hop between localized states before their recombination with respect to the exciton lifetime [81]. Ultimately, the PL spectrum arises from all contributing radiative recombination of localized states. However, the exciton lifetime has some distribution depending on the exciton energy [82]. This will be discussed in Section 4.5.

Since the nature of disorder is differs from semiconductor structure to semiconductor structure, the value of the Stokes shift is also different. While a Stokes shift of 300 meV has been obtained for Ga(AsBi) at 5 K [83], it was reported to be about 60 meV for Ga(NAsP) at 10 K [84]. Furthermore, the Stokes shift depends on the temperature as well as the excitation intensity. Under sufficiently low excitation conditions, the temperature-dependent Stokes shift shows some character that is fruitfully utilized to quantify the disorder in semiconductors, as it will be presented in Section 5.4. On the other hand, the Stokes shift becomes less apparent when the excitation intensity is increased due to the gradual filling of localized states, which are limited in number [85]. Yet, to some extent, the Stokes shift vanishes when the PL emission is mainly dominated by the recombination of band-to-band transitions.

4.3 Excitation Dependence

The excitation dependence of the PL spectrum of a Ga(AsBi)/GaAs single quantum well (SQW) at a temperature of 11 K is presented in the first part of this section. The second sub-section deals with the excitation-dependent PL peak energy as well as PL linewidth for a Ga(NAsP)/GaP-multiple-QWs-(MQWs) sample, which are measured at room temperature (RT). The discussion of the impact of the excitation intensity on both the PL intensity and the PL decay time at RT is postponed to Section 4.6.2.

4.3.1 Low Temperatures

Figs. 4.2(a_1) and 4.2(a_2) show the experimental results of PL spectra and corresponding normalized PL transients, respectively, for a Ga(AsBi)/GaAs SQW, which are measured over a wide range of excitation intensities at a lattice temperature of 11 K. In the case of very low excitation intensities, the PL emission peak is asymmetric and shows a characteristic low-energy flank of the PL spectrum. An exponential shape of the low-energy side of the low-temperature PL spectrum is suggested by Karcher *et al.* for disordered Ga(NAsP) semiconductors [84], which results from the recombination of electron-hole pairs trapped in localized states with an exponential energy-distribution. However, a Gaussian distribution of the localized states is proposed by Imhof *et al.* and extrapolated from the Gaussian-shaped low energy tail of the linear absorption spectrum of a Ga(AsBi) structure [86].

When the excitation intensity is increased the PL energy peak exhibits a blue-shift and, furthermore, additional signatures appear at the high energy shoulder of the PL spectrum, indicat-

Dieses Werk ist copyrightgeschützt und darf in keiner Form vervielfältigt werden noch an Dritte weitergegeben werden.
Es gilt nur für den persönlichen Gebrauch.

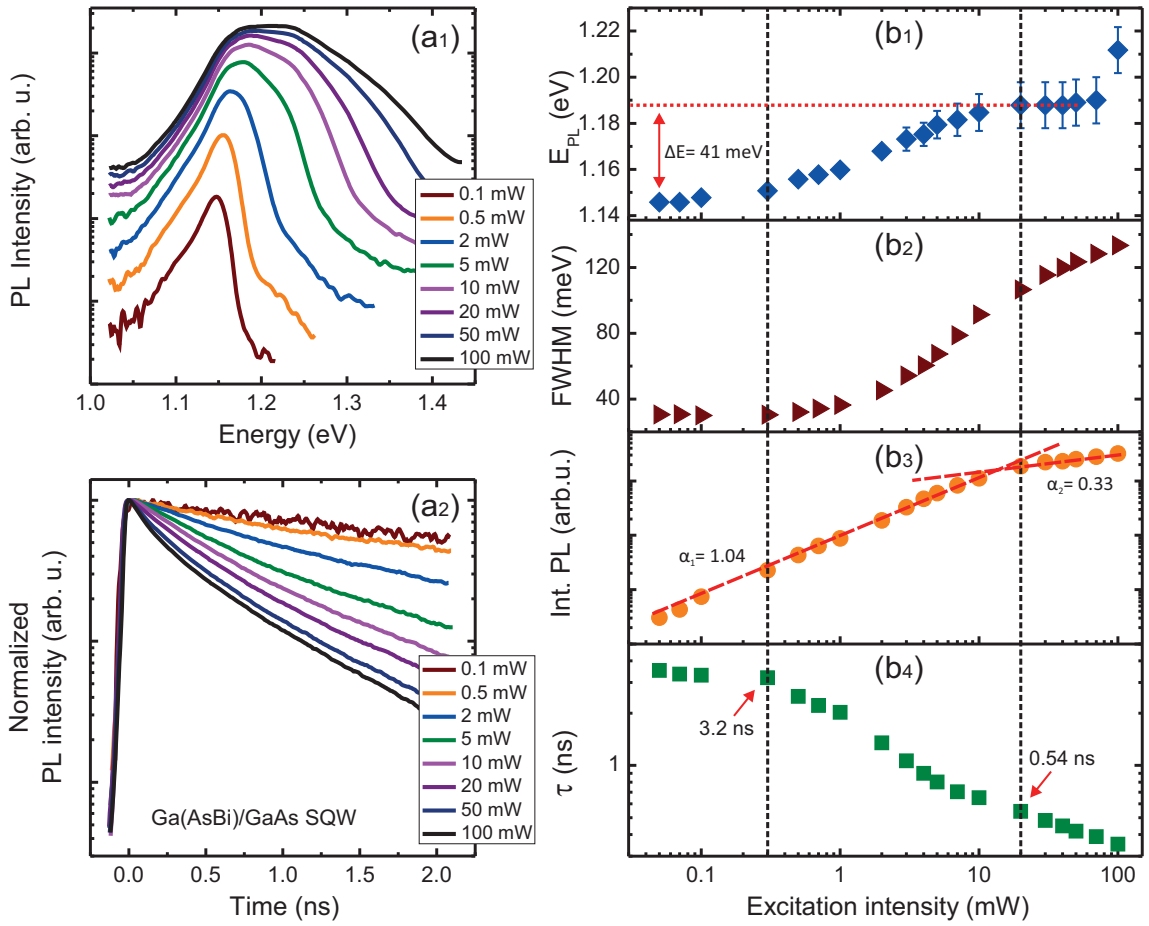

Figure 4.2: (a_1) PL spectra and (a_2) normalized corresponding PL transients of a Ga(AsBi)/GaAs SQW with Bi content of 5.5%, measured for various values of the excitation intensity at 11 K. Excitation intensity dependence of (b_1) PL peak energy, (b_2) PL FWHM, (b_3) integrated PL intensity, and (b_4) PL decay time (τ) at 11 K. The red dashed lines in (b_3) are fits generated from the power-law relation, Eq. (4.1), between the integrated PL intensity and the excitation intensity.

ing higher confined states of the studied quantum well [87]. Besides, the PL decay is observed to be slow at low excitation conditions and becomes increasingly faster for higher excitation intensities.

For further analysis of these experimental observations, the PL peak energy (E_{PL}), the PL linewidth (FWHM: full width at half maximum), the integrated PL intensity, and the PL decay time are plotted each as a function of excitation intensity in Figs. 4.2(b_1)–4.2(b_4), respectively. Here, the integrated PL intensity (I_{PL}) as a function of excitation intensity (I_{Exc}) is analyzed using a power-law with the following general form [88]:

$$I_{PL} \propto I_{Exc}^{\alpha}\,, \tag{4.1}$$

where α is the exponential factor. The red dashed lines in Fig. 4.2(b_3) refer to fits using Eq. (4.1). The experimental results, represented of the right-hand side of Fig. 4.2, can be clearly distinguished in three major regimes, shown by vertical short-dashed black lines, as follows:

Dieses Werk ist copyrightgeschützt und darf in keiner Form vervielfältigt werden noch an Dritte weitergegeben werden.
Es gilt nur für den persönlichen Gebrauch.

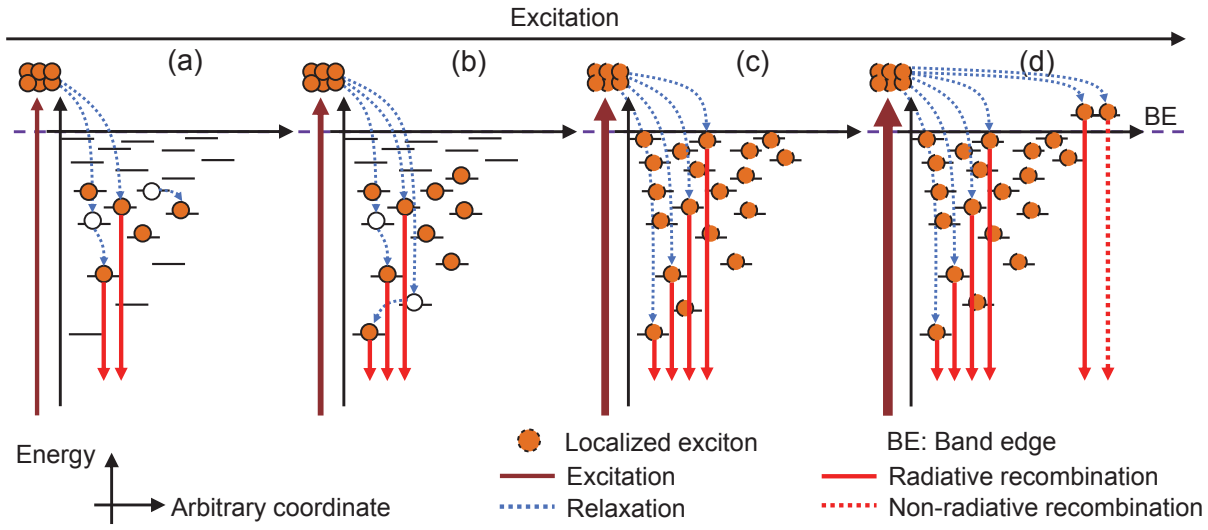

Figure 4.3: Schematic illustrations of excitation-dependent exciton dynamics in a typical disordered semiconductor.

At very low excitation intensities: the PL peak energy, the PL FWHM, and the PL decay time are almost constant while the PL emission intensity increases linearly with the excitation intensity (α_1= 1.04). This behavior can be understood respecting the excitation's finite lifetime. In particular, when the excited excitons relax downward in energy, they can be trapped in localized states or rather perform hopping transitions between these states before their radiatively decay [84], Fig. 4.3(a). The decay time is therefore understood as an average recombination time of these two possibilities.

When the excitation intensity is increased further: the PL peak energy strongly blueshifts (ΔE_{PL}= 41 meV), i.e., it shifts towards higher energies, and the PL FWHM increases strikingly. On the other hand, while the integrated PL intensity continues its linear increase, the PL decay time decreases when the excitation intensity is increased. These observations can be attributed to the gradual filling of the localized states [89], Fig. 4.3(b). In particular, the excitons can reach the deepest localized states through hopping processes, when energetically-middle-laying localized states are mainly filled. It should be noted that the presence of higher quantum states of the QW further contributes to the broadening of the PL spectrum.

Under high excitation conditions: the localized states are saturated due to their finite number [85], Fig. 4.3(c). This is reflected by rather no impact of the excitation intensity on the PL peak energy, i.e., the PL emission exhibits a maximum at 1.18 eV for the excitation range from 20 to 70 mW. However, the PL maximum shifts abruptly to 1.22 eV for the excitation intensity of 100 mW, as the second confined state of the QW becomes the dominant emission source. On the other hand, the decay time decreases with the excitation intensity. This is attributed to an increasing contribution of capture processes into defect states as the excitons become delocalized and, thus, more mobile, Fig. 4.3(d). Also, a contribution from Auger recombination [90] and/or heating effects [73] are possible. This interpretation is supported by the sub-linear dependence of the PL intensity on the excitation intensity (α_2= 0.33).

Dieses Werk ist copyrightgeschützt und darf in keiner Form vervielfältigt werden noch an Dritte weitergegeben werden.
Es gilt nur für den persönlichen Gebrauch.

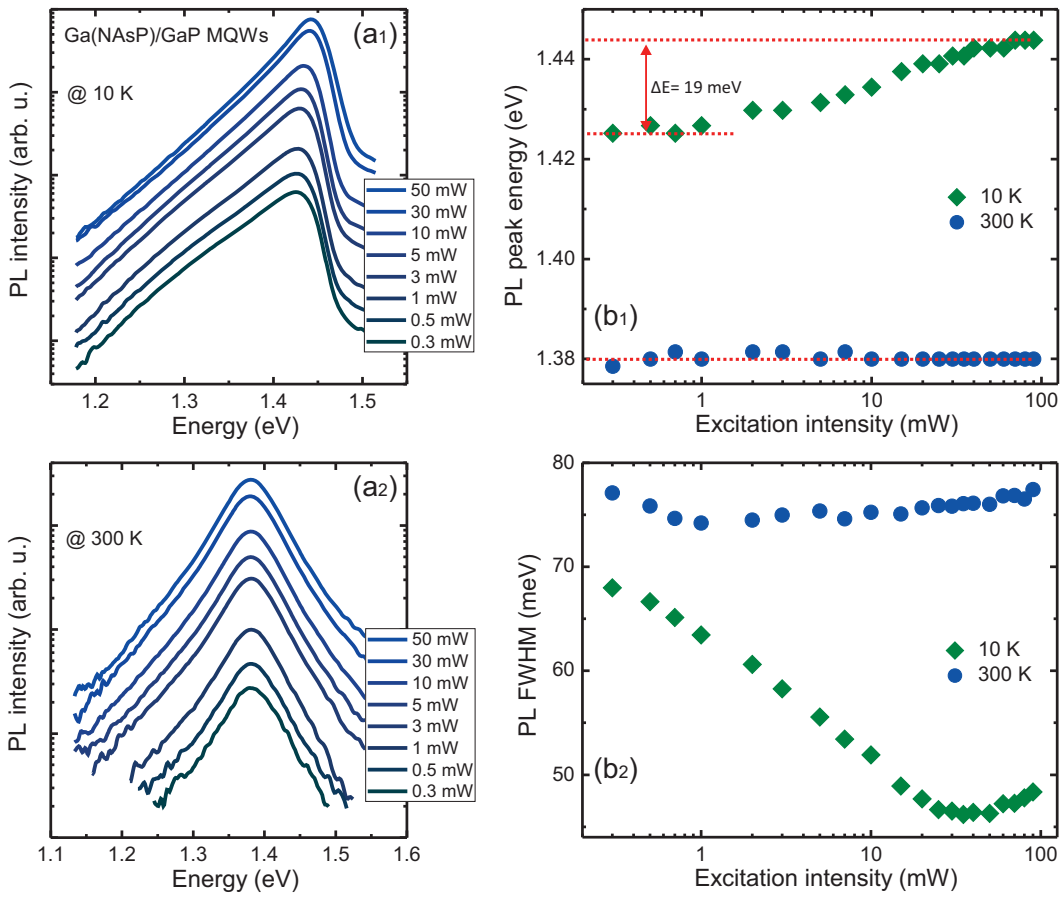

Figure 4.4: Excitation-dependent PL spectra of a Ga(NAsP)/GaP-MQWs sample with an N content of 3% measured at (a_1) 10 K and (a_2) 300 K. The corresponding (b_1) PL peak energy as well as (b_2) PL FWHM are plotted against the excitation intensity.

4.3.2 Room Temperature

Figs. 4.4(a_1) and 4.4(a_2) show the excitation-dependent PL spectra of a Ga(NAsP)/GaP-MQWs-sample, measured at 10 K and RT of 300 K, respectively. The corresponding PL peak energy and PL FWHM are presented in Figs. 4.4(b_1) and 4.4(b_2), respectively. While the PL peak energy blue-shifts by about 19 meV when the excitation intensity is increased from 0.3 to 70 mW and is close to 1.44 eV for higher intensities, it becomes excitation-independent at 300 K. The excitation-dependent behavior of the PL peak energy at low temperatures is above discussed. However, at RT, the excitons are mainly delocalized and the PL emission results form band-to-band transitions. Hence, the nearly constant value of the PL peak energy in Fig. 4.4(b_1) represents the fundamental energy band-gap energy of the studied structure at RT.

In contrast, the PL FWHM first decreases significantly when the excitation intensity is increased up to 35 mW at 10 K and then increases with a lesser extent by further increase of the excitation intensity. The excitation-dependent PL FWHM at 300 K does similarly to this at 10 K, but less pronounced. Indeed, the PL FWHM shows an excitation-independent behavior with a slight trend to increase as the excitation intensity is increased above 1 mW; it varies between 74 meV and 77 meV. A similar behavior of the excitation-dependent PL FWHM is

Dieses Werk ist copyrightgeschützt und darf in keiner Form vervielfältigt werden noch an Dritte weitergegeben werden.
Es gilt nur für den persönlichen Gebrauch.

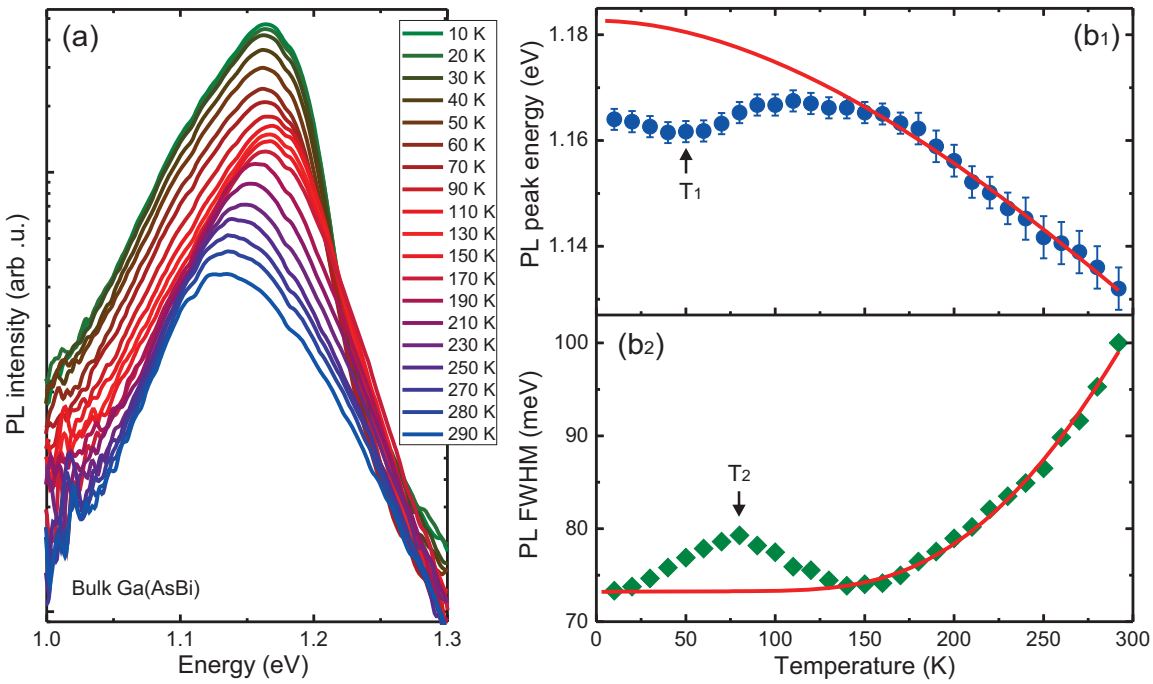

Figure 4.5: Temperature-dependent (a) PL spectra, (b_1) PL peak energy, and (b_2) PL FWHM of a bulk Ga(AsBi) sample with Bi content of 4.5%. The red solid curves in (b_1) and (b_2) are obtained from Eq. (4.2) and Eq. (4.3), respectively.

observed for (InGa)N/GaN MQWs [91]. The initial decrease of the PL FWHM is attributed to Coulomb screening of the quantum-confined Stark effect (QCSE) [92]. The latter results from the internal electric field. However, the QCSE weakens when the excitation intensity, i.e., the number of photo-generated excitons, is increased [93]. The later increase of the PL FWHM can be ascribed to band-filling effects. Besides, the weakening of Coulomb screening of the QCSE can also contribute to the observed blue-shift of the excitation-dependent PL peak energy.

4.4 Temperature Dependence

In this section the temperature-evolution of PL spectra in disordered semiconductors will be presented. First, the temperature dependence of the PL peak energy and the PL linewidth for bulk Ga(AsBi) layers is described. Then, the filling effect of localized states on the aforementioned dependences are discussed for Ga(NAsP)/GaP MQWs. The PL thermal quenching in different disordered semiconductors is shown in the second part of this section. Besides, the impact of the excitation intensity on the temperature-dependent PL intensity and the corresponding PL decay time is clarified for Ga(AsBi)/GaAs SQW's.

4.4.1 S-Shape Behavior

Fig. 4.5(a) shows PL spectra of a bulk Ga(AsBi) sample, measured at an excitation intensity of 1 mW and various temperatures in a range from 10 K up to 290 K. The PL corresponding peak

Dieses Werk ist copyrightgeschützt und darf in keiner Form vervielfältigt werden noch an Dritte weitergegeben werden.
Es gilt nur für den persönlichen Gebrauch.

energy and the PL FWHM are plotted as a function of temperature in Figs. 4.5(b_1) and 4.5(b_2), respectively. The red solid curves in Figs. 4.5(b_1) and 4.5(b_2) represent the temperature dependence of the PL peak energy and the PL FWHM, respectively, for a typical ordered semiconductor. The temperature-dependent behavior of the PL peak energy as well as the PL FWHM for studied Ga(AsBi) sample deviates obviously from that for typical ordered semiconductors. In particular, the PL peak energy as a function of temperature shows a local minimum around T_1= 50 K, i.e., the PL peak energy initially decreases (red-shift), then increases (blue-shift), and ultimately decreases (red-shift). This non-monotonic temperature-evolution of the PL peak energy is so-called S-shape behavior [94, 95]. Simultaneously, the temperature-dependent PL FWHM shows a local maximum of about 80 meV placed around T_2= 80 K. The aforementioned peculiar behaviors of the temperature-dependent PL peak energy and the PL FWHM are widely observed in disordered semiconductors such as Ga(NAsP)/GaP MQWs [71], Ga(NAs)/GaAs MQWs [76], (InGa)N/GaN MQWs [94], (InGa)As/InP SQW's [96], (GaIn)(NAs)/GaAs SQW [97], and (GaIn)(NP) alloys [98].

The disorder-induced temperature-dependent PL features can be interpreted assuming that localized excitons hop between localized states via phonon-assisted tunneling at low temperature regime [81]. In addition to this, an excited exciton is able to reach a far away localized state performing several hopping processes that must inescapable include some hops to states higher in energy. The latter transitions are probable only at relatively higher temperatures. In particular, at very low temperatures, the PL emission arises primarily from the recombination of excited excitons which are trapped by localized states in the energy band-tail, as illuminated in Fig. 4.6(a). Here, an exciton can only hop to localized states at the same level (or lower) in energy. On the other hand, the excitons do not reach the very deepest localized states; not because of their incapability to hop to states lower in energy but due to their incapability to hop to states higher in energy. However, with increasing temperature, excitons become mobile and able to hop between localized states upward in energy, overcome local potential barriers, and are thus able to reach localized states that are even lower in energy, Fig. 4.6(b). This results in an initial red-shift of the temperature-dependent PL energy peak. When the temperature is further increased, excitons' hopping transitions upward in energy are so frequent that many excitons do no relax downward in energy rapidly enough before the radiative recombination takes place, Fig. 4.6(c). As a consequence, the temperature-dependent PL energy peak exhibits a blue-shift. In the middle range of temperatures, Fig. 4.6(d), the excitons become more and more delocalized and the PL peak energy shifts toward higher energies because of the thermal depopulation of the band-tail states [78].

For even higher temperatures the majority of excitons are delocalized and, hence, PL spectra are dominated primarily by the recombination of those excitons. As a result, the PL peak energy ultimately exhibits a pronounced red-shift, following the typical temperature-induced decrease of the band-gap energy due to the increase of the interatomic spacing with increasing temperature. The latter is typically described by the well-known Varshni's empirical formula [99],

$$E_g(T) = E_0 - \frac{\alpha T^2}{T + \beta}, \tag{4.2}$$

where E_0 denotes the band-gap energy at zero temperature, and α and β are material-specific constants.

Dieses Werk ist copyrightgeschützt und darf in keiner Form vervielfältigt werden noch an Dritte weitergegeben werden.
Es gilt nur für den persönlichen Gebrauch.

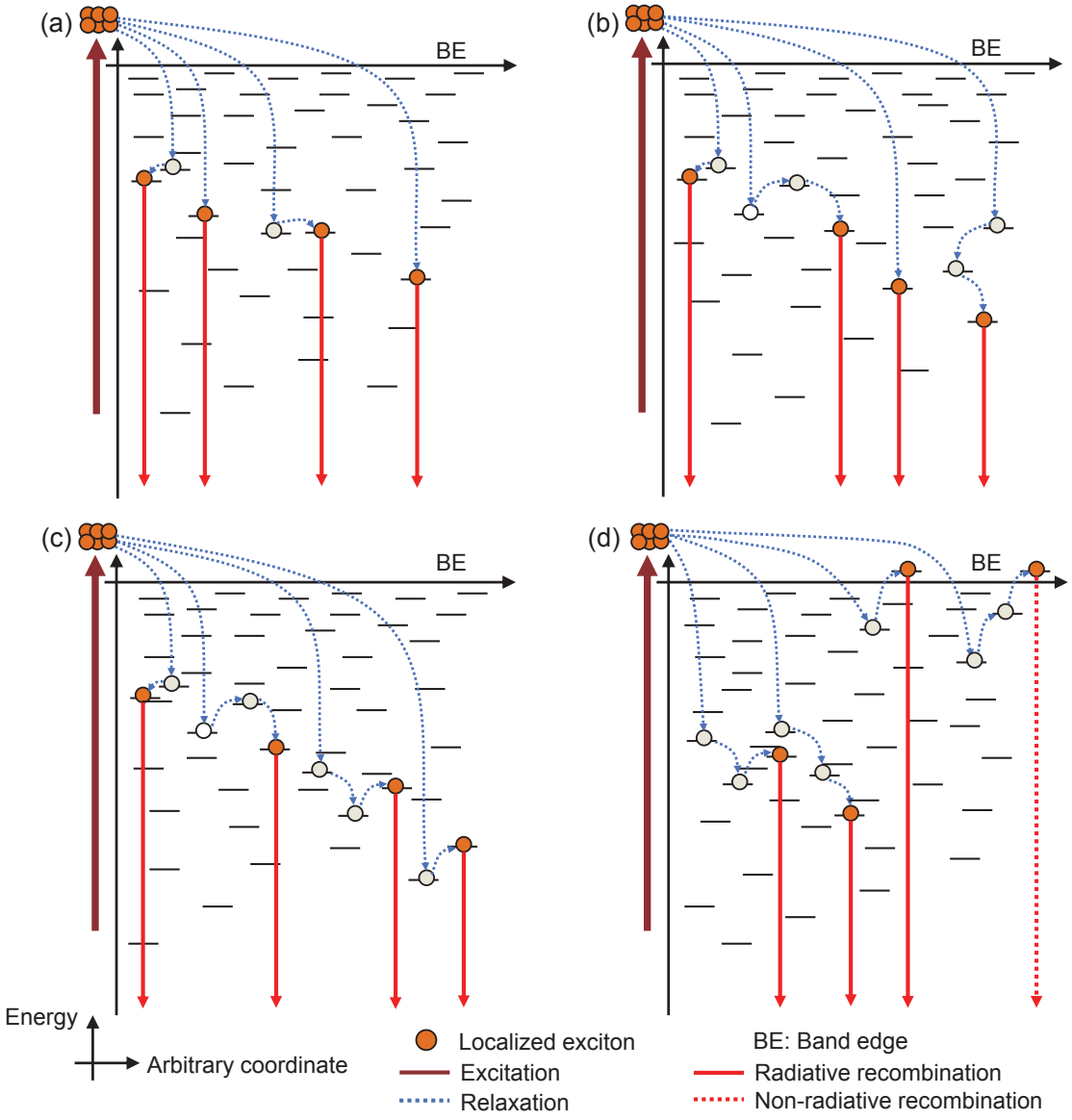

Figure 4.6: Schematic illustrations of temperature-dependent exciton dynamics in a typical disordered semiconductor.

The abrupt broadening, i.e., the rapid increase from 10 K to 80 K, of the PL FWHM is imputed to the increase in the carrier mobility with the temperature, where localized excitons recombine from a broader energy distribution of the localized states than in the case of lower temperature [96]. The shrinking of the PL FWHM between 80 and 140 K is due to the declined role of hopping transitions of localized excitons at the expense of the thermalization effect [78, 100]. The PL FWHM increases thereafter, reflecting the thermal broadening of the carrier distribution [78]. The temperature-evolution of the PL FWHM (Γ(T)) in a typical ordered semiconductor –in the presented case for the temperature range from 150 K to 290 K– can be described by the following phenomenological expression [101, 102]:

$$\Gamma(T) = \Gamma_0 + \Gamma_a T + \frac{\Gamma_{LO}}{exp(\frac{\hbar\omega_{LO}}{k_B T}) - 1}, \tag{4.3}$$

Dieses Werk ist copyrightgeschützt und darf in keiner Form vervielfältigt werden noch an Dritte weitergegeben werden.
Es gilt nur für den persönlichen Gebrauch.

where, Γ_0 is the inhomogeneous PL broadening which mainly results from the contribution of disorder, i.e., impurities, crystal imperfections. Γ_a and Γ_{LO} are coupling strengths of carriers to acoustic and LO phonons, respectively. k_B is the Boltzmann constant, and $\hbar\omega_{LO}$ is the LO phonon energy. The red solid curves in Figs. 4.5(b_1) and 4.5(b_2)) represent fit-results obtained from Eq. (4.2)[E_0= 1.183 eV,α= 48.8 meV/K , and β=524 K] and Eq. (4.3) [Γ_0= 73 meV, Γ_a= 2.38 μeV/K, Γ_{LO}= 835.4 meV, and $\hbar\omega_{LO}$= 88.7 meV] for the temperature-dependent PL peak energy and PL FWHM, respectively.

In addition to the above-mentioned qualitative explanation for both presented disorder-induced temperature-dependent PL features, a quantitative description for them is given in the next chapter.

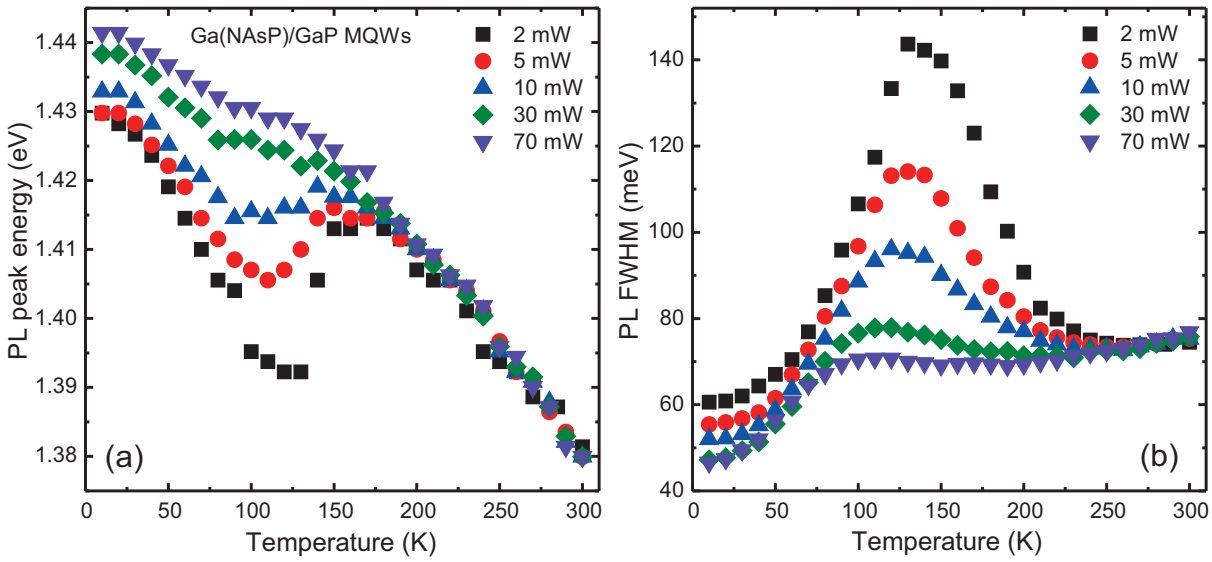

Figure 4.7: (a) the PL peak energy and (b) the PL FWHM as a function of temperature for a Ga(NAsP)/GaP MQWs-sample with an N content of 3%, measured for various excitation intensities.

Filling of Disorder-induced Localized States

The excitation-evolution of the temperature-dependent PL peak energy of a Ga(NAsP)/GaP MQWs-sample is displayed in Fig. 4.7(a). Here, the excitation intensity is varied between 2 and 70 mW, while the temperature is increased from 10 K up to 300 K. All sets of experimental data show the above-mentioned S-shape behavior. However, this feature becomes obviously less visible when the excitation intensity is increased. In other words, the degree of low-temperature blueshift of the PL peak energy as a function of temperature decreases with increasing excitation intensity. A similar behavior has been reported for (GaIn)(NAs) SQW's [103]. In contrast, as it can be seen in Fig. 4.7(b), the position and the value of the local maximum in the PL FWHM as a function of temperature shifts towards lower values with increasing excitation intensity: while it is about 144 meV at 100 K for 2 mW, it drops to about 71 meV at 130 K for 70 mW.

These aforementioned observations can be attributed to the gradual weakening of the role of disorder, since disorder-induced localized states are limited in number and ever more filled with

Dieses Werk ist copyrightgeschützt und darf in keiner Form vervielfältigt werden noch an Dritte weitergegeben werden.
Es gilt nur für den persönlichen Gebrauch.

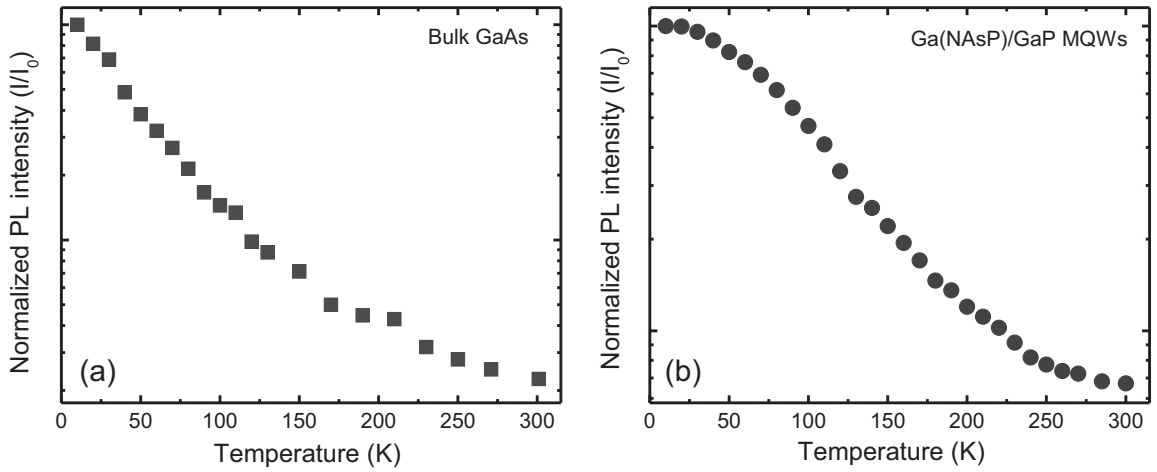

Figure 4.8: PL thermal quenching in (a) a GaAs bulk structure (after Prutskij *et al.* [104]) and (b) a Ga(NAsP)/GaP MQWs-sample with an N content of 3%, both were measured under relatively low excitation conditions. The experimental data in (a) as well as (b) is normalized to the PL intensity (I_0) obtained at zero-temperature.

increasing excitation intensity [85]. However, the continued appearance of disorder-induced PL features at even relatively high excitation intensities reflects the strong carrier localization in the presented structure.

4.4.2 Photoluminescence Thermal Quenching

The PL thermal quenching, i.e., the temperature-induced decrease of the PL intensity, in typical ordered semiconductors such as GaAs is presented in Fig. 4.8(a). The PL intensity gradually decreases when the temperature is increased. However, the decline rate of the PL intensity is lower at high temperatures. A dissimilar behavior of the temperature-dependent PL intensity is observed in disordered semiconductors such as GaNAsP/GaP MQWs (Fig. 4.8(b)). In particular, a relatively weak thermal quenching of the PL is observed at low temperatures. This is followed by a dramatic decrease of the PL intensity in an intermediate range of temperature (50 K–230 K). For higher temperatures, the PL intensity shows a slow decline and saturates close to RT. This abnormal behavior has been reported for Ga(AsBi) in the case of relatively high excitation conditions [86]. However, the PL thermal quenching in the aforementioned material (bulk as well as SQW) displays remarkably a different behavior under relatively low excitation intensities [105, 106]. The squares in Fig. 4.9(b) represent the temperature-dependent PL intensity of a Ga(AsBi)/GaAs SQW measured at an excitation intensity of 0.7 mW. Here, the PL intensity decreases when the temperature is increased, then shows a weak thermal quenching in an intermediate temperature range (55 K–115 K), and ultimately continues its decrease up to RT.

In order to gain further insight into the origin of such unexpected behavior of temperature-dependent PL intensity in disordered semiconductors, a study of the impact of the excitation intensity on the shape of the PL thermal quenching is performed. Figs. 4.9(a) and 4.9(b) show the temperature dependence of the PL decay time and the integrated PL intensity of a

Dieses Werk ist copyrightgeschützt und darf in keiner Form vervielfältigt werden noch an Dritte weitergegeben werden.
Es gilt nur für den persönlichen Gebrauch.

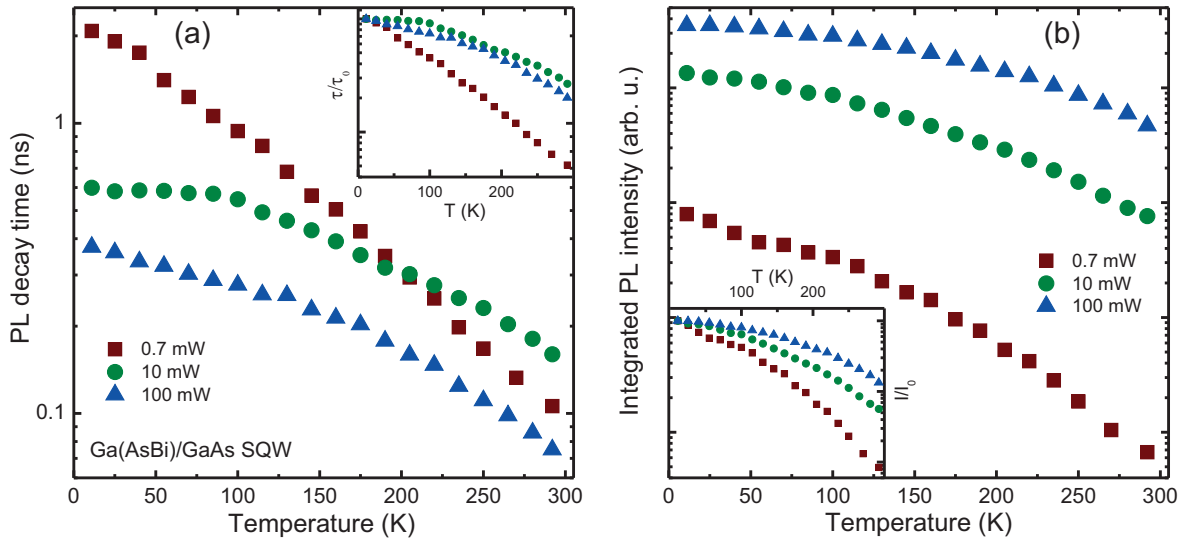

Figure 4.9: Temperature-dependent (a) PL decay time and (b) PL intensity of a Ga(AsBi)/GaAs SQW with Bi content of 5.5%, measured for three different intensities. For the sake of clarity, these results are normalized to the PL decay time (τ_0) and the PL intensity (I_0) obtained for each excitation intensity at 11 K and shown in the insets in (a) and (b), respectively.

Ga(AsBi)/GaAs SQW, respectively, carried out for three different excitation ranges. For the lowest excitation intensity the PL shows a slow decay time of about 3.2 ns. As the temperature is increased beyond 90 K, the PL decay time significantly decreases to about 0.1 ns at RT. On the other hand, for a high excitation intensity of 100 mW, the PL decay time decreases from 0.37 ns to 0.08 ns when the temperature is increased from 11 K up to RT. Strikingly, the comparison between the temperature-dependent PL decay time at 0.7 mW and 10 mW shows that while the PL decay time at 0.7 mW is longer than the one at 10 mW with rising temperature up to 215 K, they behave oppositely for higher temperatures. Furthermore, at 10 mW, the decrease rate of the PL decay time between 11 K and RT is lower than for other excitation intensities, as can be seen in the inset of Fig. 4.9(a). In contrast, while the PL intensity decreases by more than one order of magnitude at 10 mW, it quenches at 0.7 mW twice as rapidly as at 100 mW with increasing temperature up to RT. This is shown in the inset of Fig. 4.9(b).

Generally speaking, with increasing temperature, the decrease of the PL decay time is accompanied with the quenching of the PL intensity for all excitation regimes. Thus, the shortening in the PL decay time is mainly associated with a competition between radiative and non-radiative recombination channels, as widely discussed for dilute bismide and/or nitride semiconductors [6, 67, 76, 78, 94, 107, 108, 109]. In particular, for low excitation intensities, radiative recombination of localized excitons is expected to significantly contribute to the decay dynamics at low temperatures leading to a rather slow decay. However, when the excitation intensity is increased, the particular low-temperature features disappear, i.e., the temperature-dependent PL intensity shows a gradual decrease without any odd decline, since all localized states are filled –under high excitation conditions– and, hence, the PL originates mainly from band-to-band transitions. Simultaneously, the PL decay becomes faster due to the increasing contribution of non-radiative recombination. For higher temperatures, as non-radiative channels are thermally

Dieses Werk ist copyrightgeschützt und darf in keiner Form vervielfältigt werden noch an Dritte weitergegeben werden.
Es gilt nur für den persönlichen Gebrauch.

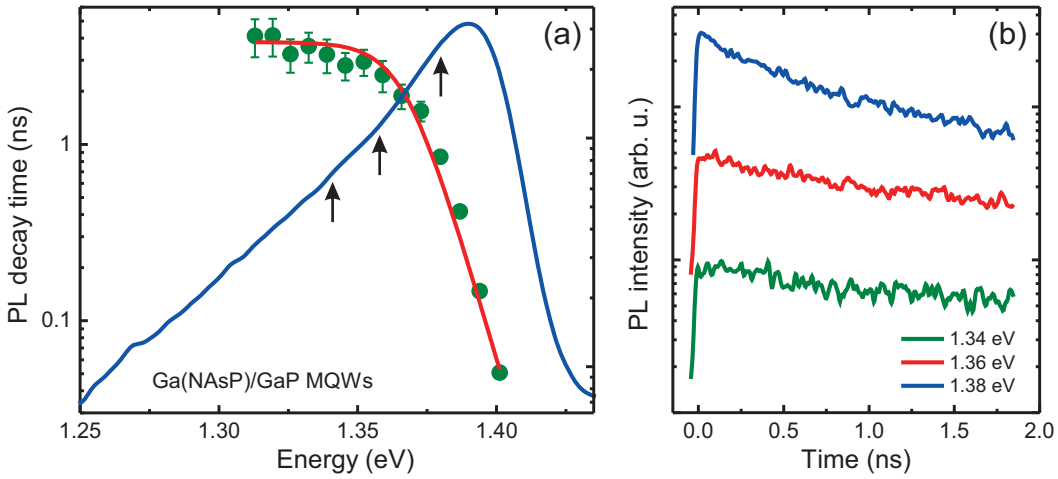

Figure 4.10: (a) the solid blue line denotes the PL spectrum of a Ga(NAsP)/GaP MQWs-sample with an N content of 4%, obtained for an excitation intensity of 3 mW at 10 K. Green circles show corresponding PL decay times for different emission energies. The solid red line represents a fit generated using the Gourdon and Lavallard model [82]. (b) selected transients for some emission energies. The transients are normalized and shifted vertically, for the sake of clarity.

activated [110], the decay time decreases. However, the unexpected behavior of the excitation-dependent PL decay time at high temperatures will be discussed in Section 4.6.2.

It is worth noting that the shape of the energy-distribution of localized states below the mobility edge plays an essential role in the quantitative explanation of the peculiar behavior of the PL thermal quenching in disordered semiconductors. A monotonous, e.g., exponential, distribution of localized states has been reported to be enough to interpret the low-temperatures flattening of the PL thermal quenching in Ga(NAsP) QWs [110], as can be seen in Fig. 4.8(b). In contrast, an approach with a non-monotonous, e.g., a combination of an exponential and Gaussian, distribution-shape of localized states[2] is indispensable to achieve a good agreement between experiment and theory for the anomalous plateau in the PL thermal quenching in Ga(AsBi) bulk layers, which is observed for relatively low excitation conditions [106]; cf. the squares in Fig. 4.9(b).

4.5 Emission Energy Dependence

Fig. 4.10(a) shows the PL spectrum together with the PL decay time as a function of emission energy for a Ga(NAsP)/GaP-MQWs-sample, measured under relatively low excitation intensity at 10 K. The PL decay strongly depends on the emission energy; PL transient profiles for some selected emission energies are shown in Fig. 4.10(b). In particular, a substantial increase with almost two orders of magnitude is observed in the PL decay time with decreasing emission energy across the PL spectrum. The shortening of the PL decay times on the high-energy side of

[2]This will be discussed in detail in Chapter 6

Dieses Werk ist copyrightgeschützt und darf in keiner Form vervielfältigt werden noch an Dritte weitergegeben werden.
Es gilt nur für den persönlichen Gebrauch.

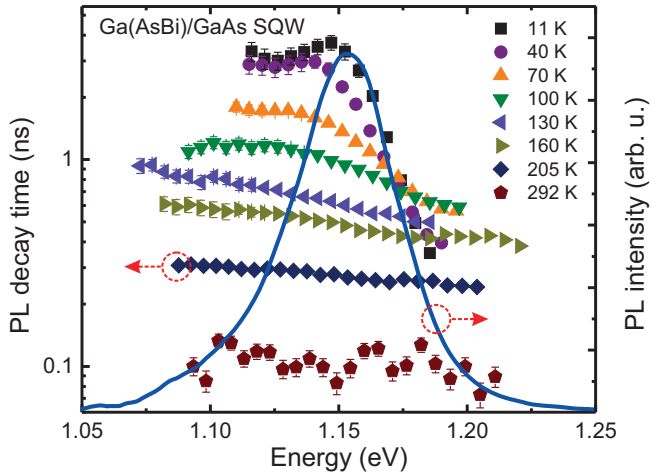

Figure 4.11: The emission energy dependence of PL decay time for a Ga(AsBi)/GaAs SQW with Bi content of 5.5%, measured for an excitation intensity of 0.7 mW at various temperatures. The blue solid line denotes the PL spectrum of presented structure at 100 K.

the PL spectrum (above 1.37 eV) can be attributed to the exciton relaxation among the band-tail states, i.e., the transfer of photo-excited excitons from higher energy states to lower empty ones [82]. On the other hand, under presented excitation condition, these excitons can hop between band-tail states, i.e., localized states, through phonon-assisted tunnelling transitions [81]. The low-energy side of the PL spectra is dominated by radiative recombination of localized excitons [80]. Given an exponential distribution of localized states, the emission-energy dependence of the PL decay time can be fitted using Gourdon and Lavallard model [82], as it is shown by the solid red curve in Fig. 4.10(b) (more details are found in the next chapter (Section 5.5.1).

Thermal Evolution

The emission-energy dependences of PL decay times at various temperatures for a Ga(AsBi)/GaAs SQW are shown in Fig. 4.11. All measurements are performed for the same relatively low excitation intensity. Below 100 K, the PL decay time strongly depends on the emission energy and follows the above-mentioned behavior. However, this trend obviously weakens with increasing temperature and disappears at RT.

These experimental observations are compatible with the qualitative description of carrier dynamics that is given in Section 4.4.1 and schematically displayed in Fig. 4.6. In particular, downward hopping relaxation transitions of localized excitons are dominant at low temperatures. When the temperature is increased, localized excitons are more mobile and gradually able to hop upward in energy. At high temperatures, most of the excitons are delocalized and, furthermore, dissociated into the band states by thermal activation. When the rates of downward and upward carrier-transfers –between energy levels– are equal, the PL decay time is quite independent on the emission energy, as can be seen at RT.

Dieses Werk ist copyrightgeschützt und darf in keiner Form vervielfältigt werden noch an Dritte weitergegeben werden.
Es gilt nur für den persönlichen Gebrauch.

4.6 Carrier Dynamics in Ga($As_{1-x}Bi_x$)/GaAs Single Quantum Well's

In this section, the impact of the Bi content (x) on the carrier recombination dynamics in a set of Ga($As_{1-x}Bi_x$) SQW's is investigated. The samples were grown by molecular beam epitaxy (MBE) on semi-insulating GaAs substrates with Bi contents of x= 1.1%, 2.1%, 5.5%, and 6.0%. More details on samples' characteristics and preparation are found in Section 3.3.2. First, the low-temperature PL emission of the studied structures is presented. Then, the temperature dependence of the carrier dynamics is discussed in the second part of this section. Finally, the PL thermal quenching together with the temperature-dependent PL decay time is described.

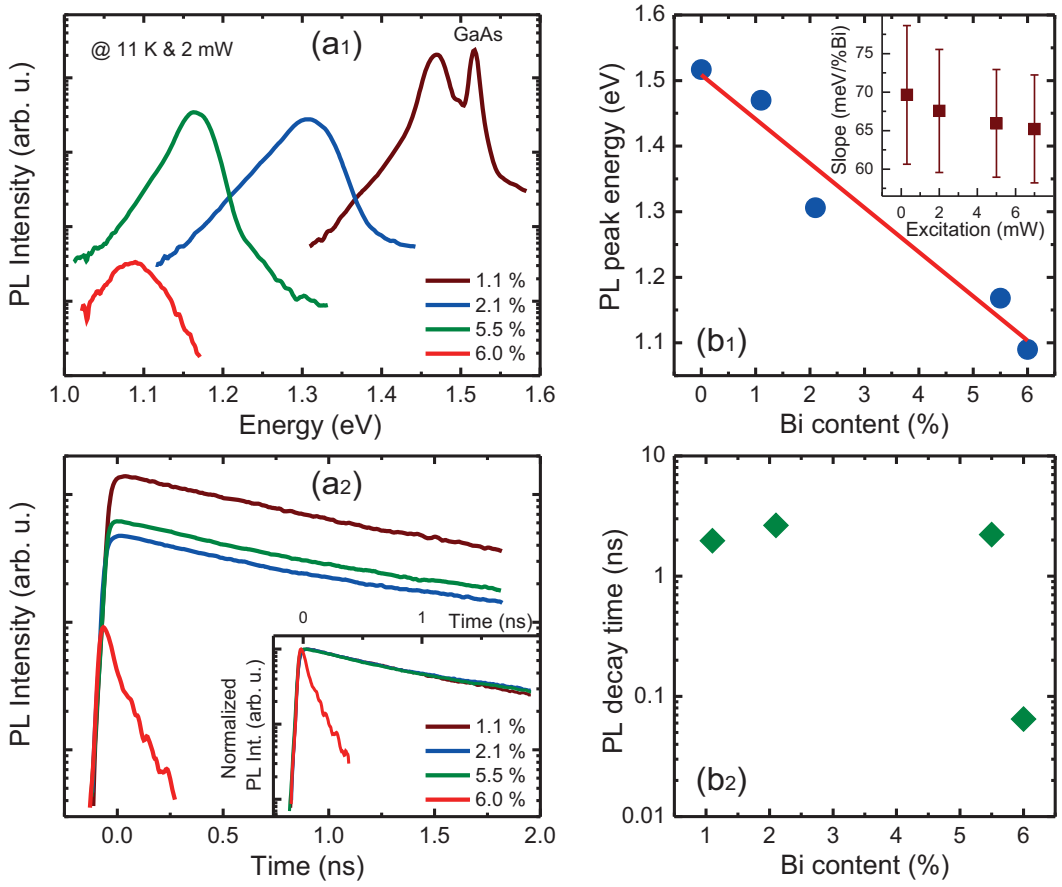

Figure 4.12: (a_1) PL spectra and (a_2) corresponding PL transients of Ga($As_{1-x}Bi_x$) SQW's, measured for 2 mW and at 11 K. PL transients are normalized in the inset in (a_2) for the sake of clarity. The PL peak energy and the PL decay time as a function of Bi content are plotted in (b_1) and (b_2), respectively. The solid red line in (b_1) represents a linear fit to the data points of PL peak energy with respect to the band-gap energy of GaAs. The inset in (b_1) shows some selected values of the absolute slope of the band-gap narrowing vs. Bi content for different excitation intensities.

Dieses Werk ist copyrightgeschützt und darf in keiner Form vervielfältigt werden noch an Dritte weitergegeben werden.
Es gilt nur für den persönlichen Gebrauch.

4.6.1 Low-Temperature Emission

Fig. 4.12(a_1) shows PL spectra of Ga($As_{1-x}Bi_x$) SQW's with different Bi contents, which are measured at an excitation intensity of 2 mW at a lattice temperature of 11 K. The corresponding PL transients are plotted in Fig. 4.12(a_2) and are normalized in the inset of this figure for the sake of clarity. As expected, the PL spectra shift toward the low energy-side with increasing Bi content. This reflects the band-gap shrinkage due to the valence-band anti-crossing interaction [45]. Based on a linear fit to the Bi content-dependent PL peak energy, plotted in Fig. 4.12(b_1), the absolute slope of the band-gap narrowing versus Bi content is 68±8 meV/%Bi with respect to the band-gap energy of GaAs. The slope is reduced by about 10% when the excitation density is increased by a factor of 10; the inset of Fig. 4.12(b_1) shows absolute values of the linear slope of the PL energy peak with Bi content for some selected excitation intensities. These values, however, are in a reasonable agreement with previously reported ones [58, 66, 111].

On the other hand, all PL spectra display a similar asymmetric form a characteristic low energy flank. The latter is attributed to the recombination of the electron-hole pairs trapped in localized states. As mentioned above, the presence of the localized states in Ga(AsBi) semiconductor alloys is attributed to disorder effects, i.e., an inhomogeneous distribution of Bi atoms and, furthermore, the existence of Bi clusters within the alloy structure. Disorder effects result, however, in a broadening of the PL emission peak [58, 112]. In the present case of QW structures, the fluctuations in the well thickness and/or strain can also lead to a certain degree of exciton localization [25, 97]. However, no clear correlation between PL linewidths and the variation of the Bi content is observed. Moreover, the increased Bi content in Ga($As_{1-x}Bi_x$) SQW's has a weak influence on PL transients up to x= 5.5%. Yet, it becomes significantly faster when the Bi content is raised to 6.0%, as shown in the inset of Fig. 4.12(a_2). The PL decay time gets reduced more than 10 times when the Bi content is increased from 5.5% to 6.0%; cf. Fig. 4.12(b_2). This point will be discussed in more detail in the following sub-section.

4.6.2 Carrier Recombination Mechanism

Low Temperatures

The integrated PL intensity and the PL decay time of the studied QW structures are plotted as a function of excitation intensity at 11 K in Figs. 4.13(a) and 4.13(b), respectively. A considerable shortening in the PL decay time by about one order of magnitude is observed when the excitation intensity is increased by three orders of magnitude. In contrast, the integrated PL intensity grows linearly with increasing excitation intensity and then sub-linearly for high excitation intensities; solid lines in Fig. 4.13(a) refer to the fits using Eq. (4.1).

The impact of the excitation intensity on the integrated PL intensity can be clearly discussed in two regimes for all studied SQW's. In particular, as the excitation intensity increases up to 10 mW, the values of the exponential factor α_1 are 0.90, 1.05, and 1.27 for SQW's with x= 2.1%, 5.5%, and 6.0%, respectively, whereas α_1 is 1.15 for x= 1.1%, as the excitation intensity is increased up to 2 mW. By a further increase in the excitation intensity, α_2 are 0.40, 0.22, 0.33, and 0.80 for the samples with x= 1.1%, 2.1%, 5.5% and 6.0%, respectively.

Dieses Werk ist copyrightgeschützt und darf in keiner Form vervielfältigt werden noch an Dritte weitergegeben werden.
Es gilt nur für den persönlichen Gebrauch.

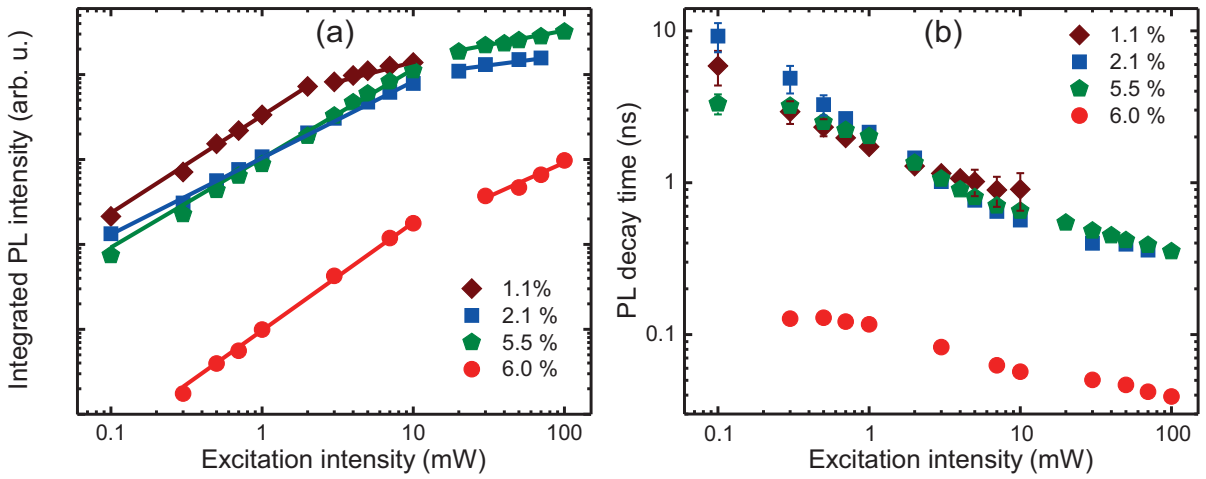

Figure 4.13: Excitation-intensity dependences of (a) the integrated PL intensity and (b) the PL decay time of Ga($As_{1-x}Bi_x$)/GaAs SQW's measured at 11 K. The solid lines in (a) indicate the fits obtained using Eq. (4.1).

As it is disscussed in Section 4.3.1, the observed decrease of the PL decay time with increasing excitation intensity, in the first excitation regime, is attributed to the dominance of radiative recombination of the electron-hole pairs trapped in the localized states, resulting in a nearly linear increase of the PL intensity as the α_1's are approximately one. When non-radiative processes dominate, a decrease of the exciton lifetime should be accompanied with a sub-linear behavior of the excitation-dependent PL intensity. This is indeed the case in the second excitation regime.

A decreasing decay time of the PL together with a sub-linear increase of the PL intensity, reflected in values of α_2 significantly lower than one, is attributed to an increasing contribution from capture processes into defect states as the excitons become delocalized and thus more mobile. Besides, further non-radiative contributions from, e.g., Auger recombination processes [90] and/or heating effects [73] are possible.

Thermal Evolution

For further investigation of carrier recombination mechanisms, the excitation dependence on the PL decay time as well as the integrated PL intensity is studied for the sample with Bi content of 5.5% at different temperatures of 11, 70, 130, 205, and 292 K. The corresponding data are shown in Fig. 4.14. The PL decay time as well as the PL intensity decreases with increasing temperature over the entire range of excitation intensities. However, the excitation-dependent PL decay time can be distinguished in three major regimes, shown by vertical short-dashed black lines in Fig. 4.14(a_1), as follows:

1. When the excitation intensity is increased up to 2 mW, the PL decay time decreases slightly at 11 K, shows very little dependence on the excitation intensity at 70 K (Fig. 4.14(b_1)), and then tends to increase with the excitation intensity for higher temperatures (e.g., at 205 K, Fig. 4.14(b_2)).

Dieses Werk ist copyrightgeschützt und darf in keiner Form vervielfältigt werden noch an Dritte weitergegeben werden.
Es gilt nur für den persönlichen Gebrauch.

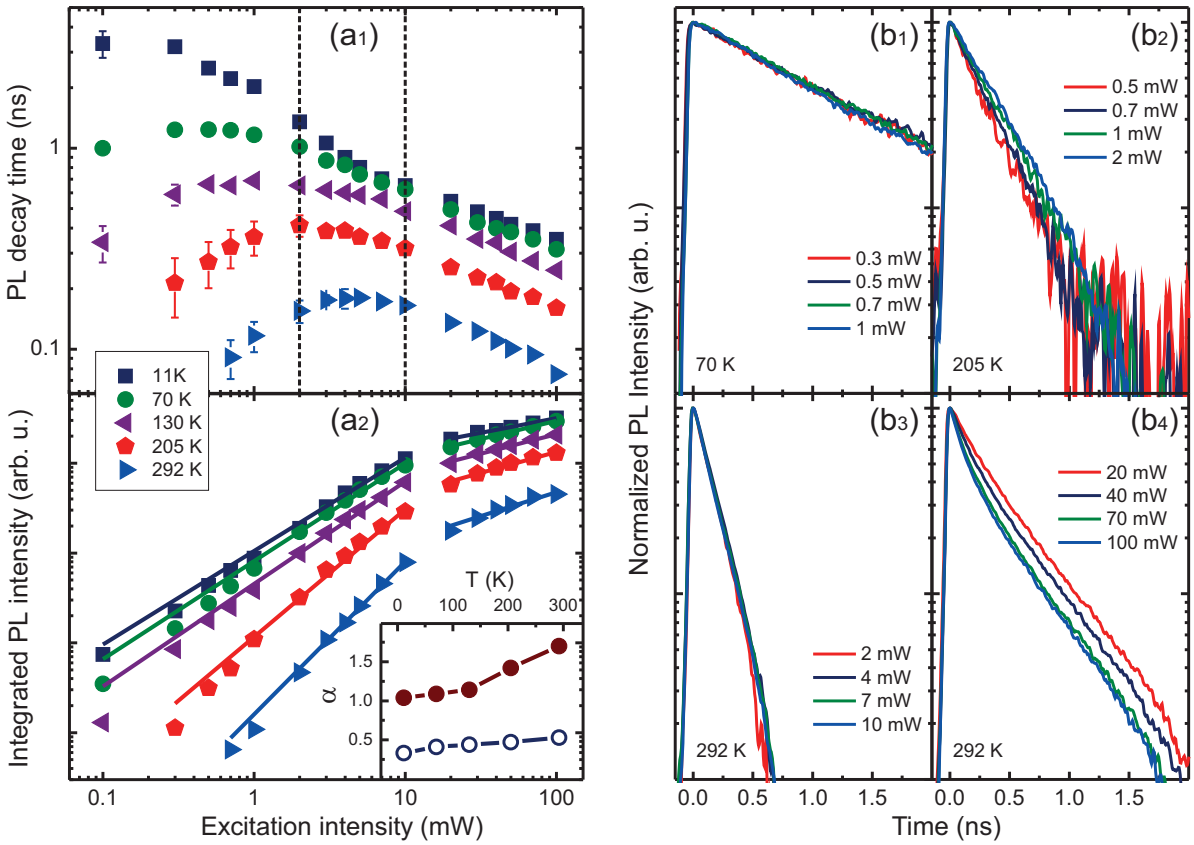

Figure 4.14: (a_1) the PL decay time and (a_2) the integrated PL intensity as a function of excitation intensity measured at different temperatures for the sample with Bi content of 5.5%. The solid lines in (a_2) indicate the fits obtained using Eq. (4.1). The corresponding exponent α vs. the temperature is shown in the inset in (a_2). (b_1), (b_2), (b_3), and (b_4) show normalized PL transients for some selected excitation intensities and temperatures.

2. By further increasing excitation intensity up to 10 mW, the PL decay time shows a weak shortening for all studied temperatures. However, the PL decay time seems to be independent of the excitation intensity at 292 K; cf. Fig. 4.14(b_3).

3. For higher excitation intensities, an obvious decrease of the PL decay time is observed when the excitation intensity is further increased (Fig. 4.14(b_4)).

In contrast, the PL intensity grows proportionally with the excitation intensity according to Eq. (4.1) and can be analyzed in two major ranges of the excitation intensity; one is from 0.1 mW to 10 mW and the second range is for higher excitation intensities up to 100 mW. The solid lines in Fig. 4.14(a_2) indicate the fits of the experimental results of the excitation-dependent PL intensity, which are obtained using Eq. (4.1). The closed and opened circles in the inset of Fig. 4.14(a_2) show the yielded exponents against the temperature for the first range of excitation intensity (α_1) and for second one (α_2), respectively.

Besides the influence of carrier localization effects, i.e., hopping relaxation processes of localized excitons between localized states before their recombination [81], the unusual excitation-dependent behavior of the PL decay time between 0.1 mW and 10 mW, with in-

Dieses Werk ist copyrightgeschützt und darf in keiner Form vervielfältigt werden noch an Dritte weitergegeben werden.
Es gilt nur für den persönlichen Gebrauch.

creased temperature is attributed to the competition between the radiative and non-radiative recombination channels [110]. In particular, the localization of excitons has a considerable impact on the carrier recombination at very low temperatures, resulting in a long PL decay time under low excitation intensities. Furthermore, PL emission is primarily dominated by radiative recombination of localized excitons [80], as above-moitioned in Section 4.3.1. However, the carrier localization is weakened with increasing either the excitation intensity due to the saturation effects of the localized states or the lattice temperature because of the thermal delocalization of the excitons. Hence, the shortening of the PL decay time with increasing temperature is attributed to the growing role of non-radiative recombination at the expense of the radiative one. This conclusion is supported by the gradual change of the relationship between the PL intensity and the excitation intensity from linear with α_1=1.05 at 11 K to super-linear with α_1=1.7 at 292 K (the inset of Fig. 4.14(a_2)). A similar behavior is reported also in Ref. [112]. On the other hand, for high lattice temperatures, the increase of the PL decay time with the excitation intensity can be attributed to the population of the non-radiative centers, which become saturated at a certain excitation intensity.

Under high excitation conditions, i.e., from 20 mW to 100 mW, a sub-linear increase of the PL intensity with the excitation intensity is observed, independent on the lattice temperature. The growing of the exponent α_2 from 0.33 to 0.53 as the temperature is raised from 11 K to 292 K, indicates a slightly reduced contribution of the energy loss processes from Auger recombination and/or heating effects. The PL decay time decreases for all temperatures in a similar way as can be seen in Fig. 4.14(a_1).

4.6.3 Temperature-Dependent Photoluminescence Intensity

Figs. 4.15(a_1) and 4.15(a_2) show the PL decay time and the integrated PL intensity of the studied Ga($As_{1-x}Bi_x$)/GaAs SQW's as a function of temperature, respectively, measured for an excitation intensity of 2 mW. A strong decrease of the PL intensity, accompanied by a shortening of the PL decay time is observed for all samples when the temperature is increased. However, the sample with Bi content of 1.1% shows an even stronger decline of the PL intensity as well as the PL decay time already in the temperature range below 100 K. Furthermore, at higher temperatures PL spectra arise mainly from the emission of the barrier's material (GaAs), as can be seen in Fig. 4.15(b). The PL intensity related to the SQW with x= 2.1% (x=5.5% as well) decreases slowly with increasing temperature up to a certain point of 150 K and then drops fast. Also the low-temperature PL decay times in these samples are relatively long at with values of around 1.5 ns and 1.2 ns for 2.1% and 5.5%, respectively. However, as the temperature is increased beyond 90 K, the PL decay decreases significantly to about 0.06 ns and 0.15 ns for 2.1% and 5.5% at 292 K, respectively.

Fig. 4.15(c) shows, e.g., the temperature-dependent PL transient of the sample with a Bi content of 2.1%. Furthermore, the PL intensity decreases by almost one order of magnitude when the Bi content is raised from 5.5% to 6.0% over the whole temperature range. A very short PL decay time of about 0.1 ns is observed at 11 K for the SQW with x= 6.0%. In addition, the PL decay time for this sample is reduced by less than one order of magnitude when the temperature is increased up to 292 K.

Dieses Werk ist copyrightgeschützt und darf in keiner Form vervielfältigt werden noch an Dritte weitergegeben werden.
Es gilt nur für den persönlichen Gebrauch.

The quenching of the PL intensity as well as the shortening of the PL decay time is mainly associated with the competition between radiative and non-radiative processes. In particular, radiative recombination of localized excitons is expected to contribute significantly to the decay dynamics at low temperatures leading to a rather slow decay. For higher temperatures, as non-radiative channels are thermally activated [110, 113], the decay time decreases.

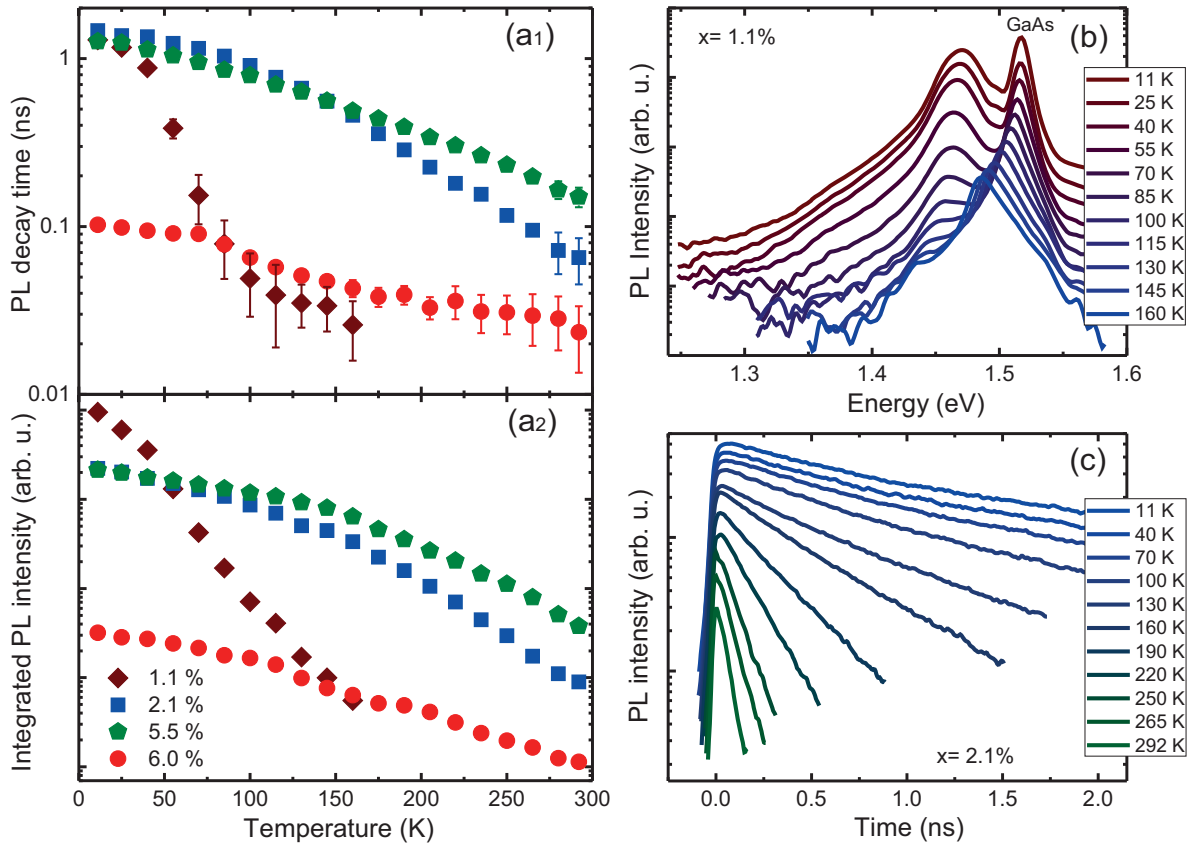

Figure 4.15: (a_1) the PL decay time and (a_2) the integrated PL intensity of Ga($As_{1-x}Bi_x$)/GaAs SQW's as a function of temperature measured at an excitation intensity of 2 mW. (b) PL spectra of the QW with x= 1.1% as well as (c) PL transients of the sample with x= 2.1% is measured at an excitation intensity of 2 mW for different temperatures.

The rapid degradation of the PL intensity as well as the PL decay time for the SQW with x= 1.1%, is attributed to the small band-gap offset between the barrier and QW. In detail, the photo-generated excitons in the QW are thermally activated and escape via GaAs barrier. Moreover, the dramatic decrease of the PL intensity as well as the corresponding decay time for the SQW with x= 6.0%, in comparison to the other SQW's, reflects an increased emergence of structural defects and subsequent degradation of the material quality of the QW [114]. In other words, the increased amount of the non-radiative centers leads to a decreased PL efficiency.

Dieses Werk ist copyrightgeschützt und darf in keiner Form vervielfältigt werden noch an Dritte weitergegeben werden.
Es gilt nur für den persönlichen Gebrauch.

4.7 Summary

A qualitative description of the most prominent PL features of disordered semiconductors is given in this chapter. Here, the impact of the excitation intensity as well as the lattice temperature on the PL emission is systematically studied for some disordered Ga(NAsP) and Ga(AsBi) nanostructures. The existence of disorder effects in a semiconductor leads to an increasing density of the localized states, which results in an extension of the energy band-edges. This is revealed by, e.g., a blueshift in the excitation-dependent PL peak energy. Furthermore, the low-temperature PL emission is mainly dominated by the radiative recombination of localized excitons. Besides, the PL decay time shows a strong dependence on the emission energy.

A peculiar temperature-dependent PL peak energy as well as PL linewidth is observed. Here, hopping relaxation processes of localized excitons between localized states are convincingly involved to interpret these unexpected behaviors. Disorder-induced PL characteristics become less visible when either the excitation intensity or the lattice temperature is increased. In particular, the increasing excitation intensity results in a gradual filling of disorder-induced localized states due to their finite number. On the other hand, localized excitons become mobile with rising temperature. Yet, most of them are delocalized at high temperatures. The PL thermal quenching as well as the shortening of the PL decay time in disordered semiconductors is mainly associated with the competition between radiative and non-radiative processes. While the quenching rate of the PL intensity decreases when the excitation intensity is increased, an odd behavior for the corresponding PL decay time is observed. In detail, the PL decay time shows firstly an increase and then a decrease as the excitation intensity is increased for high temperatures.

Ultimately, the influence of Bi content on the optical properties and carrier dynamics in $Ga(As_{1-x}Bi_x)$/GaAs SQW's is investigated. This study demonstrates that the sample with x= 5.5% has the best optical efficiency, in comparison to the other studied SQW's.

Dieses Werk ist copyrightgeschützt und darf in keiner Form vervielfältigt werden noch an Dritte weitergegeben werden.
Es gilt nur für den persönlichen Gebrauch.

5 Hopping Relaxation of Excitons in Disordered Semiconductors: Energy Scaling of Disorder

5.1 Introduction

Most of the theoretical work in the field of semiconductors assumes an ideal picture of the material's structure, where the impact of disorder is ignored. Indeed, all materials show some disorder at finite temperatures due to fundamental thermodynamics and kinetics of atomic motion within their structures. However, the disorder degree and thus its effects on the physical properties of the materials differs from one to another. For example, amorphous semiconductors (glass: amorphous SiO_2) have more disorder than crystalline ones (quartz: crystalline SiO_2).

A certain group of semiconductors possesses obviously disorder, the so-called disordered semiconductors, e.g., dilute bismuth alloys; disorder in these structures is attributed to the potential fluctuation associated with the Bi content as well as Bi clustering. Disorder can significantly affect the electronic structure of semiconductors. In particular, the presence of disorder within the material structure results in an increasing density of the localized states. This leads to an extension of the band-edge toward lower energies, the so-called band-tail states [76]. Localized states, on the other hand, lead to significant changes in carrier dynamics, which can be revealed, e.g., in photoluminescence (PL) spectra of disordered semiconductors.

The previous chapter illustrates the main PL features that are experimentally detected from disordered semiconductors. In addition, a qualitative explanation of disorder-induced PL features is given. This chapter, however, presents several models used to quantify the disorder potential in disordered semiconductors by parameters which are called energy scales of disorder. These scales are determined through comparison between simulated and experimental results of PL spectra. This chapter is organized as follows. Section 5.2 summarizes experimentally-observed disorder-induced PL features that are mainly analyzed in this chapter to estimate the disorder scales. A phenomenological model with a single energy-scale of the disorder is introduced in Section 5.3. This model has successfully interpreted the disorder-induced PL features in some disordered semiconductors such as (GaIn)(NAs), but fails for some others like Ga(NAsP). An extension of this model, presented in Section 5.4, was inescapable to correctly reproduce the experimental observations for disorder-induced PL features in these materials. The impact of the Bi content on disorder parameters in Ga(AsBi) single quantum wells is studied in Section 5.5, while the influence of the N content on the energy-scale related to the compositional disorder in Ga(NAsP) multi quantum wells is presented in Section 5.6.

Dieses Werk ist copyrightgeschützt und darf in keiner Form vervielfältigt werden noch an Dritte weitergegeben werden.
Es gilt nur für den persönlichen Gebrauch.

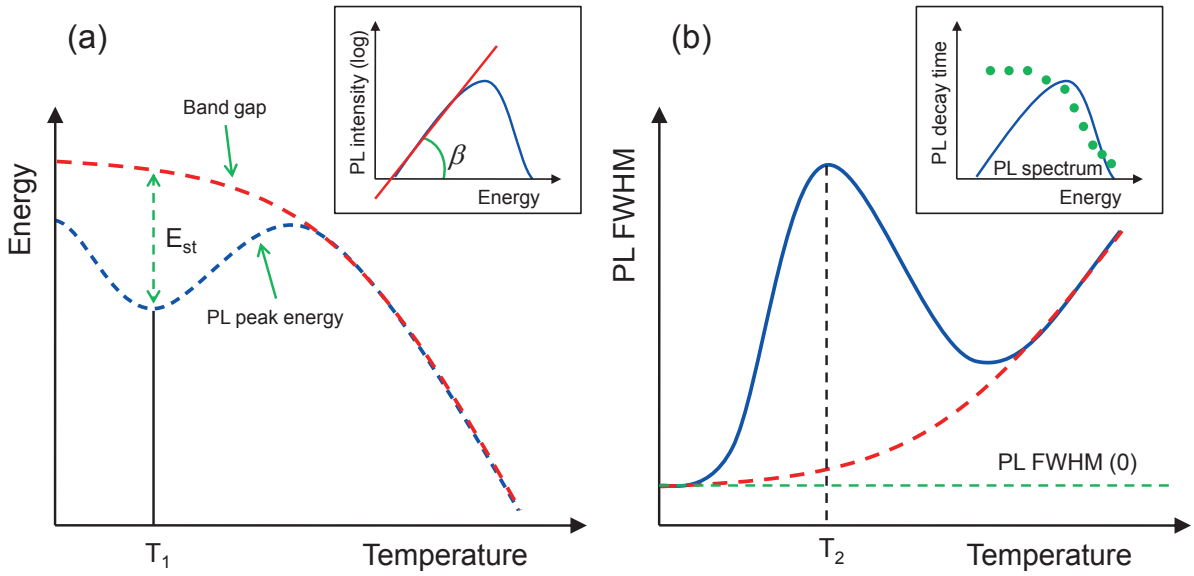

Figure 5.1: The blue curves in (a) and (b) represent the temperature dependence of the PL peak energy (a) and the PL FWHM (b) for disordered semiconductors, respectively. The dashed red lines in (a) and (b) indicate the PL features for typical semiconductors The inset in (a) shows the low-temperature PL spectrum with logarithmic slope β. The inset in (b) shows the PL decay time as a function of the emission energy.

5.2 Experimental PL Characteristics

The disorder-induced PL features, which will be analyzed in this chapter to estimate the disorder scales, are

- An asymmetric spectral shape of the PL peak emission measured at low temperatures as well as low excitation intensities. Given an exponential character of the low energy flank of the PL spectrum, this behavior is characterized by the logarithmic slope (β) of this character, i.e., the PL emission intensity vs. the emission energy (the inset of Fig. 5.1(a)).
- A strong dependence of the PL decay time on emission energy: the lower the PL emission energy, the longer is the PL decay time. A typical spectral distribution of PL decay times is represented in the inset of Fig. 5.1(b).
- A red shift, followed by an unusual blue shift, and then by a red shift of the temperature-dependent PL peak energy, shown as a blue curve in Fig. 5.1(a). This behavior is typically called S-shape, and is characterized by the temperature (T_1), at which the PL peak energy has its local minimum within the S-shape. This temperature T_1 indicates also the maximum of the Stokes shift, i.e., the energetic difference between the absorption edge and the PL emission maximum [115]. The dashed red curve in Fig. 5.1(a) indicates the behavior of the temperature-dependent PL peak energy of typical semiconductors, which follows the semi-phenomenological Varshni formula [99].
- A significant broadening of the PL linewidth in an intermediate range of temperatures, corresponding with a local maximum of the temperature-dependent PL FWHM (FWHM: full width at half maximum). This non-monotonous behavior is characterized by the

Dieses Werk ist copyrightgeschützt und darf in keiner Form vervielfältigt werden noch an Dritte weitergegeben werden.
Es gilt nur für den persönlichen Gebrauch.

temperature (T_2), shown in Fig. 5.1(b). However, the behavior of the temperature-dependent PL FWHM of typical semiconductors is represented by the dashed red curve in Fig. 5.1(b).

In addition to the above-mentioned PL trends, an anomalous behavior of the PL thermal quenching in disordered semiconductors is observed. This is, however, reserved for a separate chapter (Chapter 6).

5.3 Baranovskii-Eichmann Model: Single Energy-Scale of Disorder

In 1998, a phenomenological model with microscopic parameters has been suggested by Baranovskii *et al.* (further, BE-model: Baranovskii-Eichmann model) for an universally applicable description of energy relaxation processes in disordered material structures such as quantum wells (QWs) [81]. In this model, at very low temperatures as well as low excitation intensities and directly after the excitation, the generated electrons and holes are captured as excitons into localized states. The center-of-mass of such an exciton can perform phonon-assisted transitions (hopping transitions) via uncorrelated localized states, which are spatially as well as energetically distributed. While the localized states are randomly distributed in space, the distribution of their energies forming the band tail is considered either purely exponential or purely Gaussian. However, the energy distribution of localized states in a two-dimensional rectangle of the linear size $N_0^{1/2}$ containing N_0 sites can be expressed in the general form [84, 100]

$$g(E) = A\, f\left(\frac{E}{E_0}\right), \tag{5.1}$$

where A is the normalization parameter, E_0 is the characteristic energy scale, and $f(E/E_0)$ is a function that represents the shape of the band tail.

In comparison with theoretical models proposed earlier than the BE-model to interpret disorder-induced PL features, the BE-model takes following aspects into account [81]:

- The dependence of the hopping transition rate on the distances between the localized states: this dependence is very strong due to the *spatial* localization of excitons.
- The dependence of the hopping transition rate on the hopping distance –*combined energetic and spatial*– of excitons between localized states, in the case of tunneling transitions: since this dependence is assumed to be exponential (Eq. (5.2)), the rates for hopping transitions upward in energy are very low at low temperatures, and the rates for hopping transitions downward in energy depend strongly on the energy of localized states as the concentrations of available localized states differ at different energies. In other words, the hop length between localized states varies depending on their energies.

As above-mentioned, during its lifetime (τ_0) the exciton can perform hopping transitions. The hopping transition rate from an occupied site i to an empty site j over a distance r_{ij} is determined by the Miller-Abrahams expression [116]

Dieses Werk ist copyrightgeschützt und darf in keiner Form vervielfältigt werden noch an Dritte weitergegeben werden.
Es gilt nur für den persönlichen Gebrauch.

$$\nu_{ij} = \nu_0 \exp\left(-\frac{2r_{ij}}{\alpha}\right) \exp\left(-\frac{E_j - E_i + \mid E_j - E_i \mid}{2k_B T}\right), \tag{5.2}$$

where E_i and E_j are the energies of the states i and j, respectively, α is the decay length of the exciton center-of-mass wave function in the localized states, and ν_0 is the attempt-to-escape frequency.

Since, from an experimental point of view, the excitons can relax independently from each other in the case of low excitation intensities, their hopping and recombination are also independently simulated. However, a large number of mutually independent excitons is taken into account, where the decay rate of an exciton at site i is calculated as [81]

$$\nu_i = \tau_0^{-1} + \sum_j \nu_{ij} \ , \tag{5.3}$$

where τ_0^{-1} is the radiative recombination rate, which is assumed -for simplicity- independent of both temperature and energy. $\sum_j \nu_{ij}$ is the total hopping rate. The summation index j runs over all possible target states.

In addition to the hopping relaxation of the excitons, the possibility of thermal activation from a localized state with energy E into extended states above the mobility edge is introduced by Rubel *et al.* [110]. The rate of thermal-activated transitions of excitons is given by

$$\nu_a = \nu_0 \, exp\left(\frac{E}{k_B T}\right), \tag{5.4}$$

Being thermal-activated to the mobility edge, excitons can either be captured by non-radiative centers or they can be recaptured into radiative trapping sites. Taking into account the ratio of the concentration of non-radiative centers (N_{nr}) to the sum concentration of non-radiative and radiative recombination (N_r) centers, $N_{nr}/(N_{nr} + N_r)$[1], this opens the possibility to simulate the thermal quenching of the PL intensity [110].

The next sub-section presents an example of utilizing the BE-model to obtain a quantitative description of the energy scale of the disorder potential in (GaIn)(NAs) QWs.

5.3.1 Disorder in (GaIn)(NAs)/GaAs Quantum Wells

Quaternary (GaIn)(NAs) semiconductors alloys have received much attention in past two decades due to their unusual physical properties [42] and potential application in long-wavelength optoelectronic devices [117]. Bandgap engineering is achieved in these materials by changing the In and/or N contents. However, the incorporation of In as well as N atoms into GaAs affects dramatically the lattice of the host material due to the differences in size and electronegativity from substituted anions. Consequently, (GaIn)(NAs) alloys inevitably possess a certain degree of disorder due to inhomogeneous potential fluctuations of the alloy composition. Besides, imperfect interfaces lead also to disorder in the case of heterostructures, e.g., (GaIn)(NAs)/GaAs QWs [100].

[1] Here, it is assumed that the capture cross sections of radiative and non-radiative centers are equal.

Dieses Werk ist copyrightgeschützt und darf in keiner Form vervielfältigt werden noch an Dritte weitergegeben werden.
Es gilt nur für den persönlichen Gebrauch.

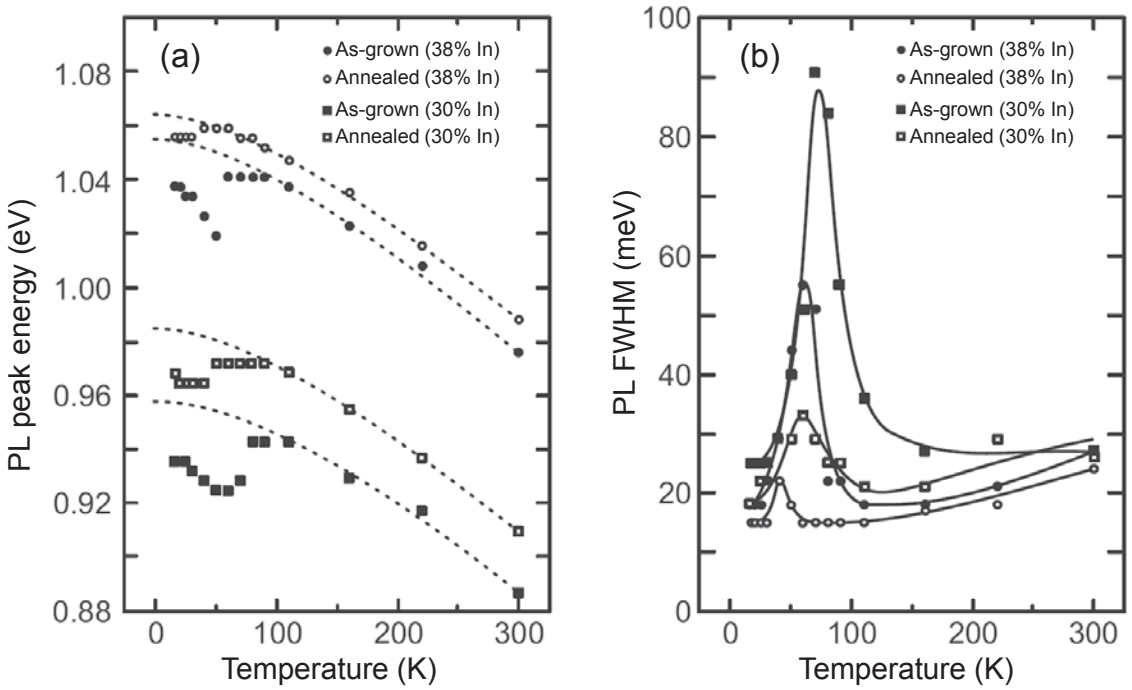

Figure 5.2: Experimental data for (a) the PL peak energy and (b) the PL FWHM vs. temperature for two $(Ga_{1-x}In_x)(N_{0.016}As)$/GaAs QW's. The filled and open symbols correspond to results taken from as-grown and annealed samples, respectively. The dashed curves on panel (a) show the band-gap variation with temperature obtained by the Varshni fit [99], while the solid lines in (a) and (b) are guides to the eye. (After Rubel *et al.* [110])

The above-mentioned disorder effects result in an increasing density of localized states, which significantly affects carrier dynamics, and thus the optical properties of the disordered (GaIn)(NAs) semiconductor structures. This is typically reflected in a non-monotonous behavior of the temperature-dependent PL peak energy as well as PL linewidth. Solid circles and squares represent experimental results for the PL peak energy (Fig. 5.2(a)) and the PL FWHM (Fig. 5.2(b)) for two as-grown $(Ga_{1-x}In_x)(N_{0.016}As)$/GaAs QW's with x= 30% and x= 38%, respectively.

Kinetic Monte-Carlo simulations based on the BE-model have been performed by Grüning *et al.* [118] to explain the disorder-induced PL features of (GaIn)(NAs) QW's, taking into account an exponential shape of the band tail. Thus, Eq. (5.1) can be written as follows

$$g(E) = \frac{N_0}{E_0}\, exp\left(\frac{E}{E_0}\right), \tag{5.5}$$

where E_0 is the energy scale of disorder and N_0 is the number of localized states. This choice of an exponential distribution of the localized states stems from the exponential low-energy tail of PL spectra at low temperatures and low excitation intensities. However, using a Gaussian energy distribution to describe localized states within BE-model fails to fit disorder-induced PL features in (GaIn)(NAs) QW's [118], since it results in a saturation of the temperature-evolution of the PL linewidth at high temperatures that indeed disagrees with experimental observations.

Dieses Werk ist copyrightgeschützt und darf in keiner Form vervielfältigt werden noch an Dritte weitergegeben werden.
Es gilt nur für den persönlichen Gebrauch.

The characteristic-energy scale of disorder potential E_0 is quantified through comparison between simulated and experimental results and can be determined by means of some experimentally observed PL characteristics [100], in particular

$$\beta = E_0^{-1} \tag{5.6a}$$

where β is the logarithmic slope of the low-temperature PL spectra in its deep-energy part,

$$FWHM(0) = (2.5 - 2.7)E_0 \tag{5.6b}$$

where, $FWHM(0)$ is the full width at half maximum of the PL spectra at low temperature, and

$$k_B T_1 = (0.75 - 0.80)E_0\,, \tag{5.6c}$$
$$k_B T_2 = (1.10 - 1.15)E_0 \tag{5.6d}$$

where T_1 and T_2 are the temperatures corresponding to the local minimum of the PL peak energy and to the local maximum of the FWHM. Using these relations to estimate the value of E_0, it is found that E_0 range between 4–7 meV and between 5–10 meV for the considered samples with x= 30% and x= 38%, respectively.

An interesting utilization of the BE-model and the relations derived therefrom is to quantify the effect of the annealing on compositional/potential fluctuations in disordered semiconductors. Fig. 5.2(a) and Fig. 5.2(b) show the experimental results for the PL peak energy and the PL FWHM of annealed $(Ga_{1-x}In_x)(N_{0.016}As)$/GaAs QW's with x= 30% (open circles) and x= 38% (open squares), respectively. From the effect of the annealing on PL spectra of the considered samples it can be recapitulated that the general trends of disorder-induced PL features still appear but less pronounced in comparison with as-grown QW's. Quantitatively, the values of E_0 decrease by about 20% for annealed samples in comparison with that for as-grown samples [100]. This results from the improvement of the crystal quality in annealed samples. In particular, due to the annealing process, compositional fluctuations are smoothed [119], nitrogen local environment is changed [120], and the nitrogen complexes (N-clusters) are broken [121].

5.4 Extension of the Baranovskii-Eichmann Model: Two Energy-Scales of Disorder

The BE-model has been successfully utilized to reproduce the disorder-induced PL features in several disordered material systems like (GaIn)(NAs) quantum wells [100], GaP(N) bulk materials [122], and (ZnCd)Se quantum dots (QDs) [123]. Despite this success, however, the BE-model with a single energy-scale of disorder cannot correctly fit PL features in a certain group of disordered semiconductors such as Ga(NAsP) quantum wells [84] and Ga(AsBi) bulk structure [86]. An extension on the standard BE-model was inescapable for a good interpretation of the experimental observations in these materials. This has been realized by introducing an additional energy-scale of disorder.

Next, the extended BE-model with two different energy-scales of disorder is discussed for two disordered semiconductors, i.e., Ga(NAsP) and Ga(AsBi) bulk structures.

Dieses Werk ist copyrightgeschützt und darf in keiner Form vervielfältigt werden noch an Dritte weitergegeben werden.
Es gilt nur für den persönlichen Gebrauch.

5.4.1 Disorder in Ga(NAsP) Bulk Structures

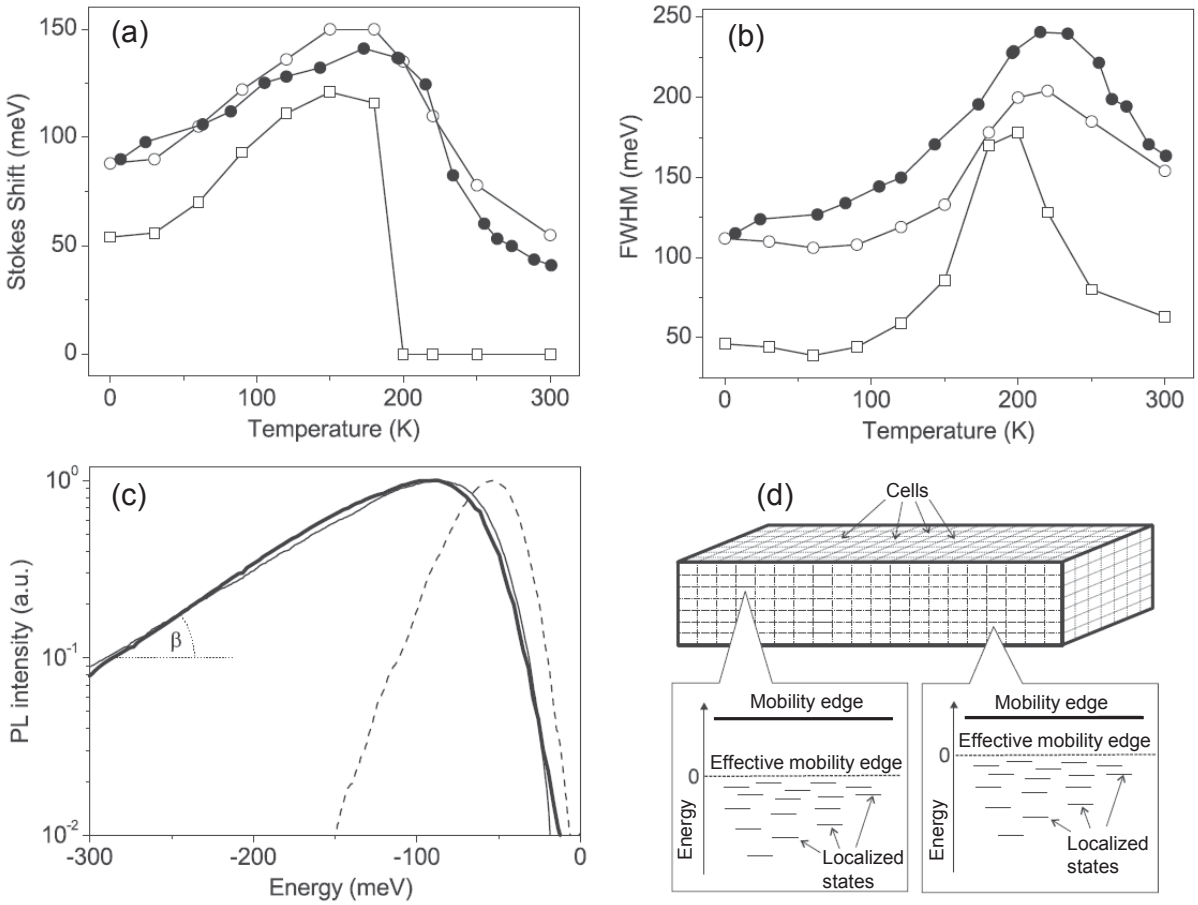

Figure 5.3: Temperature-dependent (a) Stokes-shift and (b) PL FWHM for the $Ga(N_{0.03}As_{0.14}P_{0.83})$ bulk structure. Solid circles indicate experimental results, while simulated results using a single-energy-scale model and a two-energy-scales model are represented by open rectangles and open circles, respectively. The solid line in (c) indicates the experimentally-observed low-temperature PL spectrum. PL spectra which are simulated using a single-energy-scale model and a two-energy-scales model are represented by a dashed and a thin line, respectively. (d) schematic representation of the bulk structure as an ensemble of cells. The insets show schematic energy structures of different cells. (After Jandieri *et al.* [21])

The BE-model with above-mentioned discussion for (GaIn)(NAs) cannot well describe disorder-induced PL features of Ga(NAsP) [21, 84]. This can be clearly seen from the obvious deviation between experimental and theoretical results, shown in Figs. 5.3(a)–5.3(c) for $Ga(N_{0.03}As_{0.14}P_{0.83})$ bulk structure[2]. Furthermore, the values of the characteristic energy scale E_0, estimated from the relations (5.6a)–(5.6b) based on the single-energy-scale model, are ultimately different: E_0 ranges from 16 to 80 meV. Therefore, an extension of the conventional one-energy-scale picture of disorder by introducing a second-energy-scale was found indispensable to obtain a reasonable agreement between simulated and experimental results of PL spectra

[2]More details on the extraction of the temperature-dependent Stokes-shift are found in Ref. [21].

Dieses Werk ist copyrightgeschützt und darf in keiner Form vervielfältigt werden noch an Dritte weitergegeben werden.
Es gilt nur für den persönlichen Gebrauch.

of Ga(NAsP) [21, 84]. The two energy-scales of disorder are defined by Jandieri *et al.*, in the case of Ga(NAsP) bulk structure, as follows [21]

- Long energy-scale of disorder (E_L), represents the long-range disorder-potential arising from compositional fluctuations.
- Short energy-scale of disorder (E_S), represents the short-range disorder-potential due to nitrogen-related clusters, which are typically expected to exist in dilute III-N-V semiconductor alloys [79].

Since the long-range disorder potential can be approximated as a step-like function of spatial coordinates, the whole bulk structure can be considered as an ensemble of three-dimensional cells (Fig. 5.3(d)) with the linear size determined by the spatial scale of long-range disorder. While the long-range disorder is fixed within each cell, the small-range disorder conditions hopping dynamics, including the effective mobility edge. It has been also assumed that, due to its finite lifetime, the exciton does hopping transitions and then will be captured by the recombination centers in the same cell, where this exciton was originally created [21].

It is assumed that the energy distribution of the long-range disorder-potential steps has an exponential shape and is given by

$$g_L(\varepsilon) = A\, exp\left(\frac{\varepsilon}{E_L}\right), \tag{5.7}$$

and, within each cell, the energy distribution of the localized states determined by a short-range disorder potential has also an exponential shape given by

$$g_S(E-\varepsilon) = B\, exp\left(\frac{E-\varepsilon}{E_S}\right), \tag{5.8}$$

where A and B are normalization parameters and both E_L and E_S are characteristic energy scales. Here, the energy ε is measured from some energy level identified with the mobility edge. The total energy distribution of the localized states in the whole bulk structure can be calculated as a convolution of g_L with g_S,

$$G(E) = C \int_0^E g_L(\varepsilon)\, g_S(E-\varepsilon)\, d\varepsilon\,, \tag{5.9}$$

where C is the normalization parameter, and it should be determined from the condition that the concentration of localized states N_0 is constant

$$\int_{-\infty}^{0} G(E)\, dE = N_0\,. \tag{5.10}$$

Ultimately, the total DOS of the localized states is

$$G(E) = \frac{N_0}{E_L - E_S}\left[exp\left(\frac{E}{E_L}\right) - exp\left(\frac{E}{E_S}\right)\right], \tag{5.11}$$

Taking into account this double-exponential distribution of the DOS in Kinetic Monte-Carlo simulations based on the BE-model, disorder-induced PL features of Ga(NAsP) bulk structure

Dieses Werk ist copyrightgeschützt und darf in keiner Form vervielfältigt werden noch an Dritte weitergegeben werden.
Es gilt nur für den persönlichen Gebrauch.

can be well reproduced; cf. Figs. 5.3(a)–5.3(c). Besides, a new set of relations between experimentally observed PL characteristics (β, T_1, and T_2) and both energy scales (E_S and E_L) is revealed: 5.12a–5.12d [21]. In particular, the logarithmic slope β of low-temperature PL spectra is estimated by E_L and is independent from E_S;

$$\beta = E_L^{-1}, \tag{5.12a}$$

while the disorder-induced PL features of the temperature-dependent PL peak energy as well as PL FWHM are sensitive to E_S, but insensitive to E_L;

$$k_B T_1 = (0.75 - 0.80) E_S \,, \tag{5.12b}$$

$$k_B T_2 = (1.10 - 1.15) E_S \,. \tag{5.12c}$$

On the contrary, the low-temperature PL linewidth, FWHM(0) is determined by both E_S and E_L;

$$FWHM(0) = 2.75\, E_S + 0.85\, E_L \,. \tag{5.12d}$$

Since β is purely determined by E_L(relation 5.12a), this means that the shape of the low-energy side of low-temperature PL spectra is dependent only on the energy distribution of localized states in the whole sample and, on the other hand, does not absolutely depend on the hopping transitions of excitons. In contrast, the abnormal temperature-dependent PL behavior is primarily determined by the hopping relaxations of excitons between localized states that are described by the short-range disorder, represented by E_L (relations 5.12b and 5.12c).

For the considered sample, i.e., Ga($N_{0.03}As_{0.14}P_{0.83}$) bulk structure, the scaling energies are estimated by the relations 5.12a–5.12d, and they are found to be E_S= 17 meV and E_L= 80 meV.

In the case of Ga(NAsP) QWs, the energy scaling of disorder is analyzed in a similar way to that presented here. However, the long-range disorder-potential is attributed to long-range interface imperfections between the QW and barriers, where the whole QW layer is considered as a sequence of individual quantum-well-cells of different width. In contrast, short-range imperfections and/or alloy fluctuations within each of quantum-well-cells give rise to short-range disorder-potential [84].

5.4.2 Disorder in Ga(AsBi) Bulk Structures

Similar to the effect of nitrogen in dilute III-V nitride semiconductors, the incorporation of Bi atoms in GaAs causes a certain degree of disorder in novel Ga(AsBi). The disorder in Ga(AsBi) is attributed to the potential fluctuation associated with the Bi content together with the emergence of Bi clusters within the alloy structure [23]. The disorder in Ga(AsBi) leads to a broadening in the density of localized states, corresponding with an extension of the band-edge toward lower energies. This translates into, e.g, experimentally-observed peculiarities in the PL spectra. In particular, the temperature-dependent PL peak energy as well as the corresponding Stokes-shift[3] exhibits the pronounced S-shaped behavior, while the temperature-dependent PL

[3]More details on the extraction of the temperature-dependent Stokes-shift are found in Ref. [124].

Dieses Werk ist copyrightgeschützt und darf in keiner Form vervielfältigt werden noch an Dritte weitergegeben werden.
Es gilt nur für den persönlichen Gebrauch.

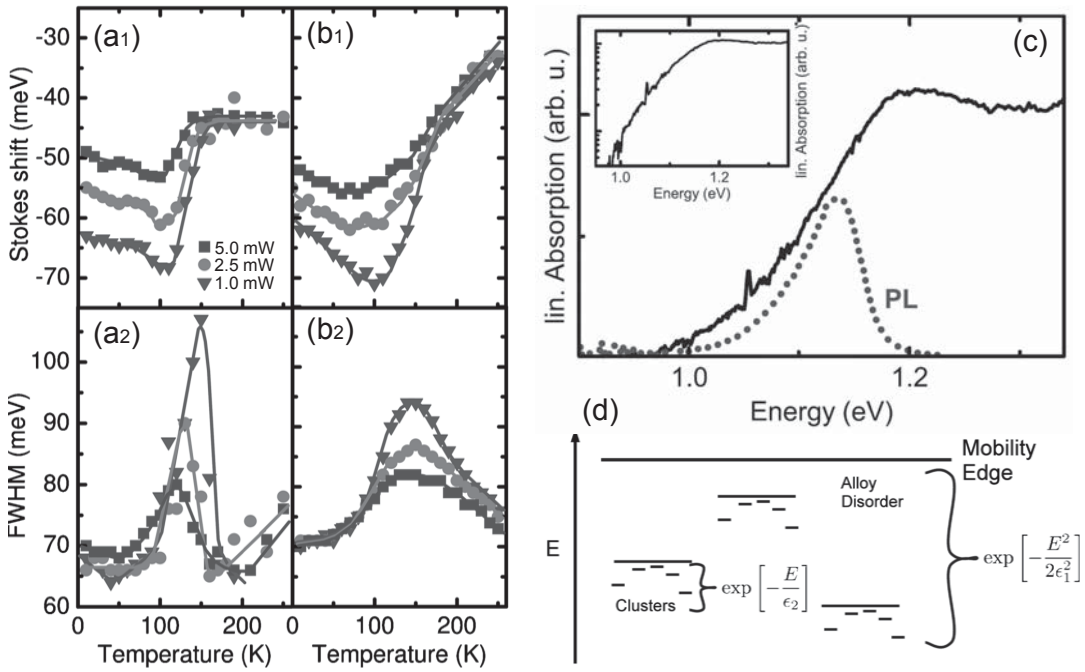

Figure 5.4: Temperature-dependent Stokes-shift and PL FWHM, obtained at different excitation intensities, for a Ga(AsBi) bulk structure with Bi content of about 4%–5%, where (a_1) and (a_2) are experimental results and (b_1) and (b_2) are simulated ones. The solid lines are guides to the eye. (c) linear absorption (solid line) and PL (dots) at 2.5 mW and 10 K. The inset in (c) shows the linear absorption on a logarithmic scale. (d) schematic representation of localized states assuming two energy-scales of disorder within Ga(AsBi) structure. (After Imhof *et al.* [86] and Imhof *et al.* [124])

FWHM shows a local maximum. Figs. 5.4(a_1) and 5.4(a_2) show the experimental data of the dependence of the temperature on the PL peak energy and the PL FWHM for a Ga(AsBi) sample with Bi content of about 4%–5%, respectively.

The energy scaling of disorder in Ga(AsBi) has been achieved through kinetic Monte-Carlo simulations of the above-mentioned disorder-induced PL features [86]. Since a conventional BE-model with a single energy-scale cannot bring the experimental and simulated results into agreement, the introduction of an additional energy-scale was inevitable to well reproduce the experimental observations from Ga(AsBi). Here, on the one hand, the long energy-scale of disorder reflects the spatially large fluctuations of the Bi content, which are assumed to have a Gaussian shape of the energy distribution, $\sim exp\,(-E^2/2E_L^2)$. The latter is strengthened by the pronounced Gaussian band tail at low energies of the linear absorption spectrum at low temperature, as shown in the inset of Fig. 5.4(c). On the other hand, the short energy-scale of disorder subdivides the long one and is attributed to the spatially short fluctuations of the sites among some cluster that have an exponential energy distribution, $\sim exp\,(-E/E_S)$. According to these assumptions, and as shown in Fig. 5.4(d), the excited exciton firstly exhibits transitions between the sites regarding the long energy-scale of disorder. Thereafter, the same exciton relaxes to some cluster and then performs hopping transitions regarding the short energy-scale of disorder, i.e, between localized states within this cluster [86].

Dieses Werk ist copyrightgeschützt und darf in keiner Form vervielfältigt werden noch an Dritte weitergegeben werden.
Es gilt nur für den persönlichen Gebrauch.

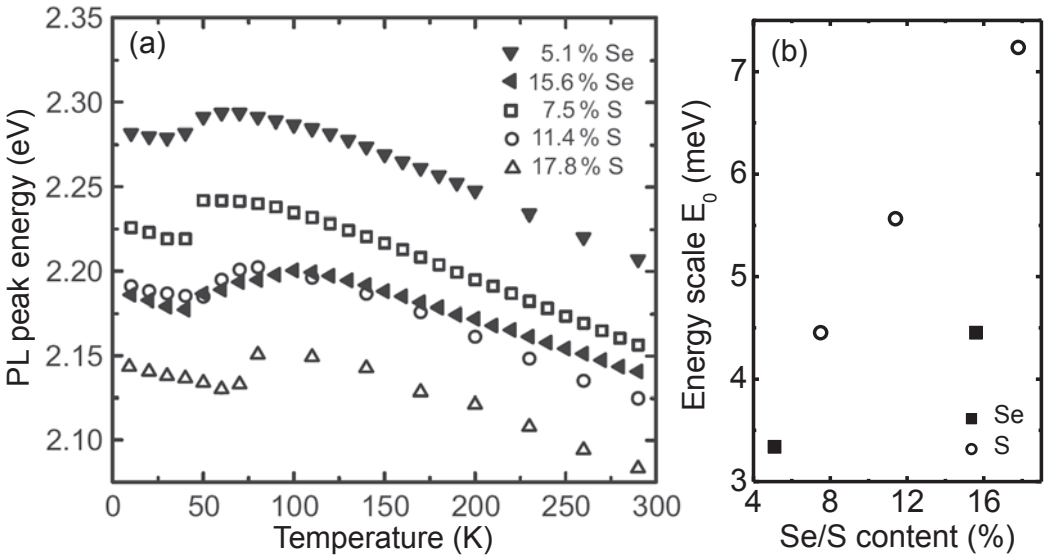

Figure 5.5: (a) temperature-dependent PL peak energy for Zn(X,Te)/GaAs structures with different X contents. Here, X is either Se or S. (After Karcher [126]) (b) energy scale of disorder (E_0) as a function of Se/S content.

A good agreement between the experimental and simulated results for Ga(AsBi) has been obtained by using this algorithm as can be seen on the left-hand side of Fig. 5.4. For the considered sample with Bi content of about 4%–5%, the short and long energy scales are estimated from the comparison between experimental and simulated results; and they are found to be E_S= 11 meV and E_L= 45 meV.

5.5 Fluctuation of Disorder Scales in Ga(AsBi)

Dilute III-V bismide (nitride) semiconductor alloys have received increasing attention in recent years due to their potential application in long-wavelength optoelectronic devices. The desired band gap is mainly achieved in these materials by varying the Bi (N) content. In particular, the higher the Bi (N) content, the smaller the band gap is (or rather the longer the wavelength is). On the other hand, the incorporation of Bi (N) in the III-V lattice results in essential amount of disorder due to the differences in size and electronegativity from substituted anions [57]. Thus, compositional fluctuations are expected in dilute III-V bismide (nitride) semiconductors alloys.

Intuitively, the degree of disorder potential in disordered semiconductors should increase when the content of the fluctuating compositional component is increased due to the rise of the absolute deviation of the composition from the average one [125]. An example is the increasing content of X (X is either Se or S) in Zn(X,Te) [126]. Fig. 5.5(a) shows the temperature-dependent PL peak energy for Zn(X,Te)/GaAs structures with different X contents. According to the relation 5.6c between the PL characteristic temperature T_1 and the energy scale of disorder E_0, the latter increases with T_1 accordingly. Fig. 5.5(b) shows E_0 as a function of X content in Zn(X,Te)/GaAs.

Dieses Werk ist copyrightgeschützt und darf in keiner Form vervielfältigt werden noch an Dritte weitergegeben werden.
Es gilt nur für den persönlichen Gebrauch.

In spite of the intuitive thought that the energy scales of disorder potential have to increase with the concentration of the fluctuating compositional component, a decrease of these scales is observed for the Ga(NAsP) MQWs when the N content is increased [21] (This will be discussed in Section 5.6). However, in the case of Ga(AsBi) structures the energy scales of disorder show a weak dependence of the Bi content [67]. In this section, a study of the impact of the Bi content on disorder potential in Ga(AsBi) is presented. The samples used in this study are a series of $Ga(As_{1-x}Bi_x)$ single quantum wells (SQW's), which were grown by molecular beam epitaxy (MBE) on semi-insulating GaAs substrates with Bi contents of x= 2.1%, 2.1%, 5.5%, and 6.0%. More details on samples' characteristics and prepration are given in Section 3.3.2. The experimental techniques employed are continuous-wave (CW) and time-resolved PL (TRPL).

Two theoretical models are used to quantify the disorder-parameters, i.e., energy scales of disorder, in considered Ga(AsBi) samples:

- The Gourdon and Lavallard model: a straightforward model with a single energy-scale is based on the carrier dynamics at very low temperatures.
- The extended BE-model model: an excitonic hopping model with two energy-scales is based on disorder-induced features of PL spectra.

5.5.1 Gourdon and Lavallard Model

In order to characterize the distribution of the localized states in $Ga(As_{1-x}Bi_x)$/GaAs SQW's, the dependence of the emission energy on the PL decay time is studied. The PL decay times against the emission energy for the four SQW's are shown as circles in Figs. 5.6(a_1)–5.6(a_4), measured at a temperature of 11 K and an excitation intensity of 1 mW. The PL decay times are determined from the spectrally integrated PL transients across $\pm$5 meV. A large increase in the PL decay time with decreasing energy is obviously observed for all samples as well. For the low emission energies of the PL spectrum, the radiative recombination is predominant due to strongly localized electron-hole pairs [127]. While, at the high energy side of the PL spectrum the carriers perform tunneling transitions toward the lower energies which lead to a shorter decay time of the PL [82, 128].

The PL decay time as a function of the emission energy is analyzed using the Gourdon and Lavallard model [82]. This model includes the mechanisms for the recombination as well as the aforementioned relaxation of the charge carriers toward lower energies. According to Gourdon and Lavallard model, the density of states is assumed to be exponential, $\sim exp(-E/E_0)$ with some characteristic energy (E_0). Hence, the PL decay times as a function of the emission energy are fitted by

$$\tau_{PL}(E) = \frac{\tau_{rec}}{1 + exp\left(\frac{E-E_{me}}{E_0}\right)}, \tag{5.13}$$

where τ_{rec} indicates the recombination lifetime and E_{me} is the energy at which the relaxation rate of an electron-hole pair toward lower-lying localized states and the recombination rate are equal. In this context, E_{me} plays a similar role as the mobility edge. The solid lines in Figs. 5.6(a_1)–5.6(a_4) are obtained from the fit to the measured data using Eq. (5.13). The obtained fitting parameters of the τ_{rec} together with E_{me} are summarized in Fig. 5.6(b) and E_0 in

Dieses Werk ist copyrightgeschützt und darf in keiner Form vervielfältigt werden noch an Dritte weitergegeben werden.
Es gilt nur für den persönlichen Gebrauch.

Fig. 5.6(c) as a function of the Bi content. E_{me} decreases linearly with increasing Bi content, reflecting the narrowing of the band-gap energy. The reduction rate of E_{me} is -64 ± 14 meV/%Bi, which is in a good agreement with the decrease of the PL peak energy of these structures (Section 4.6.1). The τ_{rec} exhibits an analogous behavior as the overall PL decay time. Up to x= 5.5%, the τ_{rec} is relatively long, and then it strongly shortens by more than one order of magnitude for the SQW with x= 6.0%. This point is already discussed in Section 4.6.1.

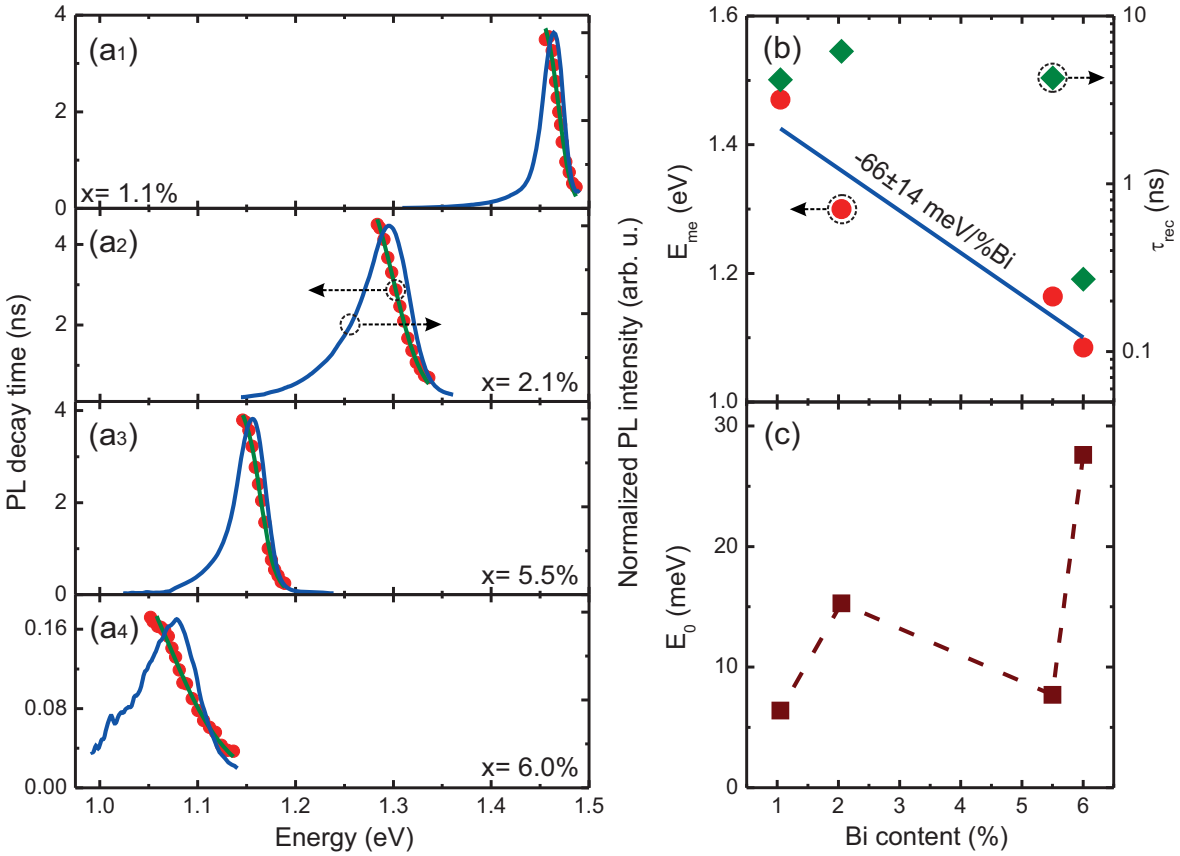

Figure 5.6: TRPL spectra for Ga($As_{1-x}Bi_x$)/GaAs SQWs with Bi contents of (a_1) 1.1%, (a_2) 2.1%, (a_3) 5.5% and (a_4) 6.0%, measured under an excitation intensity of 0.7 mW at 11 K. The red circles in (a_1)–(a_4) indicate the PL decay time as a function of the emission energy, while green lines are the fits generated using Eq. (5.13). The dependence of (b) the recombination lifetime τ_{rec} and the mobility edge E_{me}, and (c) the energy scale E_0 on the Bi content.

The obtained values of E_0 are about 6, 15, 8, and 27 meV for x= 1.1%, 2.1%, 5.5%, and 6.0%, respectively. The variation of E_0 shows a significant fluctuation with a slight tendency to increase with Bi content. A similar behavior of both E_0 and the low-temperature PL linewidth ($PL\ FWHM(0)$) versus Bi content is obviously observed in Fig. 5.6(c) and 5.7(c), respectively. The latter demonstrates the fact that the broadening of the PL spectrum is related mainly to the density of the localized states in the low energy band tail of the PL spectrum.

Dieses Werk ist copyrightgeschützt und darf in keiner Form vervielfältigt werden noch an Dritte weitergegeben werden.
Es gilt nur für den persönlichen Gebrauch.

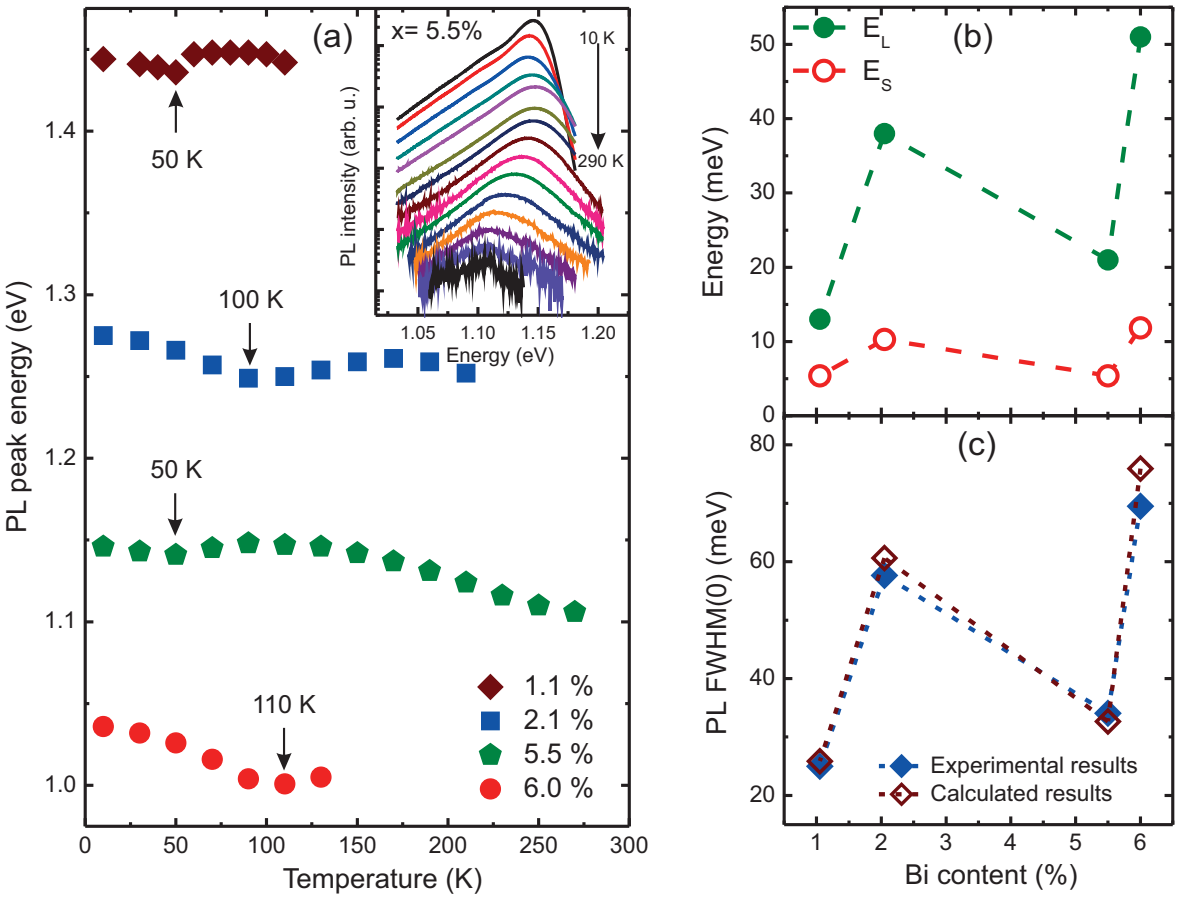

Figure 5.7: (a) temperature-dependent PL peak energy for $Ga(As_{1-x}Bi_x)$ SQW's. The inset in (a) shows emperature-dependent PL spectra for the QW with x= 5.5%. The dependence of (b) energy scales E_L and E_S, and (c) the PL linewidth on the Bi content. The values of E_L and E_S are estimated according to the extended BE-Model. The rhombuses in (c) indicate the variation of the PL linewidth; the blue closed ones are determined from TRPL spectra measured under the excitation intensity of 0.7 mW at 11 K, and the wine open ones are extracted using the relation 5.12d.

5.5.2 Extended Baranovskii-Eichmann Model

For further investigation of the impact of Bi content on the disorder in Ga(AsBi), and, on the other hand, to verify the results arise from the Gourdon and Lavallard model in the previous section, the extended BE-model by Jandieri *et al.* (Section. 5.4.1) is employed to estimate the energy-scales of disorder for the same $Ga(As_{1-x}Bi_x)$ SQW's.

Although this model has been considered for the case of bulk structure, it is used, here, for QW structures taking into account that the disorder scales can be defined as: (i) the long energy-scale of the disorder (E_L) is attributed to the potential compositional fluctuations [21] and/or the possible imperfect interfaces between the QW and the barriers [97], and (ii) the short energy-scale of the disorder (E_S) arises from the presence of Bi clusters [86] as well as the short range compositional fluctuations within the alloy structure.

Dieses Werk ist copyrightgeschützt und darf in keiner Form vervielfältigt werden noch an Dritte weitergegeben werden.
Es gilt nur für den persönlichen Gebrauch.

Experimentally, E_L relates to the energy distribution of the localized states at low temperatures and low excitation intensities and is determined from the logarithmical slope of the low-energy flank of the low-temperature PL spectrum (relation 5.12a). While E_S is extracted using the relation 5.12b with respect to the temperature (T_1) at which the PL peak energy has its local minimum within the S-shaped behavior of the temperature-dependent PL peak energy. Fig. 5.7(a) shows the temperature evolution of the PL peak energy for the four investigated samples, taken under a relatively low CW-excitation density of 8 W/cm^2 to prevent any saturation of the localized states. The long energy scale E_L is estimated to be about 25, 58, 34, and 69 meV and the short one E_S to be about 5, 10, 5, and 12 meV for *x*= 1.1%, 2.1%, 5.5%, and 6.0%, respectively. Ultimately, the low-temperature PL linewidth *PL FWHM(0)* under low excitation intensities is calculated according to the relation 5.12d. The obtained values of the *PL FWHM(0)* for the investigated structures are compared to experimental ones that are taken at 11 K in Fig. 5.7(c). An excellent agreement is obtained between the measured PL linewidth and the estimation based on the analysis of the disorder scales.

Likewise to the above-mentioned discussion on the variation in the characteristic energy scale E_0, derived from the Gourdon and Lavallard model, E_L and E_S behave similar with increasing Bi content, and obviously follow the PL linewidth; cf. Fig. 5.7(b). The fluctuation of both E_L and E_S with increasing Bi content indicates that the density of the localized states broadens differently for each sample. On the other hand, the low values of the energy scales for the SQW with a relatively high Bi content of 5.5% indicate a comparatively weak disorder potential and good optical properties of this particular sample. This is indeed desirable for long wavelength applications. Since the disorder effects are essentially related to the growth conditions, the performance of the optoelectronic devices would be enhanced if these conditions are optimized specifically.

Discussion

The above-mentioned quantitative study of the energy-scales of the disorder in Ga($As_{1-x}Bi_x$) SQW's undoubtedly demonstrates a peculiar dependence of the energy scales on the Bi content. In particular, two different theoretical models are used to estimate disorder energy-scales. The extracted energy scales fluctuate tremendously when the Bi content is varied with a weak tendency to increase with Bi content. However, the dependence of the energy-scales of the short-range disorder E_S is also performed for some Ga(AsBi) bulk structures. The results for the temperature-dependent PL peak energy for the samples with different Bi contents of 2.9%, 3.2%, 4.2%, and 4.5% are shown on the left-hand side of Fig. 5.8, where red arrows indicate the temperatures (T_1's) at which the PL peak energy curves have their local minima (within the S-shape behavior).

The values of E_S estimated by the relation 5.12b for these buk structures together with that for Ga(AsBi) SQW's studied in this thesis and other Ga(AsBi) structures previously presented in literature [108, 112, 114, 129, 130, 131], are presented on the right-hand side of Fig. 5.8. All Ga(AsBi) samples are grown by MBE technique, except the bulk structures studied in this work that are grown by MOVPE technique.

Dieses Werk ist copyrightgeschützt und darf in keiner Form vervielfältigt werden noch an Dritte weitergegeben werden.
Es gilt nur für den persönlichen Gebrauch.

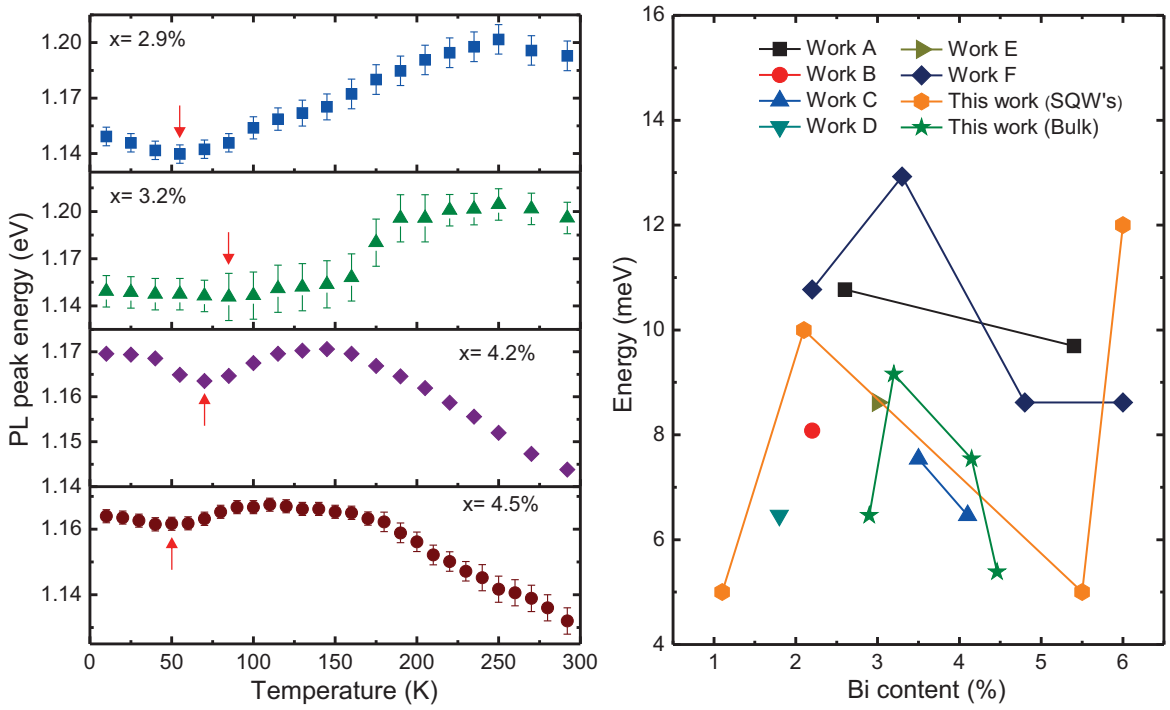

Figure 5.8: On the left-hand side: temperature dependence of the PL peak energy for the $Ga(As_{1-x}Bi_x)$/GaAs bulk structure with different Bi contents, measured under an excitation power of 1 mW. The red arrows indicate the temperatures at which the PL peak energy curves have their local minima. On the right-hand side: comparison of the short energy-scale of disorder of this work and reports in the literature: A [108], B [129], C [130], D [131], E [112], and F [114].

The behavior of E_S with increasing Bi content can be roughly summarized as follows: it increases when the Bi content is increased up to almost 3%–3.5%, decreases with increasing Bi content in the range from 3.5% to 5.5%, and ultimately saturates or dramatically increases for higher Bi content. The latter is attributed to the large increase of the defects within the Ga(AsBi) structure [67], while the reason of the behavior of the disorder energy-scales in the range of 3.5%-5.5% could be a consequence of an essential bowing of the valence band edge as a function of Bi content and of a specific compositional dependence of the hole effective mass in Ga(AsBi) compounds [132].

5.6 Energy Scaling of Compositional Disorder in Ga(NAsP)

This section deals with a study of the influence of the N content on disorder in Ga(NAsP). A set of Ga(NAsP) multi quantum wells (MQWs) with different N contents (x_N) as well as P contents (x_P) is used for this study. The studied structures were grown on (001)-oriented GaP substrate by metalorganic vapor phase epitaxy (MOVPE), where triple Ga(NAsP) layers were sandwiched pseudomorphically between GaP barriers. More details on these samples are given

Dieses Werk ist copyrightgeschützt und darf in keiner Form vervielfältigt werden noch an Dritte weitergegeben werden.
Es gilt nur für den persönlichen Gebrauch.

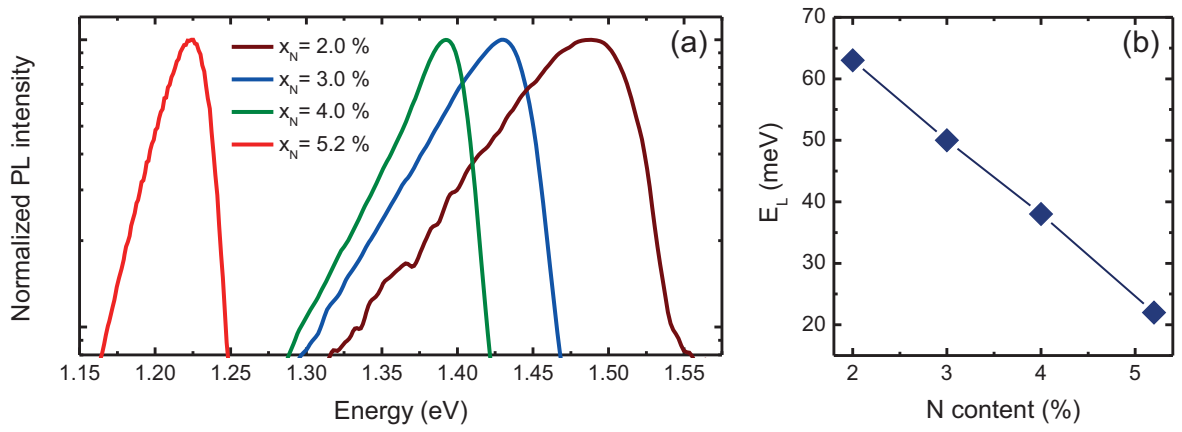

Figure 5.9: (a) low-temperature PL spectra for Ga(NAsP) MQWs with different N contents. (b) the long energy-scale of the disorder versus the N content.

in Section 3.3.1. In the following, the experimental results for disorder-induced PL features of the studied MQWs are presented. The related disorder-scales are extracted from these results. Then, an analytical theory of compositional fluctuations in semiconductor solid solutions is used for a theoretical estimation of the energy-scale of the short-range disorder. In the last part of the section, the band anti-crossing (BAC) model is employed in order to define the compositional dependence of the band gap. Furthermore, a comparison between experimental and theoretical results reveals some interesting characteristics of the studied structures.

5.6.1 Experimental Observations

Fig. 5.9(a) shows the normalized low-temperature PL spectra for the studied Ga(NAsP) MQWs[4]. The PL peak energy and the PL FWHM are shown as a function of the temperature in Figs. 5.10(a) and 5.10(b), respectively. When the nitrogen content is increased, one observes the following PL features

- For low-temperature PL spectra, both the PL peak energy and the corresponding PL linewidth decrease.
- For the temperature-dependent PL spectra, the temperatures corresponding to the local minimum of the PL peak energy as well as to the local maximum of the PL FWHM decrease.

The decrease of the low-temperature PL peak energy is common in dilute III-N-V semiconductors, e.g., N-containing III-V ternary alloys [76]. It can be well interpreted by the band-anti-crossing (BAC) model, based on the interaction between the III-V semiconductor matrix and resonant localized N states [48]. The other features, however, will be analyzed in next the sub-sections on the basis of that they could be attributed to the decrease in the energy scale of disorder with increasing N content.

[4]The experimental results for the sample with an N content of 2% are adopted from Ref. [125]

Dieses Werk ist copyrightgeschützt und darf in keiner Form vervielfältigt werden noch an Dritte weitergegeben werden.
Es gilt nur für den persönlichen Gebrauch.

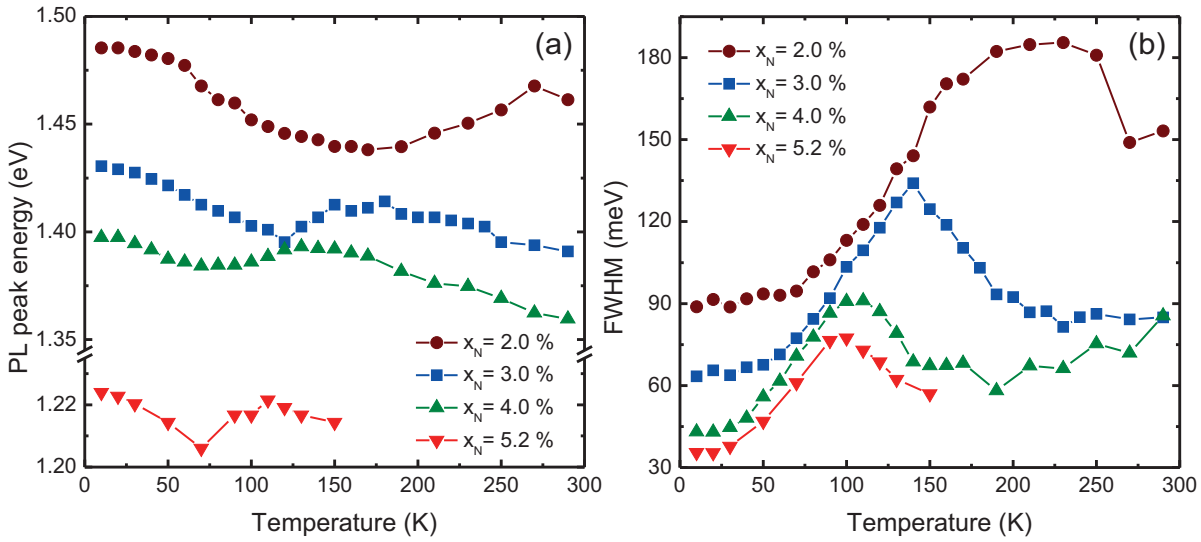

Figure 5.10: (a) the PL peak energy and (b) the PL FWHM of Ga(NAsP) MQWs as a function of the temperature.

Extraction of Disorder Energy-Scales

The disorder in Ga(NAsP) QWs is attributed to (i) long-range disorder (E_L): the long-range interface-imperfections between the QW and barriers and (ii) short-range disorder (E_S): short-range interface-imperfections and/or alloy fluctuations [84]. Taking into accounts these definitions within the extended BE-model with a double-exponential DOS (Section 5.4.1), one can extract the values of energy scales by means of the relations 5.12a, 5.12b, and 5.12c with respect, of course, to the experimental PL characteristics, i.e., β, T_1, and T_2 (Section 5.2).

Both the long energy-scale E_L and the short energy-scale E_S decrease when the N content is increased, as can be seen in Fig. 5.9(b) and Fig. 5.11(a), respectively. While E_L continuously decreases, E_S saturates for relatively high N contents, i.e., between x= 4% and x= 5.2%. Since the short range of disorder is conditioned by the compositional fluctuations, the trend of E_S is counterintuitive as the absolute deviation of the composition from the average one increases with increasing content of the fluctuating compositional component (N in the case of Ga(NAsP)). This point will be investigated in the next sub-section by applying an analytical theory for compositional fluctuations.

5.6.2 Theoretical Analysis of Compositional Disorder

In this sub-section, the energy-scale of the short-range disorder will be theoretically extracted. For this, one can utilize semiconductor solid solutions (alloys) as an example for the system with this type of disorder. The disorder in such materials arises from the random spatial distributions of their constitutive atoms that results in potential compositional fluctuations [1].

Binary semiconductor solid solutions A_xB_{1-x} (mixed crystals) are crystalline semiconductors in which the sites of the crystalline sub-lattice can be occupied by atoms of two different types, A and B. Let M be the concentration of the whole sub-lattice's sites, then x is the proba-

Dieses Werk ist copyrightgeschützt und darf in keiner Form vervielfältigt werden noch an Dritte weitergegeben werden.
Es gilt nur für den persönlichen Gebrauch.

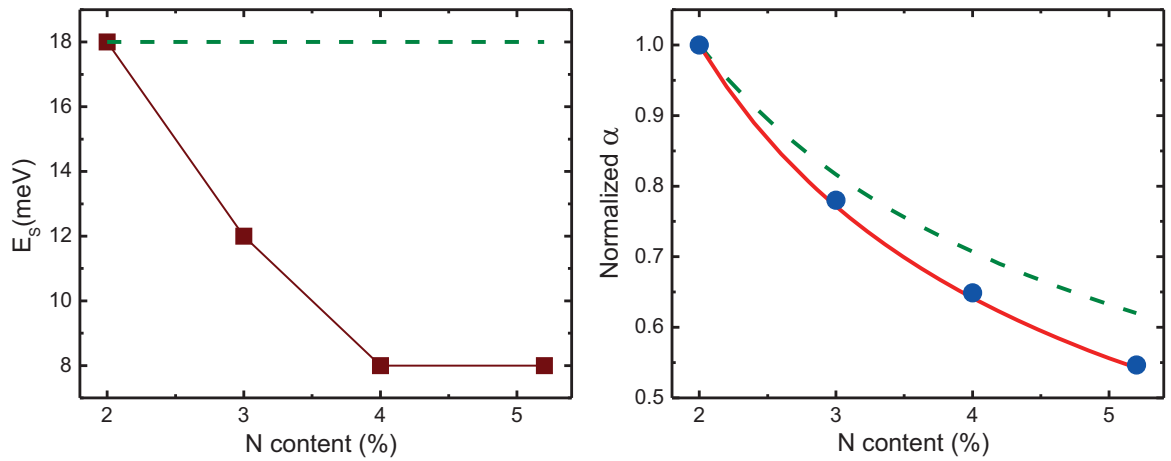

Figure 5.11: (a) the short energy-scale of the disorder (E_S or E_0) as a function of the N content: squares indicate experimentally obtained values, while the dashed line is estimated from the BAC model taking into account a constant effective-mass of the exciton. (b) the dependence of α on the N content: circles and dashed line are estimated from the theory of compositional disorder and the BAC model, respectively, for a constant value of the exciton effective-mass. The solid line shows the power dependence between α, estimated from the theory of compositional disorder, and N content.

bility that some of these sites are occupied by A atoms [133]. Since the energy-position of the band edge depends on the composition x, the fluctuations in local x values appear in the band edge, subsequently. Let us consider the impact of compositional fluctuations on the bottom of the conduction band. Fig. 5.12 shows a possible schematic dependence of the conduction band minimum E_c on the composition x. In particular, the local positions of the band edge $E_c(x)$ fluctuate around the average value $E_c(x_0)$ according to the fluctuations of the composition x around x_0, where the latter is the average composition for the considered volume $R \times R \times R$. For small fluctuations Δx, one can use the linear relation

$$E_c(x_0 + \Delta x) \simeq E_c(x_0) + \alpha\, \Delta x\,, \tag{5.14}$$

where α is the compositional variation of the conduction band edge:

$$\alpha = \left(\frac{\partial E_c(x)}{\partial x} \right)_{x=x_0}. \tag{5.15}$$

Thus, in the considered volume R^3, a potential well is formed with a height of the order

$$V \simeq \alpha\, \Delta x\,, \tag{5.16}$$

where Δx can be determined from the ratio between the excess number of atoms A to the total number of the sites among the considered volume [125], then,

$$\Delta x \simeq \frac{(x\, M\, R^3)^{1/2}}{M\, R^3}\,, \tag{5.17}$$

Dieses Werk ist copyrightgeschützt und darf in keiner Form vervielfältigt werden noch an Dritte weitergegeben werden.
Es gilt nur für den persönlichen Gebrauch.

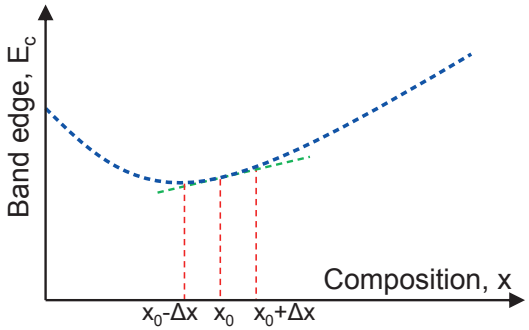

Figure 5.12: Schematic drawing of the dependence of the conduction band edge E_c on composition x in a binary semiconductor solid solution A_xB_{1-x}.

hence,

$$V \simeq \frac{\alpha\,(x\,M\,R^3)^{1/2}}{M\,R^3}\,. \tag{5.18}$$

An electronic level close to V will exist in this well, when V and R satisfy the inequality $V > \hbar^2/mR^2$, where m is the electron effective-mass. If the opposite inequality is valid, the well has no level at all.

As the energy V increases with decreasing R, the most effective of the wells are ostensibly those with small R. On the other hand, potential fluctuations in a small volume R^3, i.e., small R, should be very deep in order to play any role since $V > \hbar^2/mR^2$ must be fulfilled to get any localized states. So, it is necessary to find a compromise to set R in Eq. (5.18). However, the lowest value of R can be determined from the boundary condition, $V = \hbar^2/mR^2$, and it is

$$R \simeq \frac{M\,\hbar^4}{x\,\alpha^2\,m^2}\,. \tag{5.19}$$

Substituting Eq. (5.19) into Eq. (5.18), the smearing of the band edge is found by Baranovskii and Efros [134] of the order of

$$E_0 \simeq \frac{\alpha^4\,m^3\,x^2\,(1-x)^2}{M^2\,\hbar^6}\,. \tag{5.20}$$

This equation connects an experimental characteristic (E_0) to some crucial material characteristics (α and m). So, knowing the values of E_0 provides useful information about the studied Ga(NAsP) structures. However, to estimate E_0, using Eq. (5.20) one should take some items into account:

- **Both following conditions are fulfilled:** (i) due to the low excitation intensity the PL spectrum is dominated by the recombination of correlated electron-hole-pairs forming excitons [84, 127], and furthermore (ii) the spatial scale of exciton localization is essentially larger than the exciton radius. Here, the exciton mass is a sum of electron mass and hole mass, $m = m_e + m_h$. One can use here the mass of heavy holes for m_h owning to their large density of states [125].
- **What material component is responsible for the compositional disorder in Ga(NAsP)?** The fluctuations in both N and P contents provide localization centers for

Dieses Werk ist copyrightgeschützt und darf in keiner Form vervielfältigt werden noch an Dritte weitergegeben werden.
Es gilt nur für den persönlichen Gebrauch.

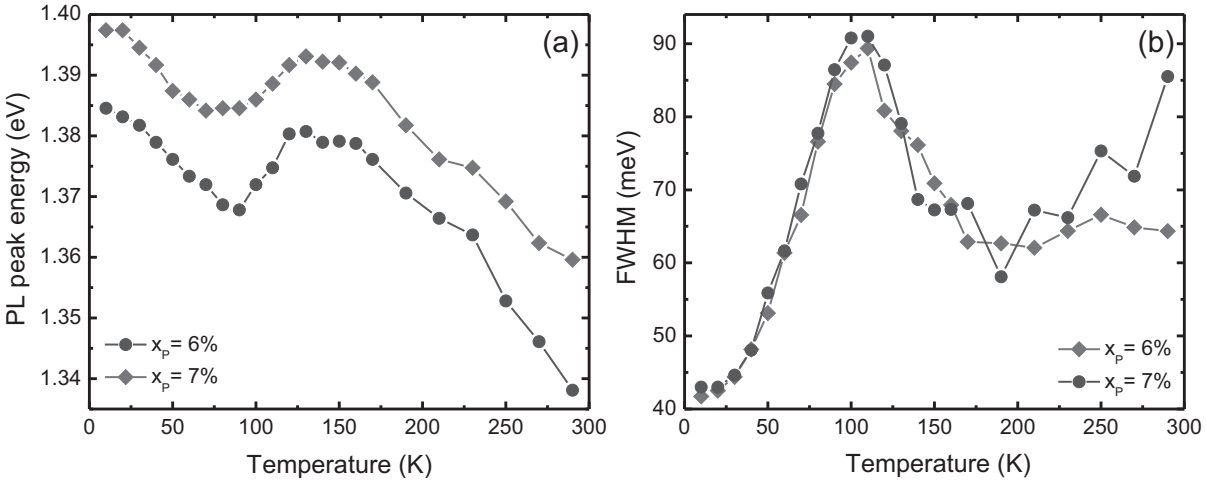

Figure 5.13: Temperature-dependent (a) PL peak energy and (b) PL FWHM for two Ga(NAsP) MQWs with different P content and a constant N content of 4%.

excitons. While the fluctuation of the P content slightly affects both conduction- and valence band-edges, the fluctuation of the N content mainly affects the conduction band edge due to the extremely strong anti-crossing interaction [41, 42] between the localized nitrogen states and the extended states of the semiconductor matrix.

From an experimental point of view, the values of $\alpha_N = \partial E_c/\partial x_N \simeq \partial E_g/\partial x_N$ in the studied samples are in the range of 6–12 eV (Fig.5.11(a)), while the values of $\alpha_P = \partial E_g/\partial x_P$ are in the range of 1.1–1.2 eV [36]. This can be also seen in the slight change in the characteristic PL features when the P content, x_P is increased from 6% to 7% for a constant N content of x_N= 4% (Fig. 5.13). The blue-shift of the PL energy peak in Fig. 5.13(a) is attributed to the change in the QW width from 6.7 nm for x_P= 6% to 5.4 nm for x_P= 7%.

On the basis of above-mentioned facts, one can conclude that the disorder energy-scale E_0 given by Eq. (5.20) is mainly determined by fluctuations of the N content in the case of Ga(NAsP). Thus, Eq. (5.20) can be specified for this case by using N content for x, where M is represented by the concentration of sites for group V elements in Ga(NAsP) structure.

- **The localization of the carrier wave-function:** the calculation of conduction- and valence-band offsets for studied samples reveals that their values are ΔE_c= 1.0 eV and ΔE_v= 0.5 eV, respectively. These values insure large depths of the QWs for conduction and valence band edges. Hence, less than 10% of the electron wave functions can penetrate into the GaP barriers, where no compositional disorder is present. For the hole wave-function the effect is even less pronounced. Therefore, wave functions of electrons and holes are taken into account to be primarily localized within the QW [125].

Dieses Werk ist copyrightgeschützt und darf in keiner Form vervielfältigt werden noch an Dritte weitergegeben werden.
Es gilt nur für den persönlichen Gebrauch.

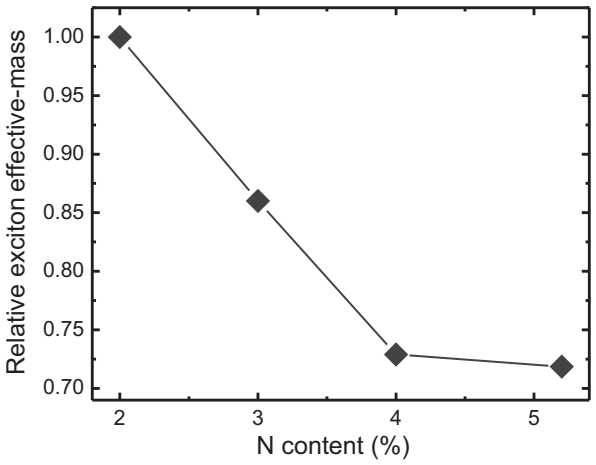

Figure 5.14: Relative exciton effective mass as a function of the N content.

Comparison between Experimental and Theoretical Results

Assuming a constant effective mass m, one can extract the compositional variation of the conduction band edge α by inserting the values of the experimentally estimated energy-scale of disorder E_S into Eq. (5.20). Solid circles in Fig. 5.11(b) show the values of α as a function of the N content x_N. Besides, the solid line in Fig. 5.11(b) indicates the power dependence, $\alpha \propto x_N^{-0.64}$, between α and N content.

On the other hand, it is possible to obtain the relation between α and x_N theoretically using the BAC model. For a fair comparison, however, a *constant* effective mass of the exciton m is taken into account through the analysis using the BAC model. This results in a power function of $\alpha \propto x_N^{-0.5}$, represented by a dashed line in Fig. 5.11(b) [125]. Yet, inserting this relation into Eq. (5.20) results in an independence of the energy scale of the compositional disorder E_0 on the nitrogen content x_N, as shown in Fig. 5.11(b) by the dashed line. However, since the experimental results evidence that the energy scale of the compositional disorder E_S decreases with increasing N content, one can conclude that a constant effective mass can be somehow a poor approximation. Therefore, one should take m into account as a *non-constant* parameter in Eq. (5.20). The exciton effective-mass in the studied samples can be predicted from the comparison between the calculated and experimentally observed energy scales of the compositional disorder. In details, α can be calculated using the BAC model and then inserted into Eq. (5.20). Thereafter, using the experimental values of the short energy-scale of the disorder E_S in Eq. (5.20) allows one to estimate the relative values of the exciton effective-mass that provide the best agreement between the experimental and calculated results [125]. Fig. 5.14 shows the values of the exciton effective mass estimated by applying the above-mentioned manner. The value of m varies with increasing N content with a trend to decrease up to x_N=4, and then it saturates for higher N contents.

Although an increase in the effective mass has been frequently reported for dilute III-N-V semiconductors with increasing N content [41, 74, 89, 135], an opposite behavior is here observed for Ga(NAsP)/GaP MQWs. Such a decrease in the effective mass with increasing N content was reported in the case of Ga(NAsP) bulk structures. In particular, the effective mass

Dieses Werk ist copyrightgeschützt und darf in keiner Form vervielfältigt werden noch an Dritte weitergegeben werden.
Es gilt nur für den persönlichen Gebrauch.

in the (100) direction was found to decrease from $0.46m_0$ ($0.23m_0$) for an N content of 1% to $0.25m_0$ ($0.15m_0$)[5] for an N content of 3%, both are for an As content of about 30% (70%) [136]. Despite the decrease in the value of the effective mass in Ga(NAsP) with increasing N content, it is still higher than that for GaAs ($m^*_{GaAs} = 0.07m_0$ [137]).

The theoretical analysis presented in this section shows that the reduced effective-mass and the specific dependence of the conduction band edge on the N content can be the reason for the reduced the energy scale of the compositional disorder in the Ga(NAsP) system.

5.7 Summary

A quantitative description of disorder-induced PL features in some disordered semiconductors is presented in this chapter. Beside the shape of the density of states (DOS) in the disorder-induced band tails, the origin of disorder effects is crucial for a well interpretation of non-monotonous behavior of PL spectra in disordered semiconductors.

A phenomenological model (BE-model) with one energy-scale of the disorder is suggested for the explanation of disorder-induced PL features. The key point of this model is phonon-assisted hopping-transitions performed by localized excitons between localized states before their recombination. The BE-model was applied successfully to analyze the disorder in (GaIn)(NAs), where the DOS has in this case an exponential shape. The energy scales of the disorder are determined through comparison between simulated and experimental results of PL spectra.

An extension of BE-model was inescapable to correctly reproduce disorder-induced PL features in some disordered semiconductors. This has been achieved by introducing an additional energy-scale of the disorder taking into account the reason for the emergence of disorder within the semiconductor structure. A double exponential shape of the DOS with two energy-scales is suggested for a study of the disorder in G(NAsP), while a combination of Gaussian and exponential energy-distributions of localized states is employed in the case of Ga(AsBi).

In spite of the intuitive thought that the energy scales of disorder potential should increase when the concentration of the fluctuating compositional component is increased, these scales show an odd dependence of the Bi content in Ga(AsBi) structures. In particular, the influence of the Bi content on the disorder, i.e., energy scales of the disorder, in Ga(AsBi) SQW's is studied using two theoretical models: (i) a straightforward model with a single energy-scale is based on the carrier dynamics at very low temperatures, and (ii) an excitonic hopping model with two energy scales (extended BE-model) is based on the features of the PL spectra. The extracted energy scales fluctuate tremendously when the Bi content is increased with a weak tendency to increase with Bi content. However, a decrease of the energy-scale related to the compositional disorder is reported in a range of Bi content from 3.5% to 5.5% for different Ga(AsBi) structures.

A decrease of disorder energy-scales is observed when the N content is increased in Ga(NAsP) MQWs. This peculiar behavior is theoretically analyzed for the energy-scale of

[5] m_0 is the free electron mass.

Dieses Werk ist copyrightgeschützt und darf in keiner Form vervielfältigt werden noch an Dritte weitergegeben werden.
Es gilt nur für den persönlichen Gebrauch.

the short-range compositional-fluctuations. This analysis is supported by some calculations using BAC model. The reason of the decrease of the short energy-scale in Ga(NAsP) MQWs is attributed to the decrease of both (i) the impact on the band structure, and (ii) the exciton effective-mass.

Dieses Werk ist copyrightgeschützt und darf in keiner Form vervielfältigt werden noch an Dritte weitergegeben werden.
Es gilt nur für den persönlichen Gebrauch.

6 Quantitative Description of the Photoluminescence Thermal Quenching in Ga(AsBi)

6.1 Introduction

In recent years, disordered Ga(AsBi) semiconductor alloys have attracted increasing interest, driven by not only their great potential in long-wavelength optoelectronic applications but also their interesting physical properties. The disorder in these novel materials is attributed to potential fluctuations associated with the Bi content [138] together with the existence of Bi clusters within the alloy structure [24]. Furthermore, potential imperfect interfaces in the case of Ga(AsBi) semiconductor heterostructures lead to an additional degree of disorder [25].

Disorder effects lead to an increasing density of localized states (DOS) and hence affect drastically carrier recombination processes. Therefore, a good understanding of carrier recombination mechanisms involved within Ga(AsBi) semiconductors indirectly provides information about the quality of their structures. For this aim, photoluminescence (PL) spectroscopy is widely used for investigating the optical properties of semiconductors andit has become a key method for characterizing material quality [67, 112]. As above-presented in Chapter 4, disorder-induced characteristics of temperature-dependent PL spectra are a non-monotonous behavior of the temperature-dependent PL peak energy (the so-called S-shape), a local maximum peak in the temperature-dependent PL linewidth within a narrow temperature range, and a strong temperature dependence of the PL intensity. While unusual temperature dependences of the PL peak energy and the PL linewidth reflect the phonon-assisted hopping-transitions of localized excitons between localized states [81], the dramatic decrease of the PL intensity with increasing temperature is attributed to the increased non-radiative recombination of thermally delocalized carriers [110].

The anomalous temperature-dependent PL peak energy as well as PL linewidth for Ga(AsBi) has been interpreted within the framework of a model with two spatial and energy scales for the disorder potential [86]. Within this two-scale model the DOS below the mobility edge is described by two different energy distributions: (i) a Gaussian energy distribution corresponding to the long-range disorder, conditioned by the fluctuations of the Bi content in the alloy and (ii) an exponential energy distribution corresponding to a short-range disorder, which was ascribed to Bi clusters. The spatially much more localized states of the exponential energy-scale form an exponential tail for each of the spatially more extended states of the Gaussian energy-scale. Hence, the overall DOS is a convolution of the Gaussian and exponential distri-

Dieses Werk ist copyrightgeschützt und darf in keiner Form vervielfältigt werden noch an Dritte weitergegeben werden.
Es gilt nur für den persönlichen Gebrauch.

bution of states. On the other hand, the thermal quenching of the integrated PL intensity within this two-scale model has been treated using only the exponential DOS corresponding to the short-range disorder. Such approach was motivated by the assumption that Gaussian states are so much extended in space that an exciton being thermally excited from the exponential DOS tail to the corresponding Gaussian state can encounter centers of non-radiative recombination from this state.

The purpose of this chapter: in this chapter, it will be demonstrated that the conventional theoretical models assuming a monotonous, e.g., exponential [86], DOS for the short-range disorder cannot be considered as an universal approach for the correct description of the temperature-induced PL quenching in Ga(AsBi) alloys. In particular, a peculiar feature is experimentally observed in Ga(AsBi)/GaAs heterostructures under relatively low excitation intensities, i.e., the temperature-induced PL quenching exhibits an anomalous plateau at intermediate temperatures. However, the calculated results based on a well-approved theoretical analysis prove that a non-monotonic DOS with at least two different components is necessary to explain the observed PL quenching. These components have different energy –but comparable spatial– scales. The localization length of the states in both components of the DOS is assumed to be so small that excitons can not encounter centers of non-radiative recombination from these states. Instead, the excitons must be excited above the mobility edge in order to recombine non-radiatively [139, 140, 141]. Therefore, in contrast to the two-scales model suggested by Imhof *et al.* [86], both components of the DOS and, hence, both energy scales are relevant for theoretical description of PL thermal quenching in Ga(AsBi) alloys.

The chapter is organized as follows. The experimental observations are given in Section 6.2. Section 6.3 presents the theoretical treatment of the observed PL thermal quenching in the framework of the suggested two-component model. Calculated results based on this theoretical analysis are presented in Section 6.4. The impact of Bi content on fit parameters is shown in Section 6.5. A number of points related to the presented theoretical analysis and the ensuing calculated results are discussed in Section 6.6.

6.2 Experimental Observations

The samples used in this study are a series of Ga($As_{1-x}Bi_x$)/GaAs heterostructures with Bi contents of $x = 2.9\%$, 3.2%, 4.2%, and 4.5%, which are grown by metal organic vapor phase epitaxy (MOVPE) on undoped exact (001) GaAs substrates. More details on the samples' characteristics and preparation are found in Section 3.3.3. Temperature-dependent measurements are performed using time-resolved PL (TRPL) technique, where the excitation intensity is set to an average laser power of 1 mW for all measurements.

Fig. 6.1(a) shows PL spectra of the sample with Bi content of 4.2% measured at various temperatures in a range from 10 K to room temperature (RT). At low temperatures PL emission peaks are significantly broad and show an asymmetric lineshape with a low energy tail. This reflects the fact that the dominant contribution to the PL arises from localized electron–hole pairs [127]. The temperature dependencies of the PL peak energy together with the corresponding full width at half maximum (FWHM), are shown in Fig. 6.1(b). They follow the main trends

Dieses Werk ist copyrightgeschützt und darf in keiner Form vervielfältigt werden noch an Dritte weitergegeben werden.
Es gilt nur für den persönlichen Gebrauch.

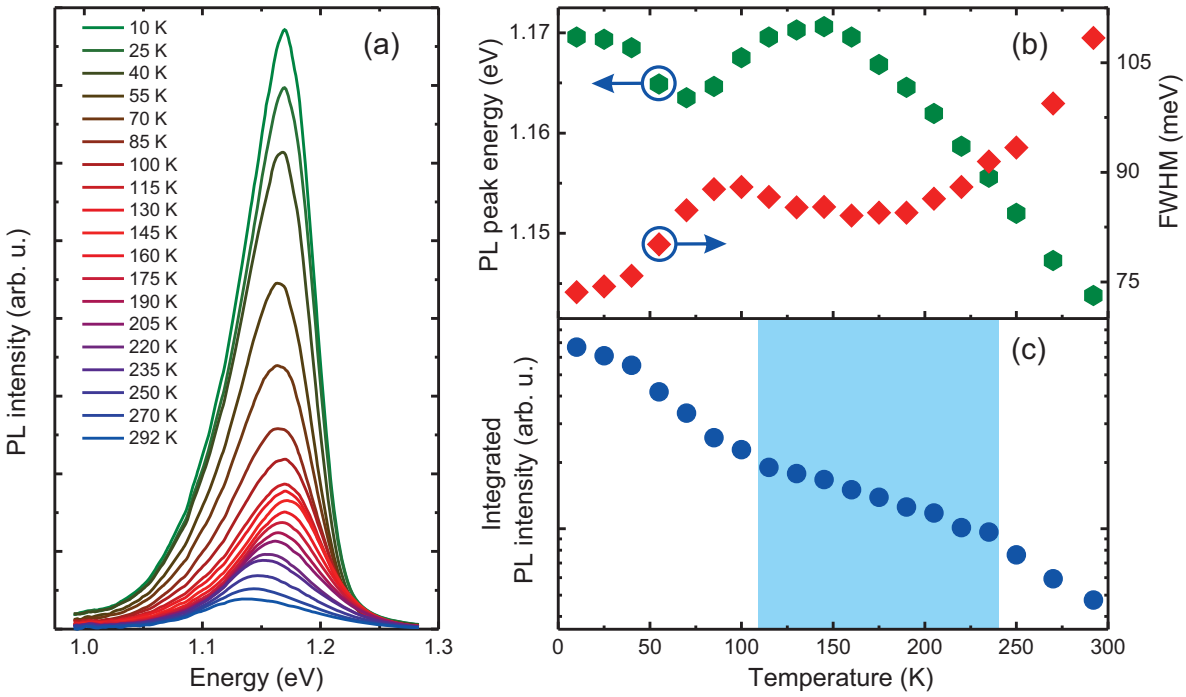

Figure 6.1: (a) temperature-dependent PL spectra of the Ga(AsBi)/GaAs heterostructure with Bi content of 4.2%, measured at an excitation intensity of 1 mW. (b) the corresponding PL peak energy together with PL FWHM as a function of the temperature. (c) the temperature dependence of the integrated PL intensity.

common for disordered compound semiconductors (Section 4.4.1). In particular, the PL peak energy exhibits a typical S-shape behavior with a local minimum around 70 K, whereas the PL FWHM shows a local maximum of about 88 meV at a temperature of approximately 100 K. These specific features are generally attributed to the hopping dynamics of photo-excited excitons between the disorder-induced localized states [81].

In contrast to the temperature dependencies of the PL peak energy and the PL FWHM, the thermal quenching of the integrated PL intensity, shown in Fig. 6.1(c), exhibits an odd behavior as compared to common tendencies previously observed in disordered semiconductors, [21, 78, 110]. The prominent characteristic of the typical PL thermal quenching in disordered semiconductors is a relatively weak temperature dependence at low temperatures, followed by a dramatic decline in an intermediate range of temperature, and ultimately, by a saturation close to RT. As an example, the typical temperature-induced quenching of the PL intensity observed in Ga(NAsP)/GaP quantum wells [110] is shown in Fig. 6.2(a). Remarkably, a similar behavior has been reported in Ga(AsBi) under relatively high excitation intensities [86] (Fig. 6.2(b)). However, in the case of relatively low excitation intensities, the situation is essentially different. The PL thermal quenching can be clearly distinguished in three regimes. A plateau area (shaded area between 115 K and 235 K in Fig. 6.1(c)) with rather weak temperature dependence separates two major regimes, where the quenching rate of the PL intensity is more pronounced. A similar peculiar behavior of the PL thermal quenching in Ga(AsBi) has been also previously observed [107].

Dieses Werk ist copyrightgeschützt und darf in keiner Form vervielfältigt werden noch an Dritte weitergegeben werden.
Es gilt nur für den persönlichen Gebrauch.

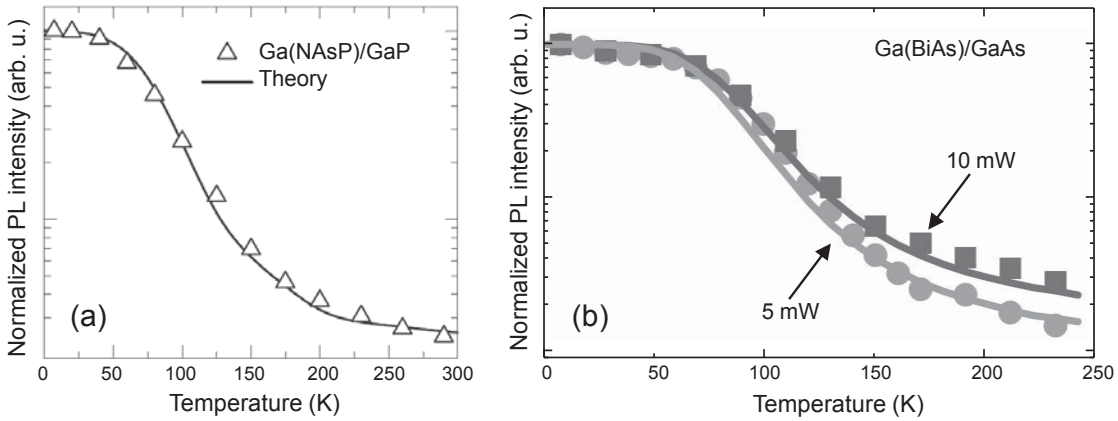

Figure 6.2: Experimental (symbols) and theoretical (lines) results for the temperature-dependent PL intensity of (a) Ga(NAsP)/GaP (after Rubel *et al.* [110]) and (b) Ga(AsBi)/GaAs (after Imhof *et al.* [86])

6.3 Theoretical analysis

The widely-known empirical formula for the expression of the temperature-induced decrease of the PL intensity in amorphous semiconductors has an exponential form [72]

$$I(T) = I_0 \exp\left(-\frac{T}{T_1}\right), \tag{6.1}$$

where I_0 is the PL intensity at T= 0 K and T_1 is a characteristic temperature.

In 1979, Gee and Kastner [142] suggested a model for the description of the PL thermal quenching in amorphous SiO_2 giving some definition of T_1 in Eq. (6.1). According to this model, the PL intensity can be theoretically calculated by

$$I = \int g(\varepsilon) \cdot p(\varepsilon,T)\, d\varepsilon\,. \tag{6.2}$$

Here, $g(\varepsilon)$ represents the distribution of activation energies for non-radiative processes, and it has an exponential form

$$g(\varepsilon) = \frac{1}{k_B T_0} \exp\left(-\frac{\varepsilon}{k_B T_0}\right), \tag{6.3}$$

with some characteristic temperature T_0. k_B is the Boltzmann constant. $p(\varepsilon,T)$ in Eq. (6.2) is the probability of radiative recombination and can be obtained from the following ratio

$$p(\varepsilon,T) = \frac{\nu_r}{\nu_r + \nu_{nr}}\,, \tag{6.4}$$

where ν_r and ν_{nr} are the radiative and non-radiative recombination rates, respectively. On the other hand, the non-radiative recombination rate ν_{nr} is given by [142]

$$\nu_{nr} = \nu_0 \cdot \exp\left(-\frac{\varepsilon}{k_B T}\right), \tag{6.5}$$

Dieses Werk ist copyrightgeschützt und darf in keiner Form vervielfältigt werden noch an Dritte weitergegeben werden.
Es gilt nur für den persönlichen Gebrauch.

where ν_0 is the attempt-to-escape frequency for the activation process. This leads to the probability of radiative recombination of the form

$$p(\varepsilon,T) = \left[1 + \frac{\nu_0}{\nu_r} \exp\left(-\frac{\varepsilon}{k_B T}\right)\right]^{-1} . \tag{6.6}$$

Substituting Eq. (6.3) and Eq. (6.6) into Eq. (6.2) indicates a proportional relation between T_0 and T_1.

Later, Orenstein and Kastner [139] and Street [109] ascribed the distribution of barriers to the density of localized states $g(\varepsilon)$ in the band tails of disordered semiconductors. Herewith was assumed that non-radiative recombination occurs via thermal activation of photo-excited excitons from radiative localized band tail states towards the mobility edge, since only mobile excitons are able to reach the spatially remote centers of non-radiative recombination. Assuming that the exciton thermally activated to the mobility edge does not necessarily recombine non-radiatively but can be recaptured into a radiative state, the non-radiative recombination rate can be expressed as

$$\nu_{nr} = \left(\frac{\sigma_{nr} N_{nr}}{\sigma_r N_r + \sigma_{nr} N_{nr}}\right) \cdot \nu_0 \cdot \exp\left(-\frac{\varepsilon}{k_\mathrm{B} T}\right) , \tag{6.7}$$

where ε is, here, the energy of the localized state measured from the mobility edge, and N_{nr}, σ_{nr} and N_r, σ_r are the density and capture cross sections of non-radiative and radiative centers, respectively. Eq. (6.7) together with the radiative recombination rate $\nu_r = \tau_0^{-1}$ [110], where τ_0 is the exciton lifetime, gives the following expression for the probability of radiative recombination

$$p(\varepsilon,T) = \left[1 + \nu_0 \tau_0 \frac{\sigma_{nr} N_{nr}}{\sigma_r N_r + \sigma_{nr} N_{nr}} \exp\left(-\frac{\varepsilon}{k_B T}\right)\right]^{-1} . \tag{6.8}$$

For a given density of localized states $g(\varepsilon)$ and for the probability of radiative recombination $p(\varepsilon,T)$ determined from Eq. (6.8), the temperature-dependent PL intensity can then be described as

$$I(T) = I_0 \int_0^\infty g(\varepsilon) \cdot p(\varepsilon,T)\, d\varepsilon , \tag{6.9}$$

where I_0 is the PL intensity at zero temperature [142].

Next, Eq. (6.9) is applied to fit the experimental results for the PL thermal quenching in studied Ga($As_{1-x}Bi_x$)/GaAs heterostructures at relatively low excitation intensities.

6.4 Calculations

In the following, for simplification, it is assumed that the radiative and non-radiative centers have the same capture cross section. Hence, Eq. (6.8) reads

$$p(\varepsilon,T) = \left[1 + \nu_0 \tau_0 \frac{N_{nr}}{N_r + N_{nr}} \exp\left(-\frac{\varepsilon}{k_B T}\right)\right]^{-1} . \tag{6.10}$$

Dieses Werk ist copyrightgeschützt und darf in keiner Form vervielfältigt werden noch an Dritte weitergegeben werden.
Es gilt nur für den persönlichen Gebrauch.

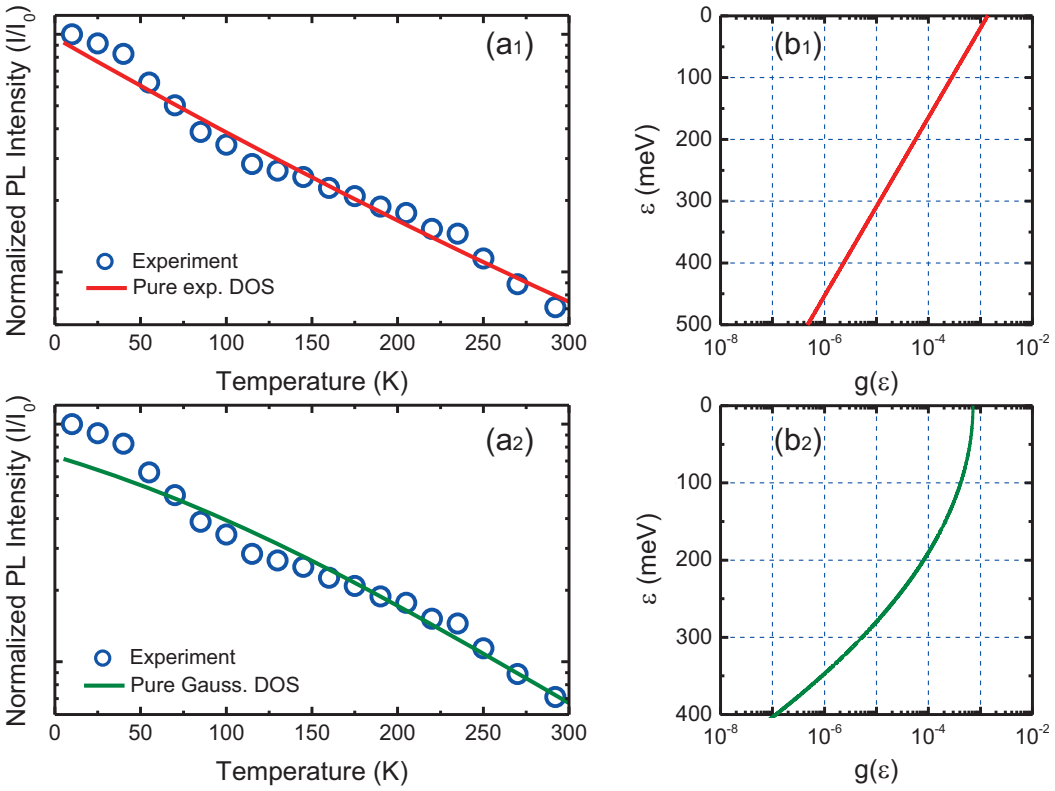

Figure 6.3: The temperature-dependent integrated PL intensity (I) of the sample with a Bi content of 4.2%. Open circles in (a_1) and (a_2) indicate the experimental data, normalized to the PL intensity at 10 K (I_0). Solid lines in (a_1) and (a_2) represent calculated results obtained from Eq. (6.11) for purely exponential DOS (b_1) and purely Gaussian DOS (b_2), respectively.

One can obtain the temperature dependence of the PL intensity by substituting Eq. (6.10) into Eq. (6.9) with a particular DOS [106],

$$I(T) = I_0 \int_0^\infty g(\varepsilon) \cdot \left[1 + \nu_0 \tau_0 \frac{N_{nr}}{N_r + N_{nr}} \exp\left(-\frac{\varepsilon}{k_B T}\right)\right]^{-1} \cdot d\varepsilon \,. \tag{6.11}$$

However, the shape of the energy distribution of the DOS plays a critical role as will be next shown, where a monotonous DOS fails to fit the odd behavior of the PL thermal quenching in Ga(AsBi), whereas a non-monotonous DOS succeeds.

6.4.1 Monotonous Density of States

To fit the experimental results for the PL thermal quenching in the Ga(AsBi) sample with a Bi content of 4.2%, prominent energy distributions of the DOS in disordered systems are used in Eq (6.11). In particular, trying to apply Eq (6.11) in combination with the commonly used exponential DOS, $g(\varepsilon) \propto \exp(-\varepsilon/\sigma)$ with some characteristic energy σ (Fig. 6.3(b_1)), one can clearly see that the calculated resultes cannot correctly fit the experimentally observed temperature-dependent PL intensity. While the measured temperature dependence of

Dieses Werk ist copyrightgeschützt und darf in keiner Form vervielfältigt werden noch an Dritte weitergegeben werden.
Es gilt nur für den persönlichen Gebrauch.

the PL intensity shows a peculiar plateau at temperatures between 115 K to 235 K, no theoretical curves based on the exponential DOS can reproduce this behavior as illustrated by the solid curve in Fig. 6.3(a_1). Moreover, replacing the exponential DOS with a Gaussian DOS, $g(\varepsilon) \propto \exp(-\varepsilon^2/2\sigma^2)$ (Fig. 6.3(b_2)), does not help to account for the plateau in the experimental results for the PL thermal quenching as illustrated by the solid curve in Fig. 6.3(a_2).

6.4.2 Non-monotonous Density of States

Since a monotonous distribution of localized states below the mobility edge fails to reproduce the plateau in the temperature dependence of PL intensity (Figs. 6.3(a_1) and 6.3(a_2)), combinations of the two most prominent energy distributions in disordered systems is assumed,

$$g(\varepsilon;\varepsilon_M,\sigma_1,\sigma_2) = (1-y)\, g_1(\varepsilon;0,\sigma_1) + y\, g_2(\varepsilon;\varepsilon_M,\sigma_2)\ , \tag{6.12}$$

where g_1 and g_2 are either of exponential (g_E) or Gaussian type (g_G) with

$$g_E(\varepsilon;\varepsilon_M,\sigma) = \Theta\left(\varepsilon-\varepsilon_M\right)\frac{1}{\sigma}\,\exp\left(-\frac{\varepsilon-\varepsilon_M}{\sigma}\right)\ , \tag{6.13}$$

and

$$g_G(\varepsilon;\varepsilon_M,\sigma) = \frac{1}{\sqrt{2\pi}\,\sigma\,\Phi\left(\frac{\varepsilon_M}{\sigma}\right)}\,\exp\left[-\frac{1}{2}\left(\frac{\varepsilon-\varepsilon_M}{\sigma}\right)^2\right]\ . \tag{6.14}$$

Here, Θ and Φ denote the Heaviside step-function and the normal cumulative distribution function, respectively, and σ_1 and σ_2 are characteristic energies. Four different distribution functions arise from this definition of $g(\varepsilon)$, a double exponential DOS, a double Gaussian DOS, and two composite DOS's with exponential and Gaussian parts. In the two cases of $g_2 = g_E$, a mathematical unsteadiness appears at ε_M in the DOS due to the Heaviside step-function which may seem unphysical. Despite this artificial structure of the unsteady DOS, all four distributions will be attempted in order to account for the experimental data. Considering ε_M, σ_1 and σ_2 as fitting parameters, an excellent agreement is obtained between the measured temperature-dependent PL intensity and theoretical curves, calculated by applying Eqs. (6.11)–(6.14) for all four possible combinations of the DOS. This is shown in Figs. 6.4(a_1)–6.4(a_4) along with the corresponding shape of the DOS in Figs. 6.4(b_1)–6.4(b_4) for the "exponential plus exponential", "exponential plus Gaussian", "Gaussian plus exponential" and "Gaussian plus Gaussian" distributions, respectively.

The respective contributions from the first $(1-y)\, g_1$ and second $y\, g_2$ parts of the DOS to the overall PL intensity are also depicted in Figs. 6.4(a_1)–6.4(a_4) by short-dashed green and long-dashed red curves, respectively. The corresponding values of fitting parameters ε_M, σ_1, σ_2 and y are summarized in Table 6.1. Around $y = 10\%$ of the states of the composite $g(\varepsilon)$ are provided by the second parts $g_2(\varepsilon;\varepsilon_M,\sigma_2)$ whose maxima ε_M vary between 129 meV and 155 meV. The characteristic energies σ_1 and σ_2 of the two parts of the composite DOS lay between 17 meV and 33 meV. It should be noted that the given values of y, ε_M, σ_1 and σ_2 do also depend upon the parameter $\nu_0\tau_0(1+N_r/N_{nr})^{-1}$ which is set to 10^{-3} after Ref. [86].

Dieses Werk ist copyrightgeschützt und darf in keiner Form vervielfältigt werden noch an Dritte weitergegeben werden.
Es gilt nur für den persönlichen Gebrauch.

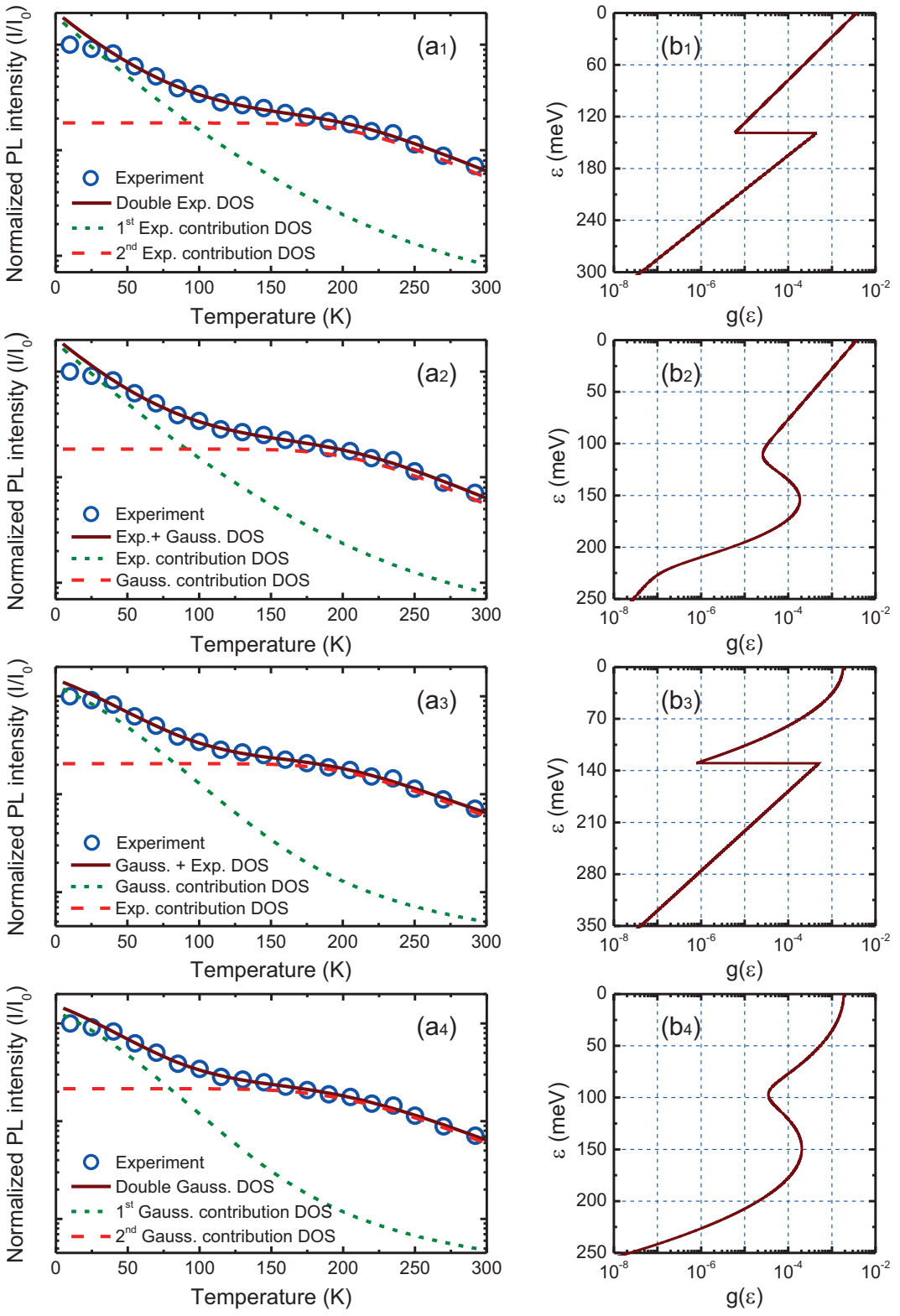

Figure 6.4: Experimental (open circles) and calculated (lines) results for the temperature-dependent PL intensity of the sample with x= 4.2% for either (a_1) double–exponential, (a_2) exponential–plus–Gaussian, (a_3) Gaussian–plus–exponential, or (a_4) double–Gaussian DOS's. (b_1), (b_2), (b_3), and (b_4) show the densities of localized states $g(\varepsilon)$ as a function of the energy difference ε from the mobility edge for each of the solid lines in (a_1), (a_2),(a_3), and (a_4), respectively.

Dieses Werk ist copyrightgeschützt und darf in keiner Form vervielfältigt werden noch an Dritte weitergegeben werden.
Es gilt nur für den persönlichen Gebrauch.

Table 6.1: Fit parameters, obtained by minimizing the deviations of $I(T)$ calculated with Eq. (6.11) from the measured one, for various DOS's extracted from Eqs. (6.12)–(6.14).

g_1	g_2	y (%)	σ_1 (meV)	σ_2 (meV)	ε_M (meV)
g_E	g_E	9	22	17	139
g_E	g_G	9	21	17	155
g_G	g_E	14	33	23	129
g_G	g_G	14	32	24	149

6.5 Impact of Bi Content

The experimental results for the temperature-dependent PL intensity of each of other Ga($As_{1-x}Bi_x$)/GaAs heterostructures are also theoretically discussed according to the above-mentioned approach. An excellent agreement is obtained between the experimental results and theoretical calculations for all studied samples. Figs. 6.5(a_1)–6.5(a_3) show the theoretical and experimental results for the samples with x= 2.9%, 3.2%, and 4.5% in the case of the DOS consists of exponential and Gaussian components (Figs. 6.5(b_1)–6.5(b_3)), respectively. The corresponding fit parameters of energy-scales are summarized in Table 6.2.

The peak position ε_M of the second component of the DOS obviously decreases with rising Bi content from around 190 meV for $x = 2.9\%$ to around 140 meV for x= 4.5%. This may be explained with increasing repulsive interactions between neighboring localized centers, lattice distortions, or the shift of the valence band edge as x increases. The width σ_1 of the first part of the DOS does also decrease with increasing Bi content from 31 meV for x= 2.9% to 12 meV for x= 4.5%. This behaviour can be related to the shrinkage of the distribution of localized states when the impurity band forms with rising Bi content [131]. Only the width σ_2 of the second part of the DOS shows no straight tendency as a function of Bi content.

Table 6.2: Fit parameters for Ga($As_{1-x}Bi_x$)/GaAs heterostructures in the case of the DOS consists of exponential and Gaussian components, respectively.

Bi-content (%)	σ_1 (meV)	σ_2 (meV)	ε_M (meV)
2.9	31	23	189
3.2	23	16	194
4.2	21	17	155
4.5	12	44	137

Dieses Werk ist copyrightgeschützt und darf in keiner Form vervielfältigt werden noch an Dritte weitergegeben werden.
Es gilt nur für den persönlichen Gebrauch.

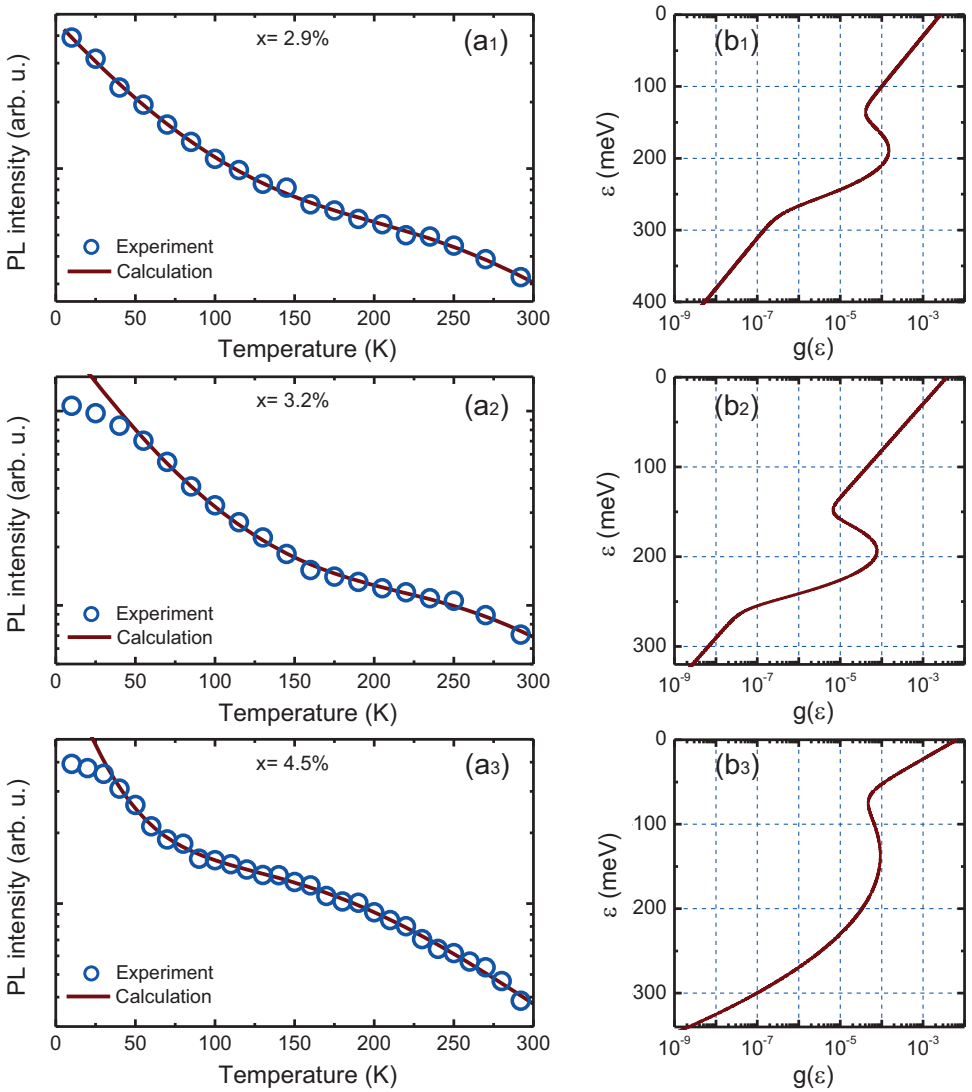

Figure 6.5: Temperature-dependent integrated PL intensities of $Ga(As_{1-x}Bi_x)$/GaAs heterostructures with x= 2.9% (a_1), 3.2% (a_2), and 4.5% (a_3) from experiment (open circles) and theory (lines). The DOS consists of exponential and Gaussian components, respectively. The densities of localized states $g(\varepsilon)$ vs. the energy difference ε from the mobility edge for each of the solid lines in (a_1), (a_2), and (a_3) are shown in (b_1), (b_2), and (b_3), respectively.

6.6 Discussion

The theoretical analysis shows that the PL thermal quenching in $Ga(As_{1-x}Bi_x)$/GaAs heterostructures is well reproduced on basis of Eq. (6.11) together with the different two-component DOS's, extracted from Eqs. (6.12)–(6.14). From a computational point of view, none of the four tested composite DOS's is more favorable than others, even though, from a physical point of view, the two steady combinations with $g_2 = g_G$ are, of course, more reasonable. This clearly demonstrates, however, how important is to extend the monotonous DOS, i.e., adding further states to an exponential or Gaussian DOS tail, in order to fit the observed temperature-dependent PL intensity with its plateau at intermediate temperatures. On the other

Dieses Werk ist copyrightgeschützt und darf in keiner Form vervielfältigt werden noch an Dritte weitergegeben werden.
Es gilt nur für den persönlichen Gebrauch.

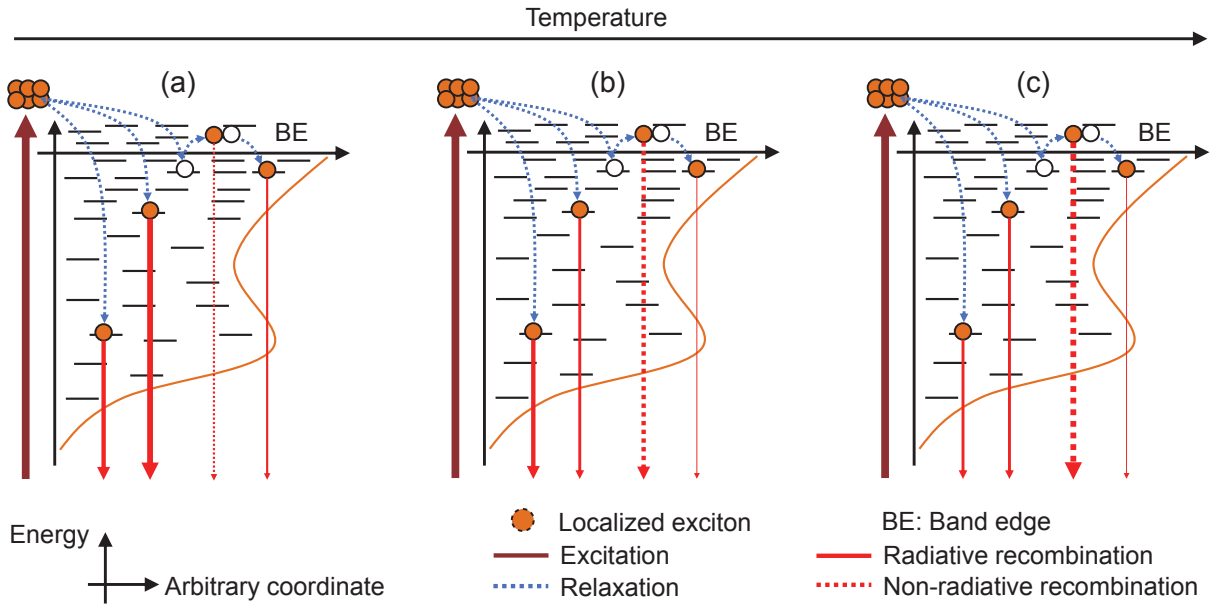

Figure 6.6: The variation of the contribution rate of the radiative and non-radiative recombination to the PL with increasing temperature, represented by changing the thicknesses of related arrows.

hand, the extension of the DOS is corresponded to the assumption of deep laying localized states. While the non-radiative recombination effectively occurs only above the mobility edge, trapped excitons in these deep states recombine radiatively, resulting in a very weak decrease of the PL intensity at intermediate temperatures. According to our results, deep localized states may be somewhere in the order of 100 meV away from the mobility (or band) edge. However, a reliable number for the bandgap energy is scarcely achievable for some currently unknown parameters in the equations like the density of non-radiative centers or their capture cross section.

The Origin of the Observed Plateau in the Temperature-Dependent PL Intensity

The plateau in the temperature-dependent PL intensity arises due to the following reason: at low temperatures the PL intensity is dominated by excitons from the shallow part of the DOS (g_1) (Fig. 6.6(a)). Due to their energetic proximity to the mobility edge, these excitons get rapidly quenched with rising temperature (Fig. 6.6(b)). On the other hand, the deeper laying excitons in the second part of the band tail are hardly affected by thermal activation at low temperatures. Thus, they keep the PL intensity at a certain level until their rates for non-radiative recombination exceed the radiative recombination rate at high temperatures (Fig. 6.6(c)).

The Absence of Two-Peaks PL Spectrum

From the existence of deep localized states, one would intuitively expect the PL spectrum to exhibit a distinct second peak which should be lower in energy and appears at intermediate

Dieses Werk ist copyrightgeschützt und darf in keiner Form vervielfältigt werden noch an Dritte weitergegeben werden.
Es gilt nur für den persönlichen Gebrauch.

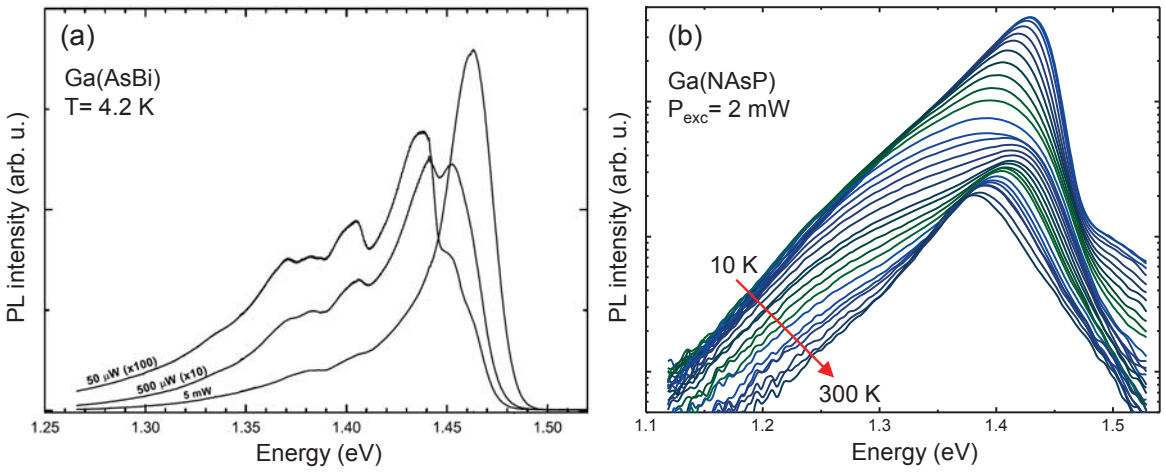

Figure 6.7: (a) low-temperature PL spectra of Ga(AsBi) sample with Bi content of 0.4% (After Francoeur *et al.* [143]). (b) temperature-dependent PL spectra for Ga(NAsP) MQWs with N and P contents of 3% and 5%, respectively.

temperatures. Fig. 6.7 shows two examples where the presence of low-energy features in the PL spectra of disordered semiconductors is clearly apparent: (i) multiple Bi bound states appear at the low-energy side of low-temperature PL spectra of a Ga(AsBi) alloy structure with a Bi content of 0.4% [143], and (ii) one can observe an additional feature on the low-energy flank of the PL main emission-peak in the temperature dependent PL spectra of a Ga(NAsP) MQWs-sample at intermediate temperatures. However, in the case of the studied sample with a Bi content of 4.2%, there are no clear additional low-energy features appearing in the PL spectra as can be seen in Fig. 6.1(a). The existing PL spectrum is very broad and, hence, might easily cover two peaks.

In most cases, the PL features caused by a non-monotonous DOS cannot be clearly distinguished due to, e.g., the short energetic distance between the localized states (or bands) [67, 78, 86]. Furthermore the broadening of the PL emission from different localized states (bands) results in an overlap between their PL spectra. At the end, all contributing PL emissions are covered by an envelope curve, which is the detected PL spectrum. Therefore, the non-existence of a second peak in the PL spectrum alone cannot be seen as indicator for invalidity of the two-components DOS model proposed here.

Exciton Hopping Transitions

Eq. (6.11), which is the basis for the theoretical analysis, does not consider hopping transitions of excitons between localized states. Such transitions are known to cause a flattening in the temperature dependence of the PL intensity only at very low temperatures [110], at which the experimentally observed PL thermal quenching has not yet started in the case of studied $Ga(As_{1-x}Bi_x)$/GaAs heterostructures.

An excitonic hopping model is suggested by Rubel *et al.* [110] to fit the temperature-dependent PL intensity in some disordered semiconductors such as Ga(NAsP)/GaP QWs

Dieses Werk ist copyrightgeschützt und darf in keiner Form vervielfältigt werden noch an Dritte weitergegeben werden.
Es gilt nur für den persönlichen Gebrauch.

(Fig. 6.2(a)). It is also applied to simulate the PL thermal quenching in Ga(AsBi) at relatively high excitation conditions [86] (Fig. 6.2(b)). This model is based on Eq. (6.10) and takes into account hopping dynamics of photo-excited excitons between the disorder-induced localized states. The latter have an exponential energy distribution, $g(\varepsilon) \propto \exp(-\varepsilon/\varepsilon_0)$ with an energy scale ε_0. However, hopping processes do not essentially affect the thermal quenching of the PL intensity at moderate temperatures under consideration in the case of Ga(AsBi) samples presented in this work. Therefore, Rubel's theoretical approach [110] is valid to study the plateau in the temperature-dependent PL intensity of Ga($As_{1-x}Bi_x$)/GaAs heterostructures at intermediate temperatures.

Comparison with Conventional Two-Energy-Scales Model

Here, the conventional two-scales model, which was proposed for the quantitative description of disorder-induced PL characteristics in Ga(AsBi) [86], is considered. The differences between this conventional to the above-discussed two-components model are stressed in the following.

In both models, the DOS consists of two-energy-scales. However, in the two-scales model the offset of the *second* exponential energy-scale follows the long-range fluctuations of the *first* Gaussian energy-scale resulting in a convolution of both energy distributions, whilst in the two-components model *both* energy distributions exist independently from each other resulting in a simple summation of both distributions. Moreover, in the two-scales model excitons do not need to be lifted above the mobility edge to recombine non-radiatively, but can be quenched already in the states of the Gaussian DOS with their large localization lengths. As a consequence of this assumption, the two-scales model reduces to an effective one-scale model with a *single* exponential-energy-distribution with respect to the PL thermal quenching since exciton quenching from localized states is driven only by the energetic difference to the states with a non-radiative recombination channel. Even without non-radiative recombination in Gaussian states, the DOS in the two-scales model would still be monotonous. Hence, the two-scales model would be incapable to reproduce a plateau in the temperature-dependent PL intensity at intermediate temperatures. An additional radiative channel, resulting from the extension of the DOS, is essential to produce the nearly temperature-independent PL intensity in the intermediate range of temperatures.

6.7 Summary

A comparative experimental and theoretical study of the thermal quenching of the PL intensity in MOVPE-grown Ga($As_{1-x}Bi_x$)/GaAs heterostructures is presented. The dependence of the PL peak energy as well as the PL FWHM on the temperature shows typical disorder-induced characteristics. An anomalous plateau in the PL thermal quenching is observed at intermediate temperatures under relatively low excitation intensities, e.g., the PL intensity is nearly temperature-independent in the range between 115 K and 235 K in the case of the sample with Bi content of 4.2%. Previously, a model with a monotonous *single-energy-scale* DOS [110] has been reported to be enough to fit the PL thermal quenching in disordered Ga(AsBi) semi-

Dieses Werk ist copyrightgeschützt und darf in keiner Form vervielfältigt werden noch an Dritte weitergegeben werden.
Es gilt nur für den persönlichen Gebrauch.

conductors under relatively high excitation intensities [86]. According to this model, hopping relaxation dynamics of the excitons are taken into account to reproduce the observed flattening in the PL thermal quenching at very low temperatures.

In contrast, it is demonstrated in this chapter that a theoretical analysis based on a well-approved approach with a non-monotonous *two-component* DOS with two-energy-scales is indispensable to achieve a good agreement between experiment and theory for the anomalous plateau in the PL thermal quenching observed at lower excitation intensities. Besides, it is assumed that an exciton thermally activated to the mobility edge does not necessarily recombine non-radiatively but can be recaptured into a radiative state located below the mobility edge, i.e., a localized state. Several shapes of two-component DOS are used to fit the experimental data of the PL thermal quenching.

By this means almost perfect matching between experiment and theory is obtained for all studied samples. The non-monotonous DOS shapes imply the presence of deep-laying localized states in the bandgap. Consequently, the observed plateau in the thermal quenching of the PL intensity is considered as a hint for the existence of such deep localized states in the bandgap of Ga(AsBi).

Dieses Werk ist copyrightgeschützt und darf in keiner Form vervielfältigt werden noch an Dritte weitergegeben werden.
Es gilt nur für den persönlichen Gebrauch.

7 Summary

In this thesis photoluminescence (PL) spectroscopy measurements are performed in order to characterize the disorder in semiconductor nanostructures. Two III-V-based semiconductors, Ga(NAsP) and Ga(AsBi) are systematically studied by means of time-resolved PL spectroscopy and continuous-wave PL spectroscopy.

The main disorder-induced PL features in these structures can be summarized in (i) a blue-shift in the excitation-dependent PL peak energy, (ii) a strong dependence of the PL decay time on the emission energy, (iii) a non-monotonous temperature-dependent PL peak energy and PL linewidth, and (iv) a strong temperature dependence of the PL intensity and the corresponding PL decay time. Hopping relaxation processes of localized excitons between localized states are convincingly involved to interpret the aforementioned peculiar behaviors. The experimental observations have demonstrated that disorder-related PL characteristics become less apparent when either the excitation intensity or the lattice temperature is increased. Here, the increasing excitation intensity results in a gradual filling of disorder-induced localized states because of their finite number. On the other hand, with increasing temperature, localized excitons become mobile and become delocalized at high temperatures. Consequently, PL intensity decreases dramatically due to the increased non-radiative recombination of thermally delocalized carriers, while the PL decay time behavior is fundamentally associated with the competition between radiative and non-radiative processes.

Beside the need of a qualitative explanation, a quantitative description of disorder effects, i.e., energy scaling of the disorder potential, is a task of crucial importance. This aspect is also discussed throughout this thesis. In spite of the intuitive thought that the energy scales of disorder potential should increase when the concentration of the fluctuating compositional component is increased, these scales show an odd dependence of the Bi content in Ga(AsBi) structures. In particular, the influence of the Bi content on the energy scales of the disorder, in Ga(AsBi) single quantum well's (SQWs) is studied using two theoretical models: (i) a straightforward model with a single energy-scale is based on the carrier dynamics at very low temperatures, and (ii) an excitonic hopping model with two energy scales is based on the features of the PL spectra. The extracted energy scales fluctuate tremendously when the Bi content is increased with a weak tendency to increase with Bi content. In contrast, in the case of Ga(NAsP) multi-QWs (MQWs), a decrease of disorder energy-scales is observed when the N content is increased. This peculiar behavior is theoretically analyzed for the energy-scale of the short-range compositional-fluctuations. This analysis is supported by some calculations using the band anti-crossing model. The reason of the decrease of the short energy-scale in Ga(NAsP) MQWs is attributed to the decrease of both the impact on the band structure and the exciton effective-mass.

Dieses Werk ist copyrightgeschützt und darf in keiner Form vervielfältigt werden noch an Dritte weitergegeben werden.
Es gilt nur für den persönlichen Gebrauch.

Furthermore, an anomalous plateau in the PL thermal quenching in Ga(AsBi)/GaAs heterostructures is observed at lower excitation intensities. It is demonstrated in my thesis that a theoretical analysis based on a well-approved approach with a non-monotonous two-component DOS with two-energy scales is indispensable to achieve a good agreement between experiment and theory for such a behavior. Here, it is assumed that an exciton thermally activated to the mobility edge does not necessarily recombine non-radiatively but can be recaptured into a radiative state located below the mobility edge, i.e., a localized state. Several shapes of two-component DOS are used to fit the experimental data of the PL thermal quenching.

In conclusion, the systematic investigation carried out in this thesis led to a better understanding of disorder effects on the electronic structure and optical properties of Ga(NAsP) and Ga(AsBi) nanostructures. This will be of importance for the development of semiconductor devices based on these material systems.

Dieses Werk ist copyrightgeschützt und darf in keiner Form vervielfältigt werden noch an Dritte weitergegeben werden.
Es gilt nur für den persönlichen Gebrauch.

Bibliography

[1] S. Kasap and P. Capper, *Springer handbook of electronic and photonic materials*. Springer, Heidelberg, Germany, 2006.

[2] A. Owens and A. Peacock, "Compound semiconductor radiation detectors," *Nucl. Instrum. Methods Phys. Res. A*, vol. 531, no. 1–2, pp. 18–37, 2004.

[3] B. G. Yacobi, *Semiconductor materials: an introduction to basic principles*. Kluwer Academic/Plenum Publishers, New York, 2003.

[4] M. Razeghi, *Fundamentals of solid state engineering*. 3ed., Springer US, 2009.

[5] A. Erol, *Dilute III-V Nitride Semiconductors and Material Systems*. Springer, Berlin-Heidelberg, Germany, 2008.

[6] H. Li and Z. M. Wang, *Bismuth-Containing Compounds*. Springer, New York, US, 2013.

[7] R. Kudrawiec, A. V. Luce, M. Gladysiewicz, M. Ting, Y. J. Kuang, C. W. Tu, O. D. Dubon, K. M. Yu, and W. Walukiewicz, "Electronic Band Structure of $\mathrm{GaN}_x\mathrm{P}_y\mathrm{As}_{1-x-y}$ Highly Mismatched Alloys: Suitability for Intermediate-Band Solar Cells," *Phys. Rev. Appl.*, vol. 1, no. 3, p. 034007, 2014.

[8] B. Kunert, A. Klehr, S. Reinhard, K. Volz and W. Stolz, "Near room temperature electrical injection lasing for dilute nitride Ga(NAsP)/GaP quantum-well structures grown by metal organic vapour phase epitaxy," *Electron. Lett.*, vol. 42, no. 10, p. 601, 2006.

[9] S. Liebich, M. Zimprich, A. Beyer, C. Lange, D. J. Franzbach, S. Chatterjee, N. Hossain, S. J. Sweeney, K. Volz, B. Kunert, and W. Stolz, "Laser operation of Ga(NAsP) lattice-matched to (001) silicon substrate," *Appl. Phys. Lett.*, vol. 99, no. 7, p. 071109, 2011.

[10] K. Bertulis, A. Krotkus, G. Aleksejenko, V. Pačebutas, R. Adomavičius, G. Molis, and S. Marcinkevičius, "Laser operation of Ga(NAsP) lattice-matched to (001) silicon substrate," *Appl. Phys. Lett.*, vol. 88, no. 20, p. 201112, 2006

[11] R. Lewis, D. Beaton, X. Lu, and T. Tiedje, "$\mathrm{GaAs}_{1-x}\mathrm{Bi}_x$ light emitting diodes," *J. Cryst. Growth*, vol. 311, no. 7, pp. 1872–1875, 2009.

[12] Y. Tominaga, K. Oe, and M. Yoshimoto, "Low Temperature Dependence of Oscillation Wavelength in $\mathrm{GaAs}_{1-x}\mathrm{Bi}_x$ Laser by Photo-Pumping," *Appl. Phys. Express*, vol. 3, no. 6, p. 062201, 2010.

[13] P. Ludewig, N. Knaub, N. Hossain, S. Reinhard, L. Nattermann, I. P. Marko, S. R. Jin, K. Hild, S. Chatterjee, W. Stolz, S. J. Sweeney, and K. Volz, "Electrical injection Ga(AsBi)/(AlGa)As single quantum well laser," *Appl. Phys. Lett.*, vol. 102, no. 24, p. 242115, 2013.

Dieses Werk ist copyrightgeschützt und darf in keiner Form vervielfältigt werden noch an Dritte weitergegeben werden.
Es gilt nur für den persönlichen Gebrauch.

[14] A. Popov, *Disordered Semiconductors: Physics and Applications*. Pan Stanford, Singapore, 2011.

[15] G. Dhanaraj, K. Byrappa, V. Prasad, and M. Dudley, *Springer Handbook of Crystal Growth*. Springer, Berlin-Heidelberg, Germany, 2010.

[16] D. R. Vij, *Luminescence of Solids*. Springer US, 1998.

[17] P. Y. Yu and M. Cardona, *Fundamentals of Semiconductors: Physics and Materials Properties*. Springer, Berlin-Heidelberg, Germany, 2010.

[18] E. N. Kaufmann, *Characterization of Materials, Volumes 1 and 2*. John Wiley & Sons, Hoboken, New Jersey, 2003.

[19] W. Martienssen and H. Warlimont, *Springer handbook of condensed matter and materials data*. Springer, Heidelberg, Germany, 2005.

[20] S. B. Zhang and S.-H.i Wei, "Nitrogen Solubility and Induced Defect Complexes in Epitaxial GaAs:N," *Phys. Rev. Lett.*, vol. 86, no. 9, pp. 1789–1792, 2001.

[21] K. Jandieri, C. Jurecka, J. Ohlmann, A. Beyer, B. Kunert, S. D. Baranovskii, K. Volz, W. Stolz, and F. Gebhard, "Hopping relaxation of photo-excited excitons in Ga(NAsP) bulk structure," *Phys. Status Solidi C*, vol. 8, no. 1, pp. 163–168, 2011.

[22] C. Karcher, K. Jandieri, B. Kunert, R. Fritz, K. Volz, W. Stolz, F. Gebhard, S. D. Baranovskii, and W. Heimbrodt, "Double-scaled disorder in Ga(N,As,P)/GaP multiquantum wells," *J. Lumin.*, vol. 133, pp. 125–128, 2013.

[23] G. Ciatto, E. C. Young, F. Glas, J. Chen, R. Alonso Mori, and T. Tiedje, "Spatial correlation between Bi atoms in dilute $GaAs_{1-x}Bi_x$: From random distribution to Bi pairing and clustering," *Phys. Rev. B*, vol. 78, p. 035325, 2008.

[24] M. Wu, E. Luna, J. Puustinen, M. Guina, and A. Trampert, "Formation and phase transformation of Bi-containing QD-like clusters in annealed GaAsBi," *Nanotechnology*, vol. 25, no. 20, p. 205605, 2014.

[25] Y. Tominaga, Y. Kinoshita, K. Oe, and M. Yoshimoto, "Structural investigation of $GaAs_{1-x}Bi_x$/GaAs multiquantum wells," *Appl. Phys. Lett.*, vol. 93, no. 13, p. 131915, 2008.

[26] H. Czichos, T. Saito, and L. Smith, *Springer Handbook of Materials Measurement Methods*. Springer, Berlin-Heidelberg, Germany, 2006.

[27] L. Vegard, "Die Konstitution der Mischkristalle und die Raumfüllung der Atome," *Z. Phys.*, vol. 5, no. 1, pp. 17–26, 1921.

[28] J. A. Van Vechten and T. K. Bergstresser, "Electronic Structures of Semiconductor Alloys," *Phys. Rev. B*, vol. 1, no. 8, pp. 3351–3358, 1970.

[29] A. G. Thompson and J. C. Woolley, "Energy-gap variation in mixed III–V alloys," *Can. J. Phys.*, vol. 45, no. 2, pp. 255–261, 1967.

[30] F. Yun, M. A. Reshchikov, L. He, T. King, H. Morkoç, S. W. Novak, and L. Wei, "Energy band bowing parameter in $Al_xGa_{1-x}N$ alloys," *J. Appl. Phys.*, vol. 92, no. 8, pp. 4837–4839, 2002.

Dieses Werk ist copyrightgeschützt und darf in keiner Form vervielfältigt werden noch an Dritte weitergegeben werden.
Es gilt nur für den persönlichen Gebrauch.

[31] D. Richardson and R. Hill, "The origins of energy gap bowings in substitutional semiconductor alloys," *J. Phys. C: Solid State Phys.*, vol. 5, no. 8, pp. 821–827, 1972.

[32] R. Hill, "Energy-gap variations in semiconductor alloys," *J. Phys. C: Solid State Phys.*, vol. 7, no. 3, pp. 521–526, 1974.

[33] E. Iliopoulos, A. Adikimenakis, C. Giesen, M. Heuken, and A. Georgakilas, "Energy bandgap bowing of InAlN alloys studied by spectroscopic ellipsometry," *Appl. Phys. Lett.*, vol. 92, no. 19, p. 191907, 2008.

[34] X. Lu, D. A. Beaton, R. B. Lewis, T. Tiedje, and Y. Zhang, "Composition dependence of photoluminescence of $GaAs_{1-x}Bi_x$ alloys," *Appl. Phys. Lett.*, vol. 95, no. 4, p. 041903, 2009.

[35] G. P. Donati, R. Kaspi, and K. J. Malloy, "Interpolating semiconductor alloy parameters: Application to quaternary III-V band gaps," *J. Appl. Phys.*, vol. 94, no. 9, pp. 5814–5819, 2003.

[36] I. Vurgaftman, J. R. Meyer, and L. R. Ram-Mohan, "Band parameters for III-V compound semiconductors and their alloys," *J. Appl. Phys.*, vol. 89, no. 11, pp. 5815–5875, 2001.

[37] A. Janotti, Su-Huai Wei, and S. B. Zhang, "Theoretical study of the effects of isovalent coalloying of Bi and N in GaAs," *Phys. Rev. B*, vol. 65, no. 11, p. 115203, 2002.

[38] J. Wu, W. Walukiewicz, K. M. Yu, J. D. Denlinger, W. Shan, J. W. Ager, A. Kimura, H. F. Tang, and T. F. Kuech, "Valence band hybridization in N-rich $GaN_{1-x}As_x$ alloys," *Phys. Rev. B*, vol. 70, no. 11, p. 115214, 2004.

[39] S.-H. Wei and A. Zunger "Giant and Composition-Dependent Optical Bowing Coefficient in GaAsN Alloys," *Phys. Rev. Lett.*, vol. 76, no. 4, pp. 664–667, 1996.

[40] T. Mattila, S.-H. Wei, and A. Zunger, "Localization and anticrossing of electron levels in $GaAs_{1-x}N_x$ alloys," *Phys. Rev. B*, vol. 60, no. 16, pp. R11245–R11248, 1999.

[41] J. Wu, W. Shan, and W. Walukiewicz, "Band anticrossing in highly mismatched III–V semiconductor alloys," *Semicond. Sci. Technol.*, vol. 17, no. 8, pp. 860–869, 2002.

[42] W. Shan, W. Walukiewicz, J. W. Ager III, E. E. Haller, J. F. Geisz, D. J. Friedman, J. M. Olson, and S. R. Kurtz, "Band Anticrossing in GaInNAs Alloys," *Phys. Rev. Lett.*, vol. 82, no. 2, pp. 1221–1224, 1999.

[43] W. Shan, W. Walukiewicz, J. W. Ager III, J. F. Geisz, D. J. Friedman, J. M. Olson, and S. R. Kurtz, "Effect of nitrogen on the band structure of GaInNAs alloys," *J. Appl. Phys.*, vol. 86, no. 4, pp. 2349–2351, 1999.

[44] S. Nacer, A. Aissat, and K. Ferdjani, "Band gap and band offsets of GaNAsBi lattice matched to GaAs substrate," *Opt. Quantum Electron.*, vol. 40, no. 9, pp. 677–683, 2008.

[45] K. Alberi, O. D. Dubon, W. Walukiewicz, K. M. Yu, K. Bertulis, and A. Krotkus, "Valence band anticrossing in $GaAs_{1-x}Bi_x$," *Appl. Phys. Lett.*, vol. 91, no. 5, p. 051909, 2007.

[46] K. Alberi, J. Wu, W. Walukiewicz, K. M. Yu, O. D. Dubon, S. P. Watkins, C. X. Wang, X. Liu, Y.-J. Cho, and J. Furdyna "Valence-band anticrossing in mismatched III-V semiconductor alloys," *Phys. Rev. B*, vol. 75, p. 045203, 2007.

Dieses Werk ist copyrightgeschützt und darf in keiner Form vervielfältigt werden noch an Dritte weitergegeben werden.
Es gilt nur für den persönlichen Gebrauch.

[47] P. W. Anderson, "Localized Magnetic States in Metals," *Phys. Rev.*, vol. 124, no. 1, pp. 41–53, 1961.

[48] W. Shan, K. M. Yu, W. Walukiewicz, J. Wu, J. W. Ager, and E. E. Haller, "Band anticrossing in dilute nitrides," *J. Phys.: Condens. Matter*, vol. 16, no. 31, pp. S3355–S3372, 2004.

[49] W. Shan, K. M. Yu, W. Walukiewicz, J. W. Beeman, J. Wu, J. W. Ager III, M. A. Scarpulla, O. D. Dubon, and E. E. Haller, "Effects of pressure on the band structure of highly mismatched $Zn_{1-y}Mn_yO_xTe_{1-x}$ alloys," *Appl. Phys. Lett.*, vol. 84, no. 6, pp. 924–926, 2004.

[50] K. Uesugi, N. Morooka, and I. Suemune, "Reexamination of N composition dependence of coherently grown GaNAs band gap energy with high-resolution x-ray diffraction mapping measurements," *Appl. Phys. Lett.*, vol. 74, no. 9, pp. 1254–1256, 1999.

[51] B. M. Keyes, J. F. Geisz, P. C. Dippo, R. Reedy, C. Kramer, D. J. Friedman, Sarah R. Kurtz, and J. M. Olson, "Optical investigation of GaNAs," *AIP Conf. Proc.*, vol. 462, no. 10, pp. 511–516, 1999.

[52] L. Malikova, Fred H. Pollak, and R. A. J. Bhat, "Composition and temperature dependence of the direct band gap of $GaAs_{1-x}N_x$ ($0 \leq x \leq 0.0232$) using contactless electroreflectance," *J. Electron. Mater.*, vol. 27, no. 5, pp. 484–487, 1998.

[53] R. Bhat, C. Caneau, L. Salamanca-Riba, W. Bi, and C. Tu, "Growth of GaAsN/GaAs, GaInAsN/GaAs and GaInAsN/GaAs quantum wells by low-pressure organometallic chemical vapor deposition," *J. Cryst. Growth*, vol. 195, no. 1–4, pp. 427–437, 1998.

[54] K. M. Yu, W. Walukiewicz, J. W. Ager, D. Bour, R. Farshchi, O. D. Dubon, S. X. Li, I. D. Sharp, and E. E. Haller, "Multiband GaNAsP quaternary alloys," *Appl. Phys. Lett.*, vol. 88, no. 9, p. 092110, 2006.

[55] R. Kudrawiec, "Parameterization of the band gap energy for $GaN_xAs_{1-x-z}P_z$ alloys," *Appl. Phys. Lett.*, vol. 101, no. 11, p. 116101, 2007.

[56] Y. Zhang, A. Mascarenhas, and L. W. Wang, "Similar and dissimilar aspects of III-V semiconductors containing Bi versus N," *Phys. Rev. B* vol. 71, no. 15, p. 155201, 2005.

[57] T. Tiedje, E. C. Young, and A. Mascarenhas, "Growth and properties of the dilute bismide semiconductor $GaAs_{1-x}Bi_x$ a complementary alloy to the dilute nitrides," *Int. J. Nanotech.*, vol. 5, no. 9-12, pp. 963–983, 2008.

[58] S. Tixier, M. Adamcyk, T. Tiedje, S. Francoeur, A. Mascarenhas, P. Wei, and F. Schiettekatte, "Molecular beam epitaxy growth of $GaAs_{1-x}Bi_x$," *Appl. Phys. Lett.*, vol. 82, no. 14, pp. 2245–2247, 2003.

[59] W. Huang, K. Oe, G. Feng, and M. Yoshimoto, "Molecular-beam epitaxy and characteristics of $GaN_yAs_{1-x-y}Bi_x$," *J. Appl. Phys.*, vol. 98, no. 5, p. 053505, 2005.

[60] S. Francoeur, M. J. Seong, A. Mascarenhas, S. Tixier, M. Adamcyk, and T. Tiedje, "Band gap of $GaAs_{1-x}Bi_x$, 0<x<3.6%," *Appl. Phys. Lett.*, vol. 82, no. 22, pp. 3874–3876, 2003.

[61] B. Kunert, K. Volz, J. Koch, and W. Stolz "MOVPE growth conditions of the novel direct band gap, diluted nitride Ga(NAsP) material system pseudomorphically strained on GaP-substrate," *J. Cryst. Growth*, vol. 298, pp. 121–125, 2007.

Dieses Werk ist copyrightgeschützt und darf in keiner Form vervielfältigt werden noch an Dritte weitergegeben werden.
Es gilt nur für den persönlichen Gebrauch.

[62] B. Kunert, K. Volz, J. Koch, and W. Stolz, "Direct-band-gap Ga(NAsP)-material system pseudomorphically grown on GaP substrate," *Appl. Phys. Lett.*, vol. 88, no. 18, p. 182108, 2006.

[63] P. Ludewig, Z. L. Bushell, L. Nattermann, N. Knaub, W. Stolz, and K. Volz, "Growth of Ga(AsBi) on GaAs by continuous flow MOVPE," *J. Cryst. Growth*, vol. 396, pp. 95–99, 2014.

[64] S. J. Pearton, *GaN and Related Materials*. Gordon and Breach Science Publications, the Netherlands 1997.

[65] M. Weyers, M. Sato, and H. Ando, "Red Shift of Photoluminescence and Absorption in Dilute GaAsN Alloy Layers," *Jpn. J. Appl. Phys.*, vol. 31, no. 7A, pp. L853–L855, 1992.

[66] V. V. Pačebutas, K. Bertulis, G. Aleksejenko, and A. Krotkus, "Molecular-beam-epitaxy grown GaBiAs for terahertz optoelectronic applications," *J. Mater. Sci.: Mater. Electron.*, vol. 20, no. 1, pp. S363–S366, 2009.

[67] M. K. Shakfa, D. Kalincev, X. Lu, S. R. Johnson, D. A. Beaton, T. Tiedje, A. Chernikov, S. Chatterjee, and M. Koch, "Quantitative study of localization effects and recombination dynamics in GaAsBi/GaAs single quantum wells," *J. Appl. Phys.*, vol. 114, no. 16, p. 164306, 2013.

[68] M. Yoshimoto, W. Huang, Y. Takehara, J. Saraie, A. Chayahara, Y. Horino, and K. Oe, "New Semiconductor GaNAsBi Alloy Grown by Molecular Beam Epitaxy," *Jpn. J. Appl. Phys.*, vol. 43, no. 7A, pp. L845–Khaled, 2004.

[69] R. Butkutė, V. Pačebutas, B. Čechavičius, R. Nedzinskas, A. Selskis, A. Arlauskas, and A. Krotkus, "Photoluminescence at up to 2.4 μm wavelengths from GaInAsBi/AlInAs quantum wells," *J. Cryst. Growth*, vol. 391, pp. 116–120, 2014.

[70] W. Shan, K. M. Yu, W. Walukiewicz, J. W. Ager III, E. E. Haller, and M. C. Ridgway, "Reduction of band-gap energy in GaNAs and AlGaNAs synthesized by N+ implantation," *Appl. Phys. Lett.*, vol. 75, no. 10, pp. 1410–1412, 1999.

[71] B. Kunert, K. Volz, I. Nemeth, and W. Stolz, "Luminescence investigations of the GaP-based dilute nitride Ga(NAsP) material system," *J. Lumin.*, vol. 121, no. 2, pp. 361–364, 2006.

[72] R. A. Street, "Luminescence in amorphous semiconductors," *Adv. Phys.*, vol. 25, no. 4, pp. 397–453, 1976.

[73] R. Kudrawiec, M. Syperek, P. Poloczek, J. Misiewicz, R. H. Mari, M. Shafi, M. Henini, Y. G. Gobato, S. V. Novikov, J. Ibanez, M. Schmidbauer, and S. I. Molina, "Carrier localization in GaBiAs probed by photomodulated transmittance and photoluminescence," *J. Appl. Phys.*, vol. 106, no. 2, p. 023518, 2009.

[74] P. J. Klar, "Recent developments in metastable dilute-N III–V semiconductors," *Prog. Solid State Chem.*, vol. 31, no. 4, pp. 301–349, 2003.

[75] G. G. Stokes, "On the change of refrangibility of light," *Phil. Trans. R. Soc. (London)*, vol. 142, pp. 463–562, 1852.

Dieses Werk ist copyrightgeschützt und darf in keiner Form vervielfältigt werden noch an Dritte weitergegeben werden.
Es gilt nur für den persönlichen Gebrauch.

[76] I. A. Buyanova, W. M. Chen, and C. W. Tu, "Recombination processes in N-containing III-V ternary alloys," *Solid-State Electron.*, vol. 47, no. 3, pp. 467–475, 2003.

[77] R. Kudrawiec, P. Poloczek, J. Misiewicz, M. Shafi, J. Ibanez, R. H. Mari, M. Henini, M. Schmidbauer, S. V. Novikov, L. Turyanska, S. I. Molina, D. L. Sales, and M. F. Chisholm, "Photomodulated transmittance of GaBiAs layers grown on (001) and (311) B GaAs substrates," *Microelectron. J.*, vol. 40, no. 3, pp. 537–539, 2009.

[78] H. D. Sun, M. Hetterich, M. D. Dawson, A. Yu. Egorov, D. Bernklau, and H. Riechert, "Optical investigations of GaInNAs/GaAs multi-quantum wells with low nitrogen content," *J. Appl. Phys.*, vol. 92, no. 3, pp. 1380–1385, 2002.

[79] P. R. C. Kent and A. Zunger, "Evolution of III-V Nitride Alloy Electronic Structure: The Localized to Delocalized Transition," *Phys. Rev. Lett.*, vol. 86, no. 12, pp. 2613–2616, 2001.

[80] S. Permogorov and A. Reznitsky, "Effect of disorder on the optical spectra of wide-gap II–VI semiconductor solid solutions," *J. Lumin.*, vol. 52, no. 1–4, pp. 201–223, 1992.

[81] S. D. Baranovskii, R. Eichmann, and P. Thomas, "Temperature-dependent exciton luminescence in quantum wells by computer simulation," *Phys. Rev. B*, vol. 58, no. 19, pp. 13081–13087, 1998.

[82] C. Gourdon and P. Lavallard, "Exciton Transfer between Localized States in $CdS_{1-x}Se_x$ Alloys," *Phys. Status Solidi B*, vol. 153, no. 2, pp. 641–652, 1989.

[83] D. Dagnelund, J. Puustinen, M. Guina, W. M. Chen, and I. A. Buyanova, "Identification of an isolated arsenic antisite defect in GaAsBi," *Appl. Phys. Lett.*, vol. 104, no. 5, p. 052110, 2014.

[84] C. Karcher, K. Jandieri, B. Kunert, R. Fritz, M. Zimprich, K. Volz, W. Stolz, F. Gebhard, S. D. Baranovskii, and W. Heimbrodt, "Peculiarities of the photoluminescence of metastable Ga(N,As,P)/GaP quantum well structures," *Phys. Rev. B*, vol. 82, p. 245309, 2010.

[85] M. Pophristic, F. H. Long, C. Tran, R. F. Karlicek, Z. C. Feng, and I. T. Ferguson, "Time-resolved spectroscopy of $In_xGa_{1-x}N$/GaN multiple quantum wells at room temperature," *Appl. Phys. Lett.*, vol. 73, no. 6, pp. 815–817, 1998.

[86] S. Imhof, A. Thränhardt, A. Chernikov, M. Koch, N. S. Köster, K. Kolata, S. Chatterjee, S. W. Koch, X. Lu, S. R. Johnson, D. A. Beaton, T. Tiedje, and O. Rubel, "Clustering effects in Ga(AsBi)," *Appl. Phys. Lett.*, vol. 96, no. 13, p. 131115, 2010.

[87] Y. I. Mazur, V. G. Dorogan, M. Schmidbauer, G. G. Tarasov, S. R. Johnson, X. Lu, S-Q. Yu, Zh. M. Wang, T. Tiedje and G. J. Salamo, "Optical evidence of a quantum well channel in low temperature molecular beam epitaxy grown Ga(AsBi)/GaAs nanostructure," *Nanotechnology*, vol. 22, no. 37, p. 375703, 2011.

[88] X. Zhongying, X. Jizong, G. Weikun, Z. Baozhen, X. Junying, and L. Yuzhang, "The excitonic properties and temperature behaviour of the photoluminescence from GaAs-GaAlAs multiple quantum well structures," *Solid State Commun.*, vol. 61, no. 11, pp. 707–711, 1987.

Dieses Werk ist copyrightgeschützt und darf in keiner Form vervielfältigt werden noch an Dritte weitergegeben werden.
Es gilt nur für den persönlichen Gebrauch.

[89] K. Nunna, S. Iyer, L. Wu, J. Li, S. Bharatan, X. Wei, R. T. Senger, and K. K. Bajaj, "Nitrogen incorporation and optical studies of GaAsSbN/GaAs single quantum well heterostructures," *J. Appl. Phys.*, vol. 102, no. 5, p. 053106, 2007.

[90] V. Pačebutas, R. Butkutė, B. Čechavičius, J. Kavaliauskas, A. Krotkus, "Photoluminescence investigation of $GaAs_{1-x}Bi_x$/GaAs heterostructures," *Thin Solid Films*, vol. 520, no. 20, pp. 6415–6418, 2012.

[91] H. Wang, Z. Ji, S. Qu, G. Wang, Y. Jiang, B. Liu, X. Xu, and H. Mino "Influence of excitation power and temperature on photoluminescence in InGaN/GaN multiple quantum wells," *Opt. Express*, vol. 20, no. 4, pp. 3932–3940, 2012.

[92] D. A. B. Miller, D. S. Chemla, T. C. Damen, A. C. Gossard, W. Wiegmann, T. H. Wood, and C. A. Burrus, "Electric field dependence of optical absorption near the band gap of quantum-well structures," *Phys. Rev. B*, vol. 32, no. 8, pp. 1043–1060, 1985.

[93] J. Zhang and N. Tansu, "Improvement in spontaneous emission rates for InGaN quantum wells on ternary InGaN substrate for light-emitting diodes," *J. Appl. Phys.*, vol. 110, no. 11, p. 113110, 2011.

[94] Y.-H. Cho, G. H. Gainer, A. J. Fischer, J. J. Song, S. Keller, U. K. Mishra, and S. P. DenBaars, ""S-shaped" temperature-dependent emission shift and carrier dynamics in InGaN/GaN multiple quantum wells," *Appl. Phys. Lett.*, vol. 73, no. 10, pp. 1370–1372, 1998.

[95] A. Kaschner, J. Holst, U. von Gfug, A. Hoffmann, F. Bertram, T. Riemann, D. Rudloff, P. Fischer, J. Christen, R. Averbeck, and H. Riechert, "Correlation between structural properties and optical amplification in InGaN/GaN heterostructures grown by molecular beam epitaxy," *MRS Proceedings*, vol. 595, p. F99W11.34, 1999.

[96] M. S. Skolnick, P. R. Tapster, S. J. Bass, A. D. Pitt, N. Apsley and S. P. Aldred, "Investigation of InGaAs-InP quantum wells by optical spectroscopy," *Semicond. Sci. Technol.*, vol. 1, no. 1, pp. 29–40, 1986.

[97] L. Grenouillet, C. Bru-Chevallier, G. Guillot, P. Gilet, P. Duvaut, C. Vannuffel, A. Million, and A. Chenevas-Paule, "Evidence of strong carrier localization below 100 K in a GaInNAs/GaAs single quantum well," *Appl. Phys. Lett.*, vol. 76, no. 16, pp. 2241–2243, 2000.

[98] M. Izadifard, J. P. Bergman, W. M. Chen, I. A. Buyanova, Y. G. Hong, and C. W. Tu, "Radiative recombination of GaInNP alloys lattice matched to GaAs," *J. Appl. Phys.*, vol. 88, no. 1, p. 011919, 2006.

[99] Y. P. Varshni, "Temperature dependence of the energy gap in semiconductors," *Physica*, vol. 34, no. 1, pp. 149–154, 1967.

[100] O. Rubel, M. Galluppi, S. D. Baranovskii, K. Volz, L. Geelhaar, H. Riechert, P. Thomas, and W. Stolz, "Quantitative description of disorder parameters in (GaIn)(NAs) quantum wells from the temperature-dependent photoluminescence spectroscopy," *J. Appl. Phys.*, vol. 98, no. 6, p. 063518, 2005.

[101] S. Rudin, T. L. Reinecke, and B. Segall, "Temperature-dependent exciton linewidths in semiconductors," *Phys. Rev. B*, vol. 42, no. 17, pp. 11218–11231, 1990.

Dieses Werk ist copyrightgeschützt und darf in keiner Form vervielfältigt werden noch an Dritte weitergegeben werden.
Es gilt nur für den persönlichen Gebrauch.

[102] A. K. Viswanath, J. I. Lee, D. Kim, C. R. Lee, and J. Y. Leem, "Exciton-phonon interactions, exciton binding energy, and their importance in the realization of room-temperature semiconductor lasers based on GaN," *Phys. Rev. B*, vol. 58, no. 24, pp. 16333–16339, 1998.

[103] S. R. Bank, M. A. Wistey, H. B. Yuen, V. Lordi, V. F. Gambin, and J. S. Harris Jr., "Effects of antimony and ion damage on carrier localization in molecular-beam-epitaxy-grown GaInNAs," *J. Vac. Sci. Technol.*, vol. 23, no. 3, pp. 1320–1323, 2005.

[104] T. Prutskij, C. Pelosi, and G. Attolini, "Temperature quenching of photoluminescence of ordered $GaInP_2$ alloy under different excitation densities," *Cryst. Res. Technol.*, vol. 46, no. 2, pp. 127–134, 2011.

[105] M. K. Shakfa, A. Chernikov, D. Kalincev, S. Chatterjee, X. Lu, S. R. Johnson, D. A. Beaton, T. Tiedje, and M. Koch, "Carrier relaxation dynamics in a Ga(AsBi) single quantum well under high-intensity excitation conditions," *Phys. Status Solidi C*, vol. 10, no. 9, pp. 1234–1237, 2013.

[106] M. K. Shakfa, M. Wiemer, P. Ludewig, K. Jandieri, K. Volz, W. Stolz, S. D. Baranovskii, and M. Koch, "Thermal quenching of photoluminescence in Ga (AsBi)," *J. Appl. Phys.*, vol. 117, no. 2, p. 025709, 2015.

[107] A. R. Mohmad, F. Bastiman, J. S. Ng, S. J. Sweeney, and J. P. R. David, "Room temperature photoluminescence intensity enhancement in $GaAs_{1-x}Bi_x$ alloys," *Phys. Status Solidi C*, vol. 9, no. 2, pp. 259–261, 2012.

[108] M. Yoshimoto, M. Itoh, Y. Tominaga, and K. Oe, "Quantitative estimation of density of Bi-induced localized states in $GaAs_{1-x}Bi_x$ grown by molecular beam epitaxy," *J. Cryst. Growth*, vol. 378, pp. 73–76, 2013.

[109] R. A. Street, *Hydrogenated Amorphous Silicon*. Cambridge University Press, Cambridge, England, 1991.

[110] O. Rubel, S. D. Baraovskii, K. Hantke, W. W. Ruhle, P. Thomas, K. Volz, and W. Stolz, "Model of temperature quenching of photoluminescence in disordered semiconductors and comparison to experiment," *Phys. Rev. B*, vol. 73, p. 233201, 2006.

[111] B. Fluegel, S. Francoeur, A. Mascarenhas, S. Tixier, E. C. Young, and T. Tiedje, "Giant Spin-Orbit Bowing in $GaAs_{1-x}Bi_x$," *Phys. Rev. Lett.*, vol. 97, no. 6, p. 067205, 2006.

[112] A. R. Mohmad, F. Bastiman, J. S. Ng, S. J. Sweeney, and J. P. R. David, "Photoluminescence investigation of high quality $GaAs_{1-x}Bi_x$ on GaAs," *Appl. Phys. Lett.*, vol. 98, no. 12, p. 122107, 2011.

[113] C. Netzel, V. Hoffmann, T. Wernicke, A. Knauer, M. Weyers, M. Kneissl, and N. Szabo, "Temperature and excitation power dependent photoluminescence intensity of GaInN quantum wells with varying charge carrier wave function overlap," *J. Appl. Phys.*, vol. 107, no. 3, p. 033510, 2010.

[114] A. R. Mohmad, F. Bastiman, C. J. Hunter, J. S. Ng, S. J. Sweeney, and J. P. R. David, "The effect of Bi composition to the optical quality of $GaAs_{1-x}Bi_x$," *Appl. Phys. Lett.*, vol. 99, no. 4, p. 042107, 2011.

Dieses Werk ist copyrightgeschützt und darf in keiner Form vervielfältigt werden noch an Dritte weitergegeben werden.
Es gilt nur für den persönlichen Gebrauch.

[115] F. Yang, M. Wilkinson, E. J. Austin, and K. P. O'Donnell, "Origin of the Stokes shift: A geometrical model of exciton spectra in 2D semiconductors," *Phys. Rev. Lett.*, vol. 70, no. 3, pp. 323–326, 1993.

[116] A. Miller and E. Abrahams, "Impurity Conduction at Low Concentrations," *Phys. Rev.*, vol. 120, no. 3, pp. 745–755, 1960.

[117] D. Bisping, S. Schneider, S. Höfling, S. Habermann, M. Fischer, J. Koeth, and A. Forchel, "1240 nm high-power GaInNAs laser diodes," *Opt. Express*, vol. 15, no. 23, pp. 15187–15192, 2007.

[118] H. Grüning, K. Kohary, S. D. Baranovskii, O. Rubel, P. J. Klar, A. Ramakrishnan, G. Ebbinghaus, P. Thomas, W. Heimbrodt, W. Stolz, and W. Rühle, "Hopping relaxation of excitons in GaInNAs/GaNAs quantum wells," *Phys. Status Solidi C*, vol. 1, no. 1, pp. 109–112, 2004.

[119] M. Albrecht, V. Grillo, T. Remmele, H. P. Strunk, A. Y. Egorov, Gh. Dumitras, H. Reichert, A. Kaschner, R. Heitz, A. Hoffman, "Effect of annealing on the In and N distribution in InGaAsN quantum wells," *Appl. Phys. Lett.*, vol. 81, no. 15, pp. 2719–2721, 2002.

[120] P. J. Klar, H. Grüning, J. Koch, S. Schäfer, K. Volz, W. Stolz, W. Heimbrodt, A. M. Kamal Saadi, A. Lindsay, and E. P. O'Reilly, "(Ga,In)(N,As)-fine structure of the band gap due to nearest-neighbor configurations of the isovalent nitrogen," *Phys. Rev. B*, vol. 64, p. 121203, 2001.

[121] O. Rubel, K. Volz, T. Torunski, S. D. Baranovskii, F. Grosse, and W. Stolz, "Columnar [001]-oriented nitrogen order in Ga(NAs) and (GaIn)(NAs) alloys," *Appl. Phys. Lett.*, vol. 85, no. 24, pp. 5908–5910, 2004.

[122] T. Niebling, O. Rubel, W. Heimbrodt, W. Stolz, S. D. Baranovskii, P. J. Klar, and J. F. Geisz, "Spectral and time dependences of the energy transfer of bound optical excitations in GaP(N)," *J. Phys.: Condens. Matter*, vol. 20, no. 1, p. 015217, 2008.

[123] B. Dal Don, K. Kohary, E. Tsitsishvili, H. Kalt, S. D. Baranovskii, and P. Thomas, "Quantitative interpretation of the phonon-assisted redistribution processes of excitons in $\mathrm{Zn}_{1-x}\mathrm{Cd}_x\mathrm{Se}$ quantum islands," *Phys. Rev. B*, vol. 69, p. 045318, 2004.

[124] S. Imhof, C. Wagner, A. Chernikov, M. Koch, K. Kolata, N. S. Köster, S. Chatterjee, S. W. Koch, X. Lu, S. R. Johnson, D. A. Beaton, T. Tiedje, O. Rubel, and A. Thränhardt, "Evidence of two disorder scales in Ga(AsBi)," *Phys. Status Solidi B*, vol. 248, no. 4, pp. 851–854, 2011.

[125] K. Jandieri, M. K. Shakfa, S. Liebich, M. Zimprich, B. Kunert, C. Karcher, A. Chernikov, K. Volz, W. Stolz, M. Koch, S. Chatterjee, W. Heimbrodt, F. Gebhard, and S. D. Baranovskii, "Energy scaling of compositional disorder in Ga(N,P,As)/GaP quantum well structures," *Phys. Rev. B*, vol. 86, p. 125318, 2012.

[126] C. Karcher, "Über den Einfluss von isoelektronischen Störstellen auf Bandbiegung und Unordnung in Verbindungshalbleitern," Ph.D. thesis, Philipps-Universität Marburg, Germany, (2011).

[127] S. Kivelson and C. D. Gelatt, "Photoluminescence in a disordered insulator: The trapped-exciton model," *Phys. Rev. B*, vol. 26, no. 8, pp. 4646–4673, 1982.

Dieses Werk ist copyrightgeschützt und darf in keiner Form vervielfältigt werden noch an Dritte weitergegeben werden.
Es gilt nur für den persönlichen Gebrauch.

[128] S. Imhof, C. Wagner, A. Thränhardt, A. Chernikov, M. Koch, N. S. Köster, S. Chatterjee, S. W. Koch, O. Rubel, X. Lu, S. R. Johnson, D. A. Beaton, and T. Tiedje, "Luminescence dynamics in Ga(AsBi)," *Appl. Phys. Lett.*, vol. 98, no. 16, p. 161104, 2011.

[129] S. Mazzucato, T. T. Zhang, H. Carrère, D. Lagarde, P. Boonpeng, A. Arnoult, G. Lacoste, A. Balocchi, T. Amand, C. Fontaine, and X. Marie, "Electron spin dynamics and g-factor in GaAsBi," *Appl. Phys. Lett.*, vol. 102, no. 25, p. 252107, 2013.

[130] Yu. I. Mazur, V. G. Dorogan, M. Benamara, M. E. Ware, M. Schmidbauer, G. G. Tarasov, S. R. Johnson, X. Lu, S.-Q. Yu, T. Tiedje, and G. J. Salamo, "Effects of spatial confinement and layer disorder in photoluminescence of $GaAs_{1-x}Bi_x$/GaAs heterostructures," *J. Phys. D: Appl. Phys.*, vol. 46, no. 6, p. 065306, 2013.

[131] S. Mazzucato, H. Lehec, H. Carrère, H. Makhloufi, A. Arnoult, C. Fontaine, T. Amand, and X. Marie, "Low-temperature photoluminescence study of exciton recombination in bulk GaAsBi," *Nanoscale Res. Lett.*, vol. 9, no. 1, p. 19, 2014.

[132] M. K. Shakfa, K. Jandieri, M. Wiemer, P. Ludewig, K. Volz, W. Stolz, S. D. Baranovskii and M. Koch, "Energy scale of compositional disorder in Ga(AsBi)," *J. Phys. D: Appl. Phys.*, vol. 48, no. 42, p. 425101, 2015.

[133] S. Baranovski, *Charge Transport in Disordered Solids with Applications in Electronics*. John Wiley & Sons, Chichester, West Sussex, UK, 2006.

[134] S. D. Baranovskii and A. L. Efros "Band Edge Smearing in Solid Solutions," *Sov. Phys. Semicond.*, vol. 12, p. 1328, 1978.

[135] C. Skierbiszewski, P. Perlin, P. Wisniewski, W. Knap, T. Suski, W. Walukiewicz, W. Shan, K. M. Yu, J. W. Ager, E. E. Haller, J. F. Geisz, and J. M. Olson, "Large, nitrogen-induced increase of the electron effective mass in $In_yGa_{1-y}N_xAs_{1-x}$," *Appl. Phys. Lett.*, vol. 76, no. 17, pp. 2409–2411, 2000.

[136] C. Robert, M. Perrin, C. Cornet, J. Even, and J. M. Jancu, "Atomistic calculations of Ga(NAsP)/GaP(N) quantum wells on silicon substrate: Band structure and optical gain," *Appl. Phys. Lett.*, vol. 100, no. 11, p. 111901, 2012.

[137] A. Raymond, J. L. Robert, and C. Bernard, "The electron effective mass in heavily doped GaAs," *J. Phys. C*, vol. 12, no. 12, pp. 2289–2293, 1979.

[138] D. F. Reyes, F. Bastiman, C. J. Hunter, D. L. Sales, A. M. Sanchez, J. P. David, and D. Gonzalez, "Bismuth incorporation and the role of ordering in GaAsBi/GaAs structures," *Nanoscale Res. Lett.*, vol. 9, no. 1, p. 23, 2014.

[139] J. Orenstein and M. A. Kastner, "Thermalization and recombination in amorphous semiconductors," *Solid State Commun.*, vol. 40, no. 1, pp. 85–89, 1981.

[140] G. J. Adriaenssens, S. D. Baranovskii, W. Fuhs, J. Jansen, and Ö. Öktü, "Photoconductivity response time in amorphous semiconductors," *Phys. Rev. B*, vol. 51, no. 15, pp. 9661–9667, 1995.

[141] H. Cordes, G. H. Bauer, and R. Brüggemann, "Transient decay from the steady state in the photoconductivity of amorphous semiconductors," *Phys. Rev. B*, vol. 58, no. 24, pp. 16160–16166, 1998.

Dieses Werk ist copyrightgeschützt und darf in keiner Form vervielfältigt werden noch an Dritte weitergegeben werden.
Es gilt nur für den persönlichen Gebrauch.

[142] C. M. Gee and Marc Kastner, “Intrinsic-defect photoluminescence in amorphous and crystalline SiO_2,” *Phys. Rev. Lett.*, vol. 42, no. 26, pp. 1765–1769, 1979.

[143] S. Francoeur, S. Tixier, E. Young, T. Tiedje, and A. Mascarenhas, “Bi isoelectronic impurities in GaAs,” *Phys. Rev. B*, vol. 77, p. 085209, 2008.

Dieses Werk ist copyrightgeschützt und darf in keiner Form vervielfältigt werden noch an Dritte weitergegeben werden.
Es gilt nur für den persönlichen Gebrauch.

Dieses Werk ist copyrightgeschützt und darf in keiner Form vervielfältigt werden noch an Dritte weitergegeben werden.
Es gilt nur für den persönlichen Gebrauch.

List of Publications

Publications in Refereed Academic Journals

- M. K. Shakfa, K. Jandieri, M. Wiemer, P. Ludewig, K. Volz, W. Stolz, S. D. Baranovskii and M. Koch, *"Energy scale of compositional disorder in Ga(AsBi),"* J. Phys. D: Appl. Phys. **48**, 425101 (2015).
- M. K. Shakfa, M. Wiemer, P. Ludewig, K. Jandieri, K. Volz, W. Stolz, S. D. Baranovskii, and M. Koch,*"Thermal quenching of photoluminescence in Ga(AsBi),"* J. Appl. Phys. **117**, 025709 (2015).
- D. Al Nakdali, M. K. Shakfa, B. Heinen, B. Kunert, W. Stolz, S. W. Koch, J. Hader, J. V. Moloney, A. Rahimi-Iman, and M. Koch,*"Analysis of optical scattering losses in vertical-external-cavity surface-emitting lasers,"* Appl. Phys. B **120**, 41 (2015).
- D. Al Nakdali, M. Gaafar, M. K. Shakfa, F. Zhang, M. Vaupel, K. A. Fedorova, A. Rahimi-Iman, E. U. Rafailov, and M. Koch,*"High-Power Operation of Quantum-Dot Semiconductor Disk Laser at 1180 nm,"* IEEE Photon. Technol. Lett. **27**, 1128 (2015).
- D. Al Nakdali, M. K. Shakfa, M. Gaafar, M. Butkus, K. A. Fedorova, M. Zulonas, M. Wichmann, F. Zhang, B. Heinen, A. Rahimi-Iman, W. Stolz, E. U. Rafailov, and M. Koch,*"High-Power Quantum-Dot Vertical-External-Cavity Surface-Emitting Laser Exceeding 8 W,"* IEEE Photon. Technol. Lett. **26**, 1561 (2014).
- M. Gaafar, D. Al Nakdali, C. Möller, K. A. Fedorova, M. Wichmann, M. K. Shakfa, F. Zhang, A. Rahimi-Iman, E. U. Rafailov, and M. Koch,*"Self-mode-locked quantum-dot vertical-external-cavity surface-emitting laser,"* Opt. Lett. **39**, 4623 (2014).
- M. K. Shakfa, D. Kalincev, X. Lu, S. R. Johnson, D. A. Beaton, T. Tiedje, A. Chernikov, S. Chatterjee, and M. Koch,*"Quantitative study of localization effects and recombination dynamics in GaAsBi/GaAs single quantum wells,"* J. Appl. Phys. **114**, 164306 (2013).
- M. Wichmann, M. K. Shakfa, F. Zhang, B. Heinen, M. Scheller, A. Rahimi-Iman, W. Stolz, J. V. Moloney, S. W. Koch, and M. Koch,*"Evolution of multi-mode operation in vertical-external-cavity surface-emitting lasers,"* Opt. Express **21**, 31940 (2013).
- A. Chernikov, M. Wichmann, J. Herrmann, B. Heinen, M. K. Shakfa, S. Chatterjee, S. W. Koch, B. Kunert, W. Stolz, T.-L. Wang, Y. Kaneda, M. Scheller, M. J. Yarborough, J. Hader, J. V. Moloney, and M. Koch,*"In-situ spectroscopy of highpower vertical-external-cavity surface-emitting lasers,"* Phys. Status Solidi B **250**, 1781 (2013).

Dieses Werk ist copyrightgeschützt und darf in keiner Form vervielfältigt werden noch an Dritte weitergegeben werden.
Es gilt nur für den persönlichen Gebrauch.

- H. Hintzsche, C. Jastrow, B. Heinen, K. Baaske, T. Kleine-Ostmann, M. Schwerdtfeger, M. K. Shakfa, U. Kärst, M. Koch, T. Schrader, and H. Stopper, *"Terahertz Radiation at 0.380 THz and 2.520 THz Does Not Lead to DNA Damage in Skin Cells In Vitro,"* Radiat. Res. **179**, 38 (2012).
- K. Jandieri, M. K. Shakfa, S. Liebich, M. Zimprich, B. Kunert, C. Karcher, A. Chernikov, K. Volz, W. Stolz, M. Koch, S. Chatterjee, W. Heimbrodt, F. Gebhard, and S. D. Baranovskii, *"Energy scaling of compositional disorder in Ga(N,P,As)/GaP quantum well structures,"* Phys. Rev. B **86**, 125318 (2012).
- A. Chernikov, M. Wichmann, M. K. Shakfa, M. Scheller, J. V. Moloney, S. W. Koch, and M. Koch, *"Time-dynamics of the two-color emission from vertical-external-cavity surface-emitting lasers,"* Appl. Phys. Lett. **100**, 041114 (2012).
- N. Vieweg, M. K. Shakfa, and M. Koch, *"Molecular Terahertz Polarizability of PCH5, PCH7 and 5OCB,"* J. Infrared Milli. Terahz. Waves **32**, 1367 (2011).
- B. Breitenstein, M. Scheller, M. K. Shakfa, T. Kinder, T. Müller-Wirts, M. Koch, and D. Selmar, *"Introducing Terahertz Technology into Plant Biology: A Novel Method to Monitor Changes in Leaf Water Status,"* J. Appl. Bot. Food Qual. **84**, 158 (2011).
- N. Vieweg, M. K. Shakfa, and M. Koch, *"BL037: A nematic mixture with high terahertz birefringence,"* Opt. Commun. **284**, 1887 (2011).
- C. Brenner, M. Hofmann, M. Scheller, M. K. Shakfa, M. Koch, I. C. Mayorga, A. Klehr, G. Erbert, and G. Tränkle, *"Compact diode-laser-based system for continuous-wave and quasi-time-domain terahertz spectroscopy,"* Opt. Lett., **35**(23), 3859 (2010).
- N. Vieweg, M. K. Shakfa, B. Scherger, M. Mikulics, and M. Koch, *"THz Properties of Nematic Liquid Crystals,"* J. Infrared Milli. Terahz. Waves **31**, 1312 (2010).
- N. Vieweg, C. Jansen, M. K. Shakfa, M. Scheller, N. Krumbholz, R. Wilk, M. Mikulics, and M. Koch, *"Molecular properties of liquid crystals in the terahertz frequency range,"* Opt. Express **18**, 6097 (2010).

Refereed Conference Publications

- A. Rahimi-Iman, M. Gaafar, D. Al Nakdali, C. Möller, F. Zhang, M. Wichmann, M. K. Shakfa, K. A. Fedorova, W. Stolz, E. U. Rafailov, and M. Koch, *"Recent Advances in the Field of Vertical-External-Cavity Surface-Emitting Lasers,"* in Proceedings of SPIE 9349, 934906, SPIE Photonics West: Vertical External Cavity Surface Emitting Lasers (VECSELs) V, San Francisco, California, USA (2015). **(invited talk)**
- M. K. Shakfa, M. Wiemer, P. Ludewig, K. Jandieri, K. Volz, W. Stolz, S. D. Baranovskii, and M. Koch, *"Two-energy-scale model for description of the thermal quenching of photoluminescence in disordered Ga(As,Bi),"* in Proceedings of 17$^{\text{th}}$ International Conference on Extended Defects in Semiconductors 2014, Göttingen, Germany (2014). **(talk)**
- M. Wichmann, M. K. Shakfa, B. Heinen, A. Rahimi-Iman, S. W. Koch, M. Koch, M. Scheller, and J. V. Moloney, *"Evolution of multi-mode emission from vertical-external-cavity surface-emitting lasers,"* in Proceedings of the 16$^{\text{th}}$ International Conference "Laser Optics 2014", Saint-Petersburg, Russia (2014). **(talk)**

Dieses Werk ist copyrightgeschützt und darf in keiner Form vervielfältigt werden noch an Dritte weitergegeben werden.
Es gilt nur für den persönlichen Gebrauch.

- M. Wichmann, M. K. Shakfa, M. Scheller, A. Rahimi-Iman, B. Heinen, J. V. Moloney, S. W. Koch, and M. Koch, *"Systematic investigation of single- and multi-mode operation in vertical-external-cavity surface-emitting lasers,"* in Proceedings of SPIE 8966, 89660N, SPIE Photonics West: Vertical External Cavity Surface Emitting Lasers (VECSELs) IV, San Francisco, California, USA (2014). **(talk)**
- M. Wichmann, A. Chernikov, M. K. Shakfa, M. Scheller, J. V. Moloney, S. W. Koch, and M. Koch, *"Room-temperature terahertz generation using vertical-external-cavity surface-emitting lasers,"* in Proceedings of CLEO/Europe-EQEC 2013: the Conference on Lasers and Electro-Optics/Europe and the European Quantum Electronics Conference, Munich, Germany (2013). **(invited talk)**
- M. K. Shakfa, A. Chernikov, D. Kalincev, S. Chatterjee, X. Lu, S. R. Johnson, D. A. Beaton, T. Tiedje, and M. Koch, *"Carrier relaxation dynamics in a Ga(AsBi) single quantum well under high-intensity excitation conditions,"* in Proceedings of NOEKS 11: the 11$^{\text{th}}$ International Workshop on Nonlinear Optics and Excitation Kinetics in Semiconductors, Stuttgart, Germany (2012). **(poster)**
- M. Wichmann, A. Chernikov, M. K. Shakfa, S. W. Koch, M. Scheller, J. V. Moloney, and M. Koch, *"Study of the two-color emission dynamics from a vertical-external-cavity surface-emitting laser,"* in Proceedings of the 37$^{\text{th}}$ International Conference on Infrared, Millimeter, and Terahertz Waves (IRMMW-THz), Wollongong, Australia (2012). **(invited talk)**
- A. Chernikov, M. Wichmann, M. K. Shakfa, S. W. Koch, M. Scheller, J. V. Moloney, and M. Koch, *"Temporal dynamics of the two-color emission in vertical-external-cavity surface-emitting lasers,"* in Proceedings of Conference on Lasers and Electro-Optics 2012 (CLEO), San Jose, California, USA (2012). **(talk)**
- M. Wichmann, A. Chernikov, M. K. Shakfa, A. Bäumner, M. Koch, M. Scheller, J. Hader, J. V. Moloney, and S. W. Koch, *"VECSELs: Nonequilibrium effects and two-color operation,"* in Proceedings of SPIE 8242-0I, 82420I, SPIE Photonics West: Vertical External Cavity Surface Emitting Lasers (VECSELs) II, San Francisco, California, USA (2012). **(invited talk)**
- M. K. Shakfa, N. Vieweg, and M. Koch, *"Liquid crystal with high THz birefringence,"* in Proceedings of the 6$^{\text{th}}$ German Microwave Conference (GeMIC), Darmstadt, Germany (2011). **(poster)**
- N. Vieweg, R. Wilk, M. K. Shakfa, J. M. Kloc, M. Scheller, C. Jansen, N. Krumbholz, M. Mikulics, and M. Koch, *"Terahertz investigation of liquid crystals from the CB family,"* in Proceedings of the IEEE Photonics Society Winter Topicals Meeting Series (WTM), Majorca, Spain (2010). **(poster)**
- S. Wietzke, C. Jansen, C. Jördens, N. Krumbholz, N. Vieweg, M. Scheller, M. K. Shakfa, D. Romeike, T. Hochrein, M. Mikulics, and M. Koch, *"Industrial applications of THz systems,"* in Proceedings of SPIE 7385-06, 738506, International Symposium on Photoelectronic Detection and Imaging 2009: Terahertz and High Energy Radiation Detection Technologies and Applications, Beijing, China (2009). **(invited talk)**

Dieses Werk ist copyrightgeschützt und darf in keiner Form vervielfältigt werden noch an Dritte weitergegeben werden.
Es gilt nur für den persönlichen Gebrauch.

- M. K. Shakfa, M. Scheller, B. Breitenstein, D. Selmar, and M. Koch,*"Monitoring the water status of economic plants with continuous wave terahertz radiation,"* in Proceedings of CLEO/Europe-EQEC 2009: the Conference on Lasers and Electro-Optics/Europe and the European Quantum Electronics Conference, Munich, Germany (2009). **(poster)**

Non-Refereed Conference Publications

- R. Woscholski, M. K. Shakfa, S. Gies, M. Wiemer, M. Zimprich, S. Reinhard, P. Ludewig, K. Jandieri, A. Rahimi-Iman, S. D. Baranovskii, W. Heimbrodt, K. Volz, W. Stolz and M. Koch,*"Time-resolved photoluminescence of Ga(NAsP) multiple quantum wells grown on Si substrate,"* in Materialforschungstag Mittelhessen 2015, Marburg, Germany (2015). **(poster)**
- D. Al Nakdali, M. K. Shakfa, M. Gaafar, M. Butkus, K. A. Fedorova, M. Zulonas, M. Wichmann, F. Zhang, A. Rahimi-Iman, E. U. Rafailov, and M. Koch,*"High-Power Operation of Infrared Quantum-Dot Vertical-External-Cavity Surface-Emitting Lasers,"* in the workshop "Women in Optics: The Castle Meeting 2015", Ebsdorfergrund, Germany (2015). **(poster)**
- M. K. Shakfa, D. Kalincev, A. Chernikov, S. Chatterjee, X. Lu, S. R. Johnson, D. A. Beaton, T. Tiedje, and M. Koch,*"Dynamics of localized carriers in GaAsBi/GaAs quantum wells,"* in the international conference "Condensed Matter in Paris", Paris, France (2014). **(poster)**
- M. K. Shakfa, D. Kalincev, A. Chernikov, S. Chatterjee, X. Lu, S. R. Johnson, D. A. Beaton, T. Tiedje, and M. Koch,*"Study of the disorder effects in Ga(AsBi) single quantum wells,"* in the German Physical Society Spring Meeting of the Condensed Matter Section (DPG-Frühjahrstagung), Dresden, Germany (2014). **(talk)**
- D. Al Nakdali, M. K. Shakfa, B. Heinen, B. Kunert, W. Stolz, S. W. Koch, J. Hader, J. V. Moloney, A. Rahimi-Iman, and M. Koch,*"Non-heating losses and thermal resistance of VECSELs,"* in the German Physical Society Spring Meeting of the Condensed Matter Section (DPG-Frühjahrstagung), Dresden, Germany (2014). **(poster)**
- M. Wichmann, M. Scheller, M. K. Shakfa, M. Stein, J. Quante, B. Heinen, A. Rahimi-Iman, W. Stolz, J. V. Moloney, S. W. Koch, and M. Koch,*"Terahertz emitting vertical-external-cavity surface-emitting laser,"* in the 2nd Annual Conference of COST MP1204 Action "Tera-MIR Radiation: Materials, Generation, Detection and Applications", Marburg, Germany (2014). **(talk)**
- D. Al Nakdali, M. K. Shakfa, B. Heinen, B. Kunert, W. Stolz, S. W. Koch, J. Hader, J. V. Moloney, A. Rahimi-Iman, and M. Koch,*"Optical Scattering Losses in VECSELs,"* in the 17th Annual German Conference of Women in Physics (Deutsche Physikerinnentagung, DPT), Heidelberg, Germany (2013). **(poster)**
- M. K. Shakfa, M. Wichmann, A. Chernikov, S. W. Koch, M. Scheller, J. V. Moloney, and M. Koch,*"Influence of Intra-cavity Losses on the Temporal Dynamics of the Dual-Wavelength Emission in VECSELs,"* in the 2nd European Workshop on VeCSELs, Montpellier, France (2013). **(talk)**

Dieses Werk ist copyrightgeschützt und darf in keiner Form vervielfältigt werden noch an Dritte weitergegeben werden.
Es gilt nur für den persönlichen Gebrauch.

- D. Al Nakdali, M. K. Shakfa, B. Heinen, B. Kunert, W. Stolz, S. W. Koch, J. Hader, J. V. Moloney, A. Rahimi-Iman, and M. Koch, *"Optical Scattering Losses in VECSELs,"* in the 2nd European Workshop on VeCSELs, Montpellier, France (2013). **(poster)**
- M. K. Shakfa, D. Kalincev, A. Chernikov, S. Chatterjee, X. Lu, S. R. Johnson, D. A. Beaton, T. Tiedje, and M. Koch, *"Carrier localization effects in Ga(AsBi)/GaAs heterostructures,"* in the E-MRS 2013 Spring Meeting (European Materials Research Society), Strasbourg, France (2013). **(talk)**
- D. Kalincev, M. K. Shakfa, A. Chernikov, S. Chatterjee, X. Lu, S. R. Johnson, D. A. Beaton, T. Tiedje, and M. Koch, *"Investigation of carrier dynamics in $Ga(As_{1-x}Bi_x)/GaAs$ heterostructures by time-resolved photoluminescence,"* in the German Physical Society Spring Meeting of the Condensed Matter Section (DPG-Frühjahrstagung), Regensburg, Germany (2013). **(poster)**
- H. Hintzsch, C. Jastrow, B. Heinen, K. Baaske, T. Kleine-Ostmann, M. Schwerdtfeger, M. K. Shakfa, U. Kärst, M. Koch, T. Schrader, and H. Stoppe, *"Does terahertz radiation cause genotoxic effects and mitotic disturbances?,"* in the 2012 Workshop on EMF & Health Risk Research, Monte Verità, Ascona, Switzerland (2012). **(talk)**
- M. K. Shakfa, D. Kalincev, A. Chernikov, S. Chatterjee, X. Lu, S. R. Johnson, D. A. Beaton, T. Tiedje, and M. Koch, *"Time-resolved photoluminescence studies of Ga(AsBi)/GaAs single quantum wells,"* in ICSNN 2012: the International Conference on Superlattices, Nanostructures and Nanodevices, Dresden, Germany (2012). **(poster)**
- M. K. Shakfa, D. Kalincev, A. Chernikov, S. Chatterjee, X. Lu, S. R. Johnson, D. A. Beaton, T. Tiedje, and M. Koch, *"Characterization of $Ga(As_{1-x}Bi_x)/GaAs$ single quantum wells using time-resolved photoluminescence,"* in Materialforschungstag Mittelhessen 2012, Marburg, Germany (2012). **(poster)**
- A. Chernikov, M. Wichmann, M. K. Shakfa, B. Heinen, S. W. Koch, J. Hermann, S. Chatterjee, B. Kunert, W. Stolz, M. Koch, M. Scheller, J. M. Yarborough, J. Hader, J. V. Moloney, *"High power vertical-external-cavity surface-emitting lasers for continuous-wave multi-mW THz applications,"* in TERA-2012: the 2nd International Conference "Terahertz and Microwave radiation: Generation, Detection and Applications", Moskow, Russia (2012). **(talk)**
- C. Jastrow, T. Kleine-Ostmann, M. Salhi, T. Schrader, H. Hintzsche, H. Stopper, U. Kärst, B. Heinen, M. K. Shakfa, M. Schwerdtfeger, T. Probst, and M. Koch, *"In vitro THz field exposition of skin cells,"* in EBEA 2011: the 10th International Congress of the European Bioelectromagnetics Association, Rome, Italy (2011). **(talk)**
- C. Brenner, M. Hofmann, M. Scheller, M. K. Shakfa, M. Koch, A. Klehr, and G. Erbert, *"Diode laser based THz homodyne system for cw and quasi time domain spectroscopy,"* in Laser Optics Berlin, Berlin, Germany (2010). **(talk)**
- C. Brenner, M. R. Hofmann, M. K. Shakfa, M. Scheller, M. Koch, A. Klehr, and G. Erbert, *"Versatile THz Homodyn System based on an amplified laser diode in an external cavity,"* in the International Workshop on Terahertz Technology 2009 (TeraTech '09), Osaka, Japan (2009). **(poster)**

Dieses Werk ist copyrightgeschützt und darf in keiner Form vervielfältigt werden noch an Dritte weitergegeben werden.
Es gilt nur für den persönlichen Gebrauch.

- M. K. Shakfa, M. Scheller, B. Breitenstein, D. Selmar, and M. Koch *"Terahertz imaging for studying the water status of plants,"* in the European Summer School on New Trends in Terahertz Imaging (NTTI 2009), Paris, France (2009). **(poster)**

Dieses Werk ist copyrightgeschützt und darf in keiner Form vervielfältigt werden noch an Dritte weitergegeben werden.
Es gilt nur für den persönlichen Gebrauch.

Dieses Werk ist copyrightgeschützt und darf in keiner Form vervielfältigt werden noch an Dritte weitergegeben werden.
Es gilt nur für den persönlichen Gebrauch.

Dieses Werk ist copyrightgeschützt und darf in keiner Form vervielfältigt werden noch an Dritte weitergegeben werden.
Es gilt nur für den persönlichen Gebrauch.